

**DEVELOPMENT AND APPLICATION OF AN IN-SITU
FORMING, BIOHYBRID SCAFFOLD
FOR WOUND REPAIR**

by

Ryan Victor Hartwell

B.Sc. Biochemistry (honours) University of Ottawa, 2007

A THESIS SUBMITTED IN PARTIAL FULFILLMENT OF THE
REQUIREMENTS FOR THE DEGREE OF

DOCTOR OF PHILOSOPHY

in

The Faculty of Graduate and Postdoctoral Studies
(Experimental Medicine)

THE UNIVERSITY OF BRITISH COLUMBIA
(Vancouver)

March 2015

© Ryan Victor Hartwell, 2015

Abstract

Tissue engineering has advanced rapidly over the past decade in an effort to address unmet medical needs in burn and chronic wound treatment. Each year, over 1 million patients seek medical attention for burn injuries in North America. Moreover, chronic wounds in the elderly and those with diabetes comprise the largest single segment of wound care. Without question current treatments are costly and challenging for healthcare professionals. When autografts are not possible, skin substitutes are often employed as alternative coverage. Although these strategies have dramatically improved healing in patients, they are limited by the time they take to fully integrate with surrounding tissue. Our idea to bridge the gap is to create a patient-ready skin substitute. Moving toward a skin substitute that is readily available for the patient, I developed an in-situ gelling scaffold that permits integration with surrounding tissue. Furthermore, it was my goal to create a system that resists cell mediated contracture and digestion, and provide an ideal environment for tissue repair.

My hypothesis was that the fabrication of a composite matrix of collagen and a blended-polymer hydrogel would result in a material that could be lyophilized, reconstituted and gel rapidly in-situ. The objectives of this work are fourfold: (1) develop, characterize, optimize and evaluate the functionality of a reconstitutable in situ forming scaffold in vitro; (2) evaluate the efficacy of the scaffold to perform within an acute wound; (3) evaluate methods to tailor the scaffold to be used as a cell delivery vehicle; and (4) develop a prototype model product that could translated to the clinic. Satisfying the objectives of this work have demonstrated that with a biocompatible concentration of hydrogel collagen fibrillogenesis activation energy can be lowered, and the mechanical and physical properties of the

resulting scaffold are enhanced. The resulting scaffold can be further lyophilized and reconstituted to form composite skin and other matrices both in vitro and in vivo. Assuming that regulatory requirements are met, the scaffold has the potential to improve the quality of life of patients with devastating chronic wounds and burns, and advance further knowledge in the field of tissue engineering.

Preface

The work presented herein is a compilation of studies that has already been published in peer-reviewed journals, conditionally accepted for publication in peer-reviewed journals, submitted and under review by a peer-reviewed journal or published in a provisional patent submitted by the UBC University Industry Liaison Office. Distribution of the work is as follows:

Chapter 2: Complete, original publication with minor modifications for improved clarity hereto. Hartwell R, Leung V, Chavez-Munoz C, Nabai L, Yang H, Ko F, and Ghahary A. A novel hydrogel-collagen composite improves functionality of an injectable extracellular matrix. Acta Biomater.7(8):3060-9. In this work Ryan Hartwell performed, alone or in-conjunction with co-authors, all experiments in addition to writing the first and final edited draft of the manuscript. Leung contributed to the experimental design and execution of the mechanical loading, calorimetry scanning electron microscope (SEM) experiments. Chavez-Munoz assisted with immunostaining and evaluating cell viability in addition to manuscript review. Nabai assisted in conducting enzyme degradation method development and experimentation. Yang contributed to the experimental design of the mechanical loading evaluation. Ko oversaw the engineering (mechanical evaluation) aspects of the manuscript, in addition to reviewing and editing the manuscript. Ghahary supervised the project and reviewed the manuscript revisions.

Chapter 3: Complete component of a US Provisional Patent Application, with minor modifications for improved clarity hereto, and prepared manuscript. Hartwell R, Chan B, Elliott K, and Ghahary A. Polyvinyl-alcohol-PEG (PVA-PEG) hydrogels improve fibrillation kinetics, mechanics and utility of collagen:GAG scaffolds. Hartwell was the project lead and performed, alone or in-conjunction with co-authors and technical service staff (contact angle and SEM), all experiments in addition to drafting and editing the manuscript and patent

application. Chan assisted in performing gel curve analysis and evaluation of cell viability and migration, as well as manuscript review. Elliott assisted in performing gel curve analysis. Ghahary supervised the project and reviewed and edited the manuscript.

Chapter 4: Complete, original publication with minor modifications for improved clarity hereto. Hartwell R, Poormasjedi-Meibod M, Chavez-Munoz C, Jalili R, Tabatabaei A and Ghahary A. An in-situ forming skin substitute improves healing outcome in a hypertrophic scar model. Journal of Tissue Engineering Part A. March 2015, 21(5-6): 861-874. Hartwell was the project lead and performed, alone or in-conjunction with co-authors, all experiments in addition to drafting and editing the manuscript. Poormasjedi-Meibod was the primary contributor for mRNA extraction and data analysis in addition to assisting with animal surgery and immunostaining. Chavez-Munoz also assisted with mRNA extraction and data analysis in addition to assisting with animal surgery, experimental design and manuscript review. Jalili assisted with experimental design, animal surgery and manuscript review. Tabatabaei assisted with mRNA extraction and data analysis and animal surgery. Ghahary supervised the project and assisted with manuscript review and editing.

Chapter 5: Component of a publication in the Canadian Journal of Diabetes. Azadeh Hosseini-Tabatabaei RBJ, Ryan Hartwell, Sanam Salimi, Ruhangiz T. Kilani, Aziz Ghahary. Embedding Islet in a liquid scaffold increases islet viability and function. Canadian Journal of Diabetes. 2013;37 (1):27-35. The central work from the aforementioned manuscript described in this thesis was performed by Ryan Hartwell in conjunction with the primary author Azadeh Hosseini-Tabatabaei. Scaffold design and fabrication and viability analysis was performed by Ryan Hartwell. Islet isolation and culturing was conducted by Azadeh Hosseini-Tabatabaei. The remaining authors contributed to aspects of the manuscript that are not discussed herein.

All research described herein was conducted under the supervision of the Principle Investigator, Dr. Aziz Ghahary. Financial support for this work was provided by CIHR and NSERC grants, in addition to support from Worksafe BC and the BC Professional Fire Fighters Burn Fund held by Dr. Aziz Ghahary.

Work described herein was conducted in accordance with University and Hospital (Vancouver Coastal Health Research Institute) Ethics approvals for research involving human subjects under protocol: H05-0103; and under approvals for research conducted on animals under protocols: A10-0147 and A10-1372.

Table of Contents

Abstract	ii
Preface	iv
Table of Contents	vii
List of Figures	xi
List of Abbreviations	xiv
Acknowledgements	xvi
1 Introduction	1
1.1 Wound healing	1
1.2 Wound care background	3
1.3 Advances in wound care	4
1.4 Skin substitutes and polymer scaffolds	5
1.5 Hydrogel-based scaffolds	6
1.6 Collagen	7
1.7 Polyvinyl alcohol (PVA)	12
1.8 Hypothesis and objectives	14
2 A novel hydrogel-collagen composite improves functionality of an injectable extracellular matrix	16
2.1 Introduction	16
2.2 Materials and methods	18
2.2.1 Collagen-glycosaminoglycan scaffolds.....	18
2.2.2 Cell populated scaffolds.....	19
2.2.3 Cell viability and morphology	20
2.2.4 Cellularity	20
2.2.5 Time to fibril formation	21
2.2.6 Mechanical strength.....	21
2.2.7 Differential scanning calorimetry (DSC) and scanning electron microscopy (SEM)	21
2.2.8 Gel contraction.....	22
2.2.9 Collagenase digestion	22
2.2.10 Bi-layered skin substitute	23

2.2.11	Statistics	23
2.3	Results	24
2.3.1	Casting time.....	24
2.3.2	Mechanical strength.....	26
2.3.3	Cell viability and morphology	28
2.3.4	Cellularity	31
2.3.5	Resistance to contraction	31
2.3.6	Thermal stability.....	33
2.3.7	Resistance to enzyme degradation	34
2.3.8	Scanning electron microscopy (SEM).....	35
2.3.9	Engineered skin substitute (ESS).....	36
2.4	Discussion	38
2.5	Conclusion	42
3	Polyvinyl alcohol-<i>graft</i>-polyethylene glycol hydrogels improve fibrillation kinetics, mechanics and utility of collagen:glycosaminoglycan scaffolds	43
3.1	Introduction	43
3.2	Materials and methods	46
3.2.1	Materials	46
3.2.2	Fabrication of collagen-polymer hybrid scaffolds.....	46
3.2.3	Crosslinker, polyvinyl alcohol and copolymer effects on gelation kinetics... 49	49
3.2.4	Mechanical strength.....	49
3.2.5	Scaffold architecture using Scanning Electron Microscopy (SEM).....	50
3.2.6	Contact angle.....	50
3.2.7	Cell viability.....	50
3.2.8	Cell adhesion and migration	51
3.2.9	Statistics	51
3.3	Results	52
3.3.1	Effect of crosslinker concentration, PVA and time on fibril formation	53
3.3.2	PVA-hydrogel addition preserves gelation and mechanical properties of gel- mixtures following lyophilization	57
3.3.3	PVA-PEG and PVA-hydrogel systems exhibit a surfactant like effect on collagen gel-mixtures	60

3.3.4	Cell viability and cell migration.....	63
3.3.5	Fibroblast morphology and scaffold architecture	65
3.4	Discussion	66
3.5	Conclusion	69
4	An in-situ forming skin substitute improves healing outcome in a hypertrophic scar model	70
4.1	Introduction	70
4.2	Materials and methods	71
4.2.1	Cell isolation and culture.....	71
4.2.2	Preparation of IDO expressing cells	72
4.2.3	Scaffold preparation.....	73
4.2.4	Cell viability and morphology	73
4.2.5	Scaffold contracture.....	73
4.2.6	Animal model.....	74
4.2.7	Healing outcome- scar elevation index, epidermal thickness & cellularity .	75
4.2.8	Collagen staining, MMP-1 and collagen expression.....	75
4.2.9	Immunofluorescence staining CD31, CD3 and PGP 9.5.....	76
4.2.10	Statistics	76
4.3	Results	77
4.3.1	IDO expression, skin cell viability and morphology within in-situ forming scaffolds	77
4.3.2	Free-floating scaffold resistance to contraction and cellular morphology	79
4.3.3	Application of the hydrogel scaffold and wound healing outcome	80
4.3.4	Matrix deposition and expression of matrix metalloproteinase-1 (MMP-1) and collagen type 1	84
4.3.5	CD3+ T-cells post wound healing.....	86
4.3.6	CD31 ⁺ immunostaining and vessel-like structures within healed wounds ...	88
4.3.7	Cutaneous innervation.....	90
4.4	Discussion	92
4.5	Conclusion	95
5	Applications of a reconstitutable matrix for in-situ tissue engineering strategies and suggestions for future work	96
5.1	General discussion.....	96

5.2 Suggestions for future work	97
Bibliography	100

List of Figures

Figure 1.1. The stages of wound healing.....	3
Figure 1.2. Collagen structure and synthesis.	9
Figure 1.3. Turbidity measurement for collagen fibrillogenesis with differing dermatan sulfate treatments described by <i>Panitich et al.</i> in US patent number: US20110020298.....	11
Figure 1.4. Structure and interactions of polyvinyl alcohol (PVA).....	13
Figure 1.5. Cartoon representation of an in-situ forming skin substitute system either applied alone or in combination with pre-made skin substitutes in the solid form.	15
Figure 2.1. Time to fibril formation and gelation of collagen-GAG scaffolds.	25
Figure 2.2. Mechanical properties of hydrated collagen-GAG gels.	27
Figure 2.3. Viability and morphology of cells cultured in or on collagen-GAG scaffolds.	29
Figure 2.4. Fibroblast cellularity when cultured within collagen-GAG scaffolds over a 10-day period.	30
Figure 2.5. Contraction of free-floating fibroblast populated collagen-GAG scaffolds (FFPC).....	32
Figure 2.6. Thermal and enzymatic stability of collagen-GAG scaffolds. ...	34
Figure 2.7. SEM micrographs of three different collagen gels.	36
Figure 2.8. Phase-contrast micrographs of engineered skin substitutes ESS.	37
Figure 3.1. Process-schematic for the fabrication of the reconstitutable, collagen scaffold. Steps 1-8 describe the process by which one can	

manufacture the scaffold, freeze-dry, then reconstitute using water or other aqueous media and easily apply to a wound bed or cell culture container.45

Figure 3.2. Effect of crosslinker concentration on fibril formation kinetics and turbidity.	52
Figure 3.3. Arrhenius plot for collagen fibrillation as a function of PVA-borate hydrogel concentration	54
Figure 3.4. Effect of PVA variants on collagen fibrillogenesis pre- and post lyophilization/reconstitution.	56
Figure 3.5 Quantification of collagen solution gelation kinetics and mechanical properties pre- and post lyophilization (freeze drying).	59
Figure 3.6. Contact angle measurements of dry gelled collagen films.	61
Figure 3.7. Cell viability and migration in collagen scaffold variants.....	62
Figure 3.7. Fibroblast morphology and scaffold architecture in collagen variants.	64
Figure 3.9. Utility of lyophilized (freeze-dried) collagen scaffold.....	67
Figure 4.1. Biocompatibility and functional evaluation of scaffolds in-vitro.	78
Figure 4.2. Macroscopic clinical evaluation of punch wounds in the rabbit ear.....	81
Figure 4.3. Histologic evaluation of hematoxylin and eosin stained sections of treated rabbit wounds on post surgical day 35.	82
Figure 4.4. Evaluation of healing outcome in rabbit ear treated wounds using Scar Elevation Index, epidermal and dermal thickness, and tissue cellularity.	83
Figure 4.5. Collagen staining and gene expression of collagen and MMP-1 in treated rabbit wounds.	85

Figure 4.6. CD3⁺ lymphocyte and CD31⁺ (platelet cell adhesion molecule) marked vessel formation in treated rabbit tissue. 87

Figure 4.7. Distribution and quantification of cutaneous neoinnervation within the treated wound tissues 35 days post-surgery. 89

Figure 4.8. Validation of IDO expression in transplanted fibroblasts. 91

List of Abbreviations

ANOVA	Analysis of variance
ASA	Alpha smooth muscle actin
AU	Absorbance Units
BHK	Baby hamster kidney cells
BPE	Bovine Pituitary Extract
DAPI	2-(4-amidinophenyl)-1H -indole-6-carboxamide
DMEM	Dulbecco's Modified Eagle's Medium
DSC	Differential Scanning Calorimetry
DT	Dermal thickness
ECM	Extracellular Matrix
EDTA	Ethylenediaminetetraacetic acid
ET	Epidermal thickness
ESS	Engineered Skin Substitute
FBS	Fetal Bovine Serum
FFPC	Free-floating Fibroblast Populated Collagen scaffold
GLY	Glycine
GAG	Glycosaminoglycan
HaCat's	Immortalized human keratinocyte cell line
HCl	Hydrochloric acid
H&E	Hematoxylin and Eosin
HEPES	2-[4-(2-hydroxyethyl)piperazin-1-yl]ethanesulfonic acid
hFF	Primary normal human fibroblast
hKC	Primary normal human keratinocyte
hIDO	Human IDO gene
hpf	High power field
IDO	Indoleamine 2,3-dioxygenase
IPN	Interpenetrating Network
IRF	Immunoreactive fiber
KSFM	Keratinocyte Serum-Free Media

MMP	Matrix metalloproteinase
mRNA	Messenger Ribonucleic Acid
NaOH	Sodium Hydroxide
PBS	Phosphate Buffered Saline
PCL	Polycaprolactone
PCR	Polymerase Chain Reaction
PDB	Protein Database
PDGF	Platelet derived growth factor
PEG	Polyethylene glycol
P-HEMA	Poly(hydroxyethylmethacrylate)
PGP	Protein Gene Product
PLA	Poly(lactic acid)
PLGA	Poly(lactic acid-co-glycolic acid)
PRP	Platelet Rich Plasma
PVA	Polyvinyl alcohol
RPE	Retinal Pigment Epithelial (cells)
SDS	Sodium dodecyl sulfate
SEI	Scar Elevation Index
SEM	Scanning Electron Microscope

Acknowledgements

A sincere thank-you to my supervisor, Dr. Aziz Ghahary and committee members, Dr. Ross MacGillivray and Dr. Frank Ko for their encouragement, mentoring, guidance and contributions. A special thank you to Doug and Heike Hartwell, who have as my parents reminded me to enjoy the journey, even if it means taking the hard road, and to think out of the box. Thank you to my brother Keenan Elliott who assisted as a summer student. Thank you to my partner, DeeDee Ryan, who has provided support and motivation during the final stages of compiling this dissertation. Thank you to all of my friends and colleagues who have, in one way or another contributed to the success of this work and continue to see it through into a realizable material one day. Finally, thanks to CIHR, NSERC and the BC Provincial Firefighters Burn Fund, Spectra Energy, and Works Safe BC for funding the body of work described herein.

1 Introduction

1.1 Wound healing

Healing, or rather tissue repair and regeneration, requires the orchestration of a spectacular array of physiological processes. The general process of wound healing involves at least three major overlapping phases: the lag phase (homeostasis, inflammation, and cytokine release), proliferative phase (fibroblast number increases, matrix deposited, epithelial cell migration, vascularization) and the remodeling phase (cell number decreases, collagen fiber organization and remodeling) (1). Myofibroblasts, a contractile fibroblast-like cell expressing alpha-smooth muscle actin (ASA), appear at the wound site, deposit collagen and facilitate contracture of the newly formed matrix in order to approximate wound margins (2, 3). The initial phase of wound re-epithelialization involves activation of basal and suprabasal keratinocytes located at the wound edge, causing them to migrate beneath the dried out portion of edges in order to reform the epidermis (4, 5). The final stages of wound healing are the epithelialization and remodeling phases in which the granulation tissue is replaced with new-dermis, which is then matured and remodeled. The latter of these phases is crucial to control in regard to scarring.

When an injury is too large for the wound edges to be approximated, granulation and fibrous tissue formation comprises the wound bed until cells of papillary dermal (and mid dermal) appendages (hair follicles and sweat glands) migrate and rapidly proliferate to form a new epidermal layer. In the chronic wound this process is often hindered resulting in a hyperplastic epidermal tongue along the wound margin (pseudoeplitheliomatous hyperplasia) (6). Thus, surviving a large surface area injury to the skin depends heavily on the efficiency of an epidermal lining to be restored over the wound site (7). Keratinocytes are not only the main cellular component of the epidermis, but are also one of the major sources of cytokines and growth factors in healing process (8).

To encourage survival of cells that have either migrated from the wound margins or transplanted on the wound bed, a matrix or scaffold is required. In chronic wounds, oxidative stress, sheer stress and proteolytic enzymes can inhibit or retard the matrix deposition process (9). In an acute complicated injury, such as a burn, normal matrix deposition and epidermal repair are retarded, therein leading to contracture and scarring (10). Conversely in the case of a burn, there is an initial influx of matrix producing cells that exhibit prolonged matrix deposition, with reduced matrix remodeling together resulting in scar formation (10, 11). In diabetes, complicated etiology often leads to retarded matrix deposition, glycosylation of proteins, poor circulation and excessive inflammation that ultimately leads to a chronic wound (12, 13). Finally, in the elderly patient cellular senescence often leads to both impaired migration and matrix deposition, therein delaying wound closure of what otherwise would have been an acute wound (14-16).

Collagen (type I and III) are the two major matrix proteins found in the wound healing process, whereby collagen III is often replaced in part by collagen I over the natural course of late stage wound healing. Nonetheless, the right scaffolding (extracellular matrix (ECM)) is opportune to drastically accelerate wound healing, reducing scarring, and when combined with cell transplantation, can offer a means to deliver cells to the tissue as means of replacement. Initially a fibrin clot offers a temporary matrix in which fibroblasts can migrate within and remodel while depositing collagen. The greater the volume of tissue required to be regenerated through the wound healing process, the greater the length of time to heal, the greater the amount of matrix deposited, and thus, the greater likelihood of scarring and/or incomplete wound closure. Communication between dermal cells and epidermal cells is essential for homeostasis following wound healing, and the faster a matrix can be deposited within a wound, the sooner the epithelial tongue can migrate across (10, 17).

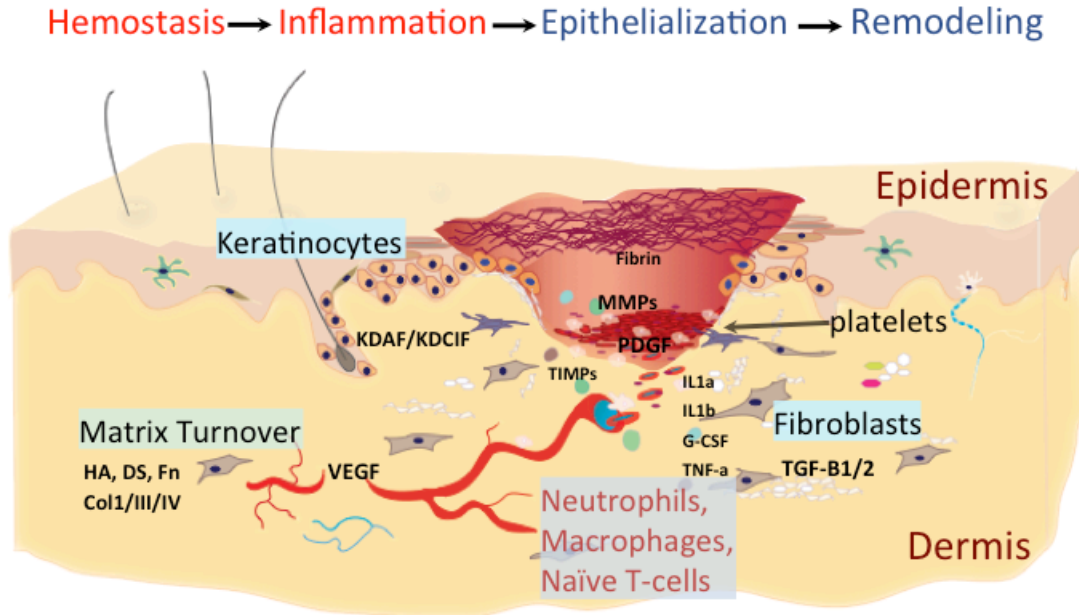


Figure 1.1. The stages of wound healing.

Cartoon schematic depicting the four stages of wound healing (top) commencing with hemostasis, cessation of bleeding, and transiting through an inflammatory phase (neutrophils initially followed by macrophages and T-cells) ending with remodeling of matrix proteins once the wound is closed. Core constituents of normal wound healing are cellular cross-talk between cells of the epidermis and dermis, the extent of the inflammatory response and the extracellular deposition/turnover of matrix.

1.2 Wound care background

The wound care market transcends age, nationality and demographic, and is one of the most costly segments in healthcare. Valued at roughly \$16 billion the worldwide market is expansive and innovative, despite the fact that complicated wound healing can lead to prolonged and recurring hospital stays, even amputations (15, 18-21). Major diseases such as obesity and diabetes, together with an aging population, are among the many driving forces behind the prevalence of complications in wound care. Normally acute wounds, typically with

little intervention, progress through the normal stages of wound healing. On the other hand, complicated wounds such as chronic wounds (ulcers) and burns may have retarded healing at the cellular level or be colonized with bioburden, and in either regard remain open. The longer a wound remains open the greater the chance of infection and scarring. For many patients who suffer from burns and chronic wounds such as diabetic ulcers, the use of autologous grafting is not an option due to either lack of skin or the high risk of generating another non-healing wound. Advanced wound care has for these reasons placed a tremendous amount of interest in developing biological wound coverage. One strategy for tissue repair and regeneration is the use of biomimetic scaffolds that foster the growth and development of a tissue toward restoring normal architecture. Many currently marketed scaffolds and dressings are solid, sheet-like materials. One major problem with solid (sheet) scaffolds is their inability to conform to wounds of varying shapes and sizes. Where injectable materials may be useful, current commercially available materials are weak in comparison to surrounding tissue. Nonetheless, with or without cells, injectable *in situ* gelling extracellular matrices are opportune to improve cell transplant and other surgical procedures if some of the major caveats can be resolved.

1.3 Advances in wound care

Numerous strategies have been employed to address chronic and complicated wounds. Pioneering approaches utilized cadaveric skin and semi-synthetic biomaterials such as Biobrane™ (a collagen-nylon based dressing). Cadaveric tissue offers biological wound coverage and a source of growth factors and nutrients, but the major pitfall is that the tissue is allogeneic and the cells are in some cases, already dead. Technological advancement has led to the creation of cultured epithelial auto and allografts, and then to engineered skin substitutes such as Apligraf® and Dermagraft®, both of which are a skin substitute containing cells. Supply chain logistics for these products is laborious and costly, perhaps leading to the fewer number of products containing cells when compared to acellular scaffolds and injectable matrix. Advanced wound care has

witnessed a large insurgence of biological, acellular scaffolds over the past 10 years, resulting in wound care's most rapidly growing segment (15, 18, 20). *Ideally, the best tissue repair therapy is an off-the-shelf, patient ready, and completely integrative, composite tissue replacement.* Moving toward the ideal therapy companies have developed products such as Stratagraft®, Apligraf®, Integra®, Dermagraft®, Oasis® and Lifecell®, all of which are variations of modern scaffold technology and have taken the approach of using sheet like materials (solid pre-formed constructs) (15, 18, 20). These sheet-based materials are indeed patient ready; however, they require time to integrate with surrounding tissue, where gaps may form and fill with biological fluids between the uniform scaffold surface and the uneven wound bed. Naturally gaps will impair cellular infiltration and neovascularization. On the other hand, Integra Lifesciences has commercialized a powdered version of their product, Integra® Flowable, which results in an opaque matrix that will form a gelled-slurry at room temperature (15, 18, 20). Albeit that the gelled-slurry is lacking the mechanical and architectural attributes of the sheet scaffolds, it can easily conform to the uneven and irregularity of the chronic wound. Finally, the third niche product group within advanced wound care, in addition to skin substitutes and injectable matrices, are growth factors. Despite the number of trials for products that target wound closure and scarring, the only successful growth factor therapy today is Regranex® (platelet derived growth factor (PDGF)), which is thought to stimulate granulation tissue formation and the recruitment and proliferation of cells in chronic wounds (22) (18).

1.4 Skin substitutes and polymer scaffolds

Numerous novel scaffolds that have been created at the research level have yet to make it to clinic. Tremendous efforts have been made to create nanofibrous scaffolds that exhibit superior uniformity, mechanical and physical characteristics over conventional methods. A large majority of these scaffolds utilize polymers such as gelatin, polyethylene glycol—*block*-epsilon-caprolactone), poly(lactic-co-glycolic acid) (PLGA), polylactic acid (PLA), polycaprolactone (PCL) and

variations of the same, as they are easily electrospun (23-34). Conventional methods of scaffold preparation typically have comprised various crosslinking methods to improve the mechanical properties of biopolymers collagen, hyaluronic acid, chondroitin sulfate and chitosan (15, 25, 33, 35-37). These scaffolds can therein be further modified with growth factors and gradients of polymer to permit the fabrication of a more bio-equivalent engineered tissue. The downside of many of these scaffolds is that they typically lack the heterogeneity of a complex tissue. De-cellularized matrix has become a popular option to preserve the appendages and architecture, yet still requires a lengthy preparation time from processing to cellular infiltration (38, 39). Where the lack of complex tissue architecture can be sacrificed for reduced fabrication time, scaffold integration with the surrounding tissue, and immediate cell infiltration (or integration via mixing) hydrogels stand to offer a promising solution (39-42).

1.5 Hydrogel-based scaffolds

Apart from bone, the majority of soft tissue comprises of a mix of collagens (predominantly type I), hyaluronic acid and sulfated-proteoglycans (i.e dermatan sulfate) that form amorphous hydrogel-like scaffolds. Hyaluronic acid is the largest and only non-sulfated glycosaminoglycan in the body. As with most biopolymers, collagen and hyaluronic acid both contain cell receptor motifs (structures) that can engage cell signaling pathways (43-48). Apart from the signaling motifs the hydrogel itself, structures that are formed provide a mechanical stimulus for cells (45). Soft hydrogel-like material is found in tissues such as the spinal cord, whereas harder (tougher) hydrogel-like material is found in the skin (49-51). In principle, a hydrogel is a network of partially insoluble polymers that retain fluid. The mechanics of the tissue scaffold are dependent on the composition of the biopolymer. For example, elastin is a hydrophobic protein that is a major constituent of skin providing elasticity, while collagen typically provides rigidity. Interestingly very few engineered scaffolds contain elastin, and those that do often combine it with another biopolymer (52). The formation of the neo-scaffold in the wound healing setting begins with a temporary, soft, nutrient

rich matrix (fibrin and type III collagen, also regarded as a blood-clot) that is over time degraded, replaced and remodeled into skin (12, 53). The initial matrix fills all the uneven pockets of the wound, stops bleeding and bridges the uninjured tissue so that stromal cells can begin the process of repair. Similarly, a tissue-engineered hydrogel permits the incorporation of cells (via mixing) and the ability for a structure to be created within a wound bed. This is particularly advantageous for the chronic wound. However, the caveat of most hydrogels is first and foremost strength and secondly application. For example, collagen and hyaluronan dermal fillers can easily and adequately fill spaces within a tissue, but are not able to form a contiguous solidified structure. The mechanical properties of a matrix material can have profound effects on cell physiology, which under a stress response could exacerbate scarring and inflammation (45). Ideally a hydrogel that could undergo solidification in situ would be ideal for several clinical modalities (54, 55). As described herein, a number of such scaffolds do exist; however in many cases encumber the unknown risks of using synthetic materials or, in the case of biopolymers, are not inert. It is for these reasons that we turned our attention to a simplified approach using collagen and polyvinyl alcohol. The hydrogel attributes of both polymers underscored their versatility in fabrication of scaffold, but more so that as a surfactant polyvinyl alcohol may possibly enhance the properties of collagen.

1.6 Collagen

Collagen is the most abundant protein in the human body. By weight, it comprises roughly 25% of all the protein in the body. Although it may play an obvious and essential structural need, its unique physical properties have demonstrated that it is constantly in a dynamic state as its melting temperature is 37°C. Collagen is a highly conserved protein. There are at least 28 isoforms, fibrillar and non-fibrillar, with the most common being Type I (56). Collagen production involves first the synthesis of pro-collagen into a right-handed triple helix structure that is later cleaved into its structural form outside of the cell (57). Figure 1.2 describes the collagen synthesis pathway, where it is first translated

into three left-handed helical polypeptide chains (two α -1 and one α -2). Together, the polypeptide trimer forms a right-handed triple helix. Collagen has a distinctly unique amino acid sequence of Gly-X-Y, where X is most often proline and Y is any other amino acid, but most often hydroxyproline (unique to collagen). The glycine and hydroxyproline content of collagen are thought to stabilize the triple helix structure. The thermal stability of collagen is thus driven by the amino acid sequence, wherein particular the glycine and hydroxyproline content heavily determine the thermal properties of collagen (58-60). The rise of the right handed atypical, triple helix, is 2.9Å per amino acid (versus 1.5Å for a typical α -helix)(57). Each turn corresponds to approximately 3.3 amino acids, and the span between glycine residues is nearly 1nm (57). Stability of a collagen triple helix is largely the result of the hydroxyproline and proline hydrogen bonding via water molecules (58, 59). In diseases such as Osteogenesis Imperfecta and other collage-like peptides, substitution of alanine for the glycine results in higher melting points and reduced fibrillogenesis in vivo (58).

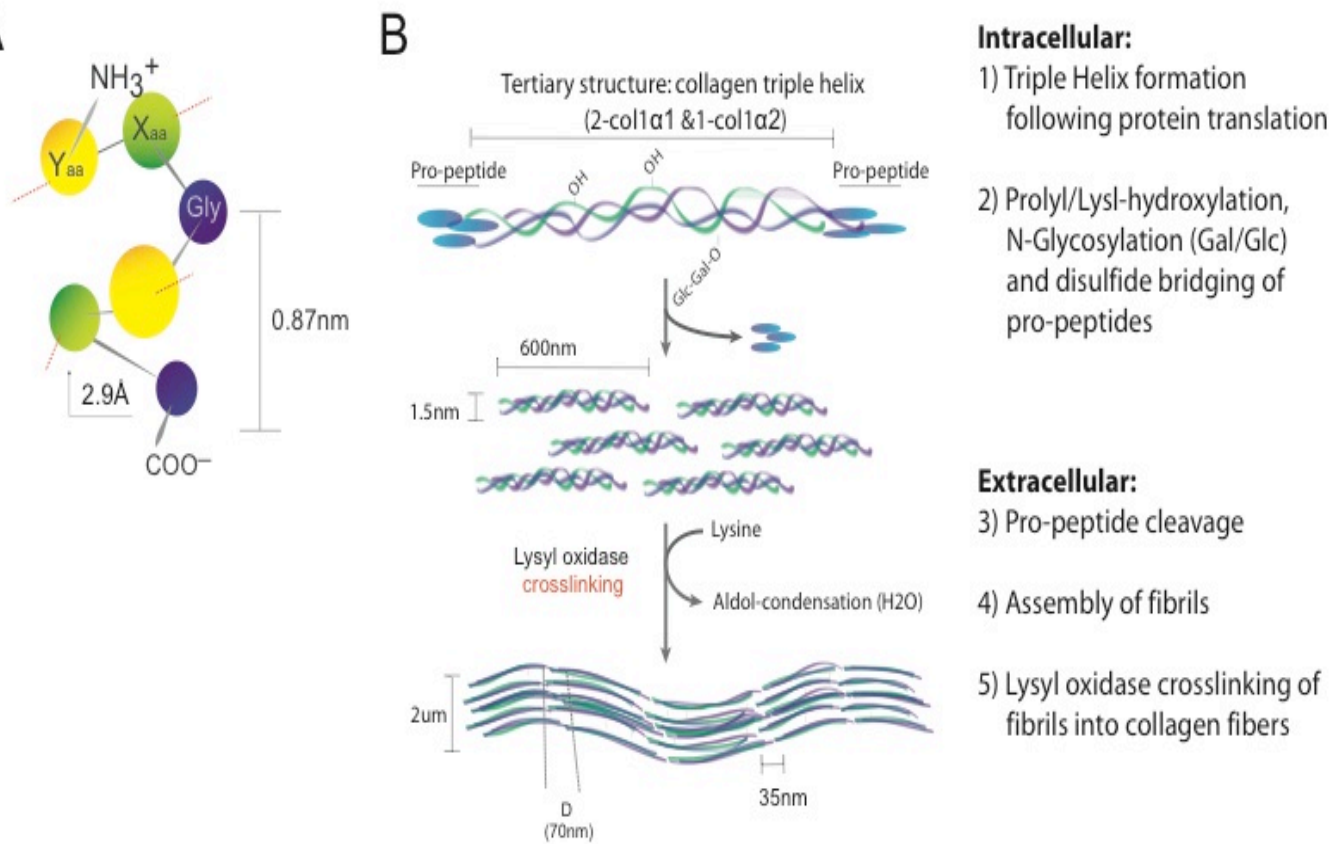


Figure 1.2. Collagen structure and synthesis¹.

(A) Cartoon ball and stick representation of primary alpha helix collagen sequence and structure. Typical sequence patterns for collagen are follow a Gly-Xaa-Yaa repeat, whereat Xaa is Proline and Yaa is Hydroxyproline, but may represent other amino acids. (B) Collagen synthesis begins at the endoplasmic reticulum, whereat collagen mRNA is translated. The protein of type 1 (fibrillar) collagen is formed through the favourable formation of a right-handed triple helix containing two alpha-one peptides and an alpha-two peptide. The trimer, tertiary structure, is then glycosylated and hydroxylated (prolyl hydroxylase and lysyl

¹ Adapted from Grisham, Biochemistry57. Grisham RHGaCM. Biochemistry. 3rd ed. CA, USA: Thomson Learning Inc.; 2005. 169-71 p.

hydroxylase) which requires the conversion of alpha ketoglutarate into succinate together with the co-factor ascorbic acid. The resultant tropocollagen is then released from the cell whereat the propeptide is cleaved. Cleaved collagen triple helix is roughly 300nm in length and 1.5nm in diameter. Gaps of approximately 40nm form between fibrous collagen helices, whereby sugars and glycoproteins collect and participate in collagen assembly (57). The helices are then, as a result of hydrogen bonding and solvation effects, assembled into fibrils where lysyl oxidase presence can easily convert lysines to reactive aldehyde-reactive-lysine, which through aldol condensation form crosslinks between and among triple helices. The pattern then forms fibers containing notable “D” domains that show shadow effect or banding of collagen superstructure and span roughly 70nm in distance (56, 57). The final fiber size of collagen is, on average on the order of 2-20 μ m in size (61).

Gelation of collagen has classically been measured through the turbidity of a soluble collagen gel solution. As fibrils form the solution becomes less translucent absorbing light at 313nm, eventually forming a gel (59, 60, 62, 63). The gelation curve in Figure 1.3 represents the gelation of collagen, through the formation of fibrils, as indicated by a change in solution turbidity and the impact of proteoglycans and glycosaminoglycans (GAG) on the gelation (fibrillation) kinetics. The time at $\frac{1}{2}$ maximum absorbance ($t_{1/2max}$) represents the gelation time, and the time from the start of gelation through to gelation represents the lag time (t_{lag}). Unless amino acid substitution occurs, collagen typically follows a curve with a delta max of 1 to 1.5 AU at 37°C. A typical scaffold should undergo gelation within 1 to 2h at concentrations of 2-3mg/ml without the addition of glycosaminoglycan, crosslinker or other additive, such as a surfactant. Conversely additives may reduce the rate at which gelation occurs, or even prevent it altogether. In his 2009 doctoral thesis, Li, Y. investigated the role of surfactants on the kinetics of collagen fibril formation (64). Therein he described that the surfactant sodium dodecyl sulfate (SDS) is able to reduce the gelation

time significantly. Moreover the surfactant markedly reduced the activation energy required for gelation. Unfortunately many surfactants, including SDS, are not suitable for human use. As with any protein, stability is often affected by changes in pH and temperature. Surfactants as biochemical agents are known to improve solubility and denature or alter the structure of proteins. Unique to collagen is that its denaturation leads, in some conditions, to a more stable-fibrous structure.

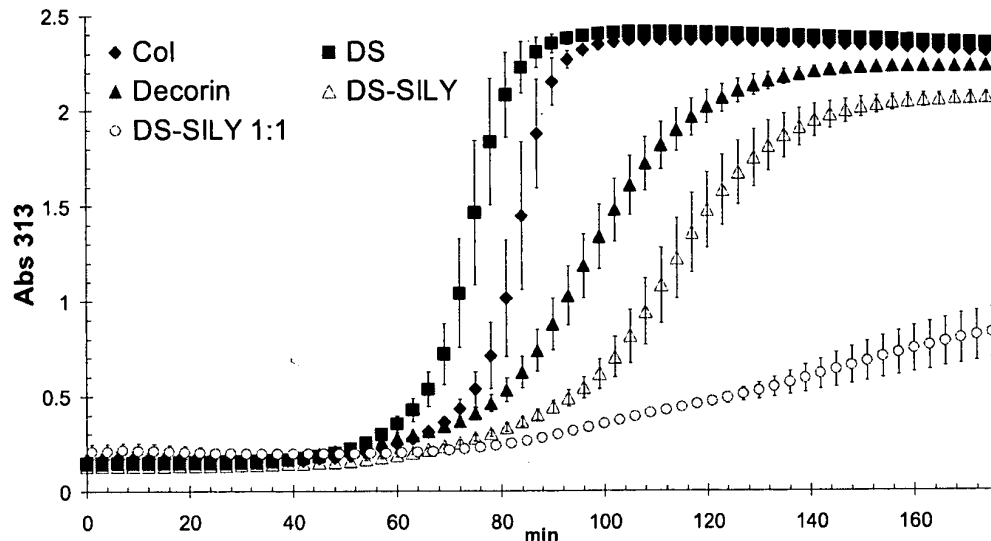


Figure 1.3. Turbidity measurement for collagen fibrillogenesis with differing dermatan sulfate treatments described by *Panitich et al.* in US patent number: US20110020298.

Gel solutions (50ul) of 4mg/ml collagen and additive were maintained at 4°C until turbidity measurements were obtained at 37°C. The figure demonstrates that the rate of collagen fibrillogenesis is enhanced by the proteoglycan dermatan sulfate (DS) when compared to collagen alone (Col) and collagen in the presence of decorin (a glycosaminoglycan, mucoadhesive protein) (63).

1.7 Polyvinyl alcohol (PVA)

Polyvinyl alcohol is a well-characterized, versatile polymer and surfactant. Depending upon the degree of acetate hydrolysis, polyvinyl alcohol is miscible with a wide range of solvents (65, 66). It is amphipathic, making it available to associate with hydrophobic and hydrophilic interfaces (67). The simple repeating carbon backbone and hydroxyl side groups permit a helical structure in water that is also known to function of a mild, non-ionic surfactant (68, 69). PVA is derived from vinyl acetate, following free radical polymerization of the vinyl functional group and hydrolysis of the acetate group. The degree of hydrolysis represents the extent to which the polymer chains are hydrolyzed from acetate. The more hydrolyzed derivatives are in fact slightly less soluble than the partially hydrolyzed structures. PVA is an approved excipient in pharmaceutical formulations, and often used for encapsulation. When combined with borate ions it readily forms a hydrogel, serving as a tackifying agent when the pH is at or above neutral pH by thickening a solution (67, 70, 71). As a biomimetic of hyaluronic acid, it can when crosslinked into a gel, serve similar hydrating and hydrogel functions without any known receptor/ligand interactions that can have adverse effects. As a non-sugar, homopolymer it is possibly less opportune to elicit immune reactions through the innate immune responses (i.e. complement) despite being known to bind with C5 found in plasma at statistically lower levels when compared with agarose and Zymosan A (72, 73).

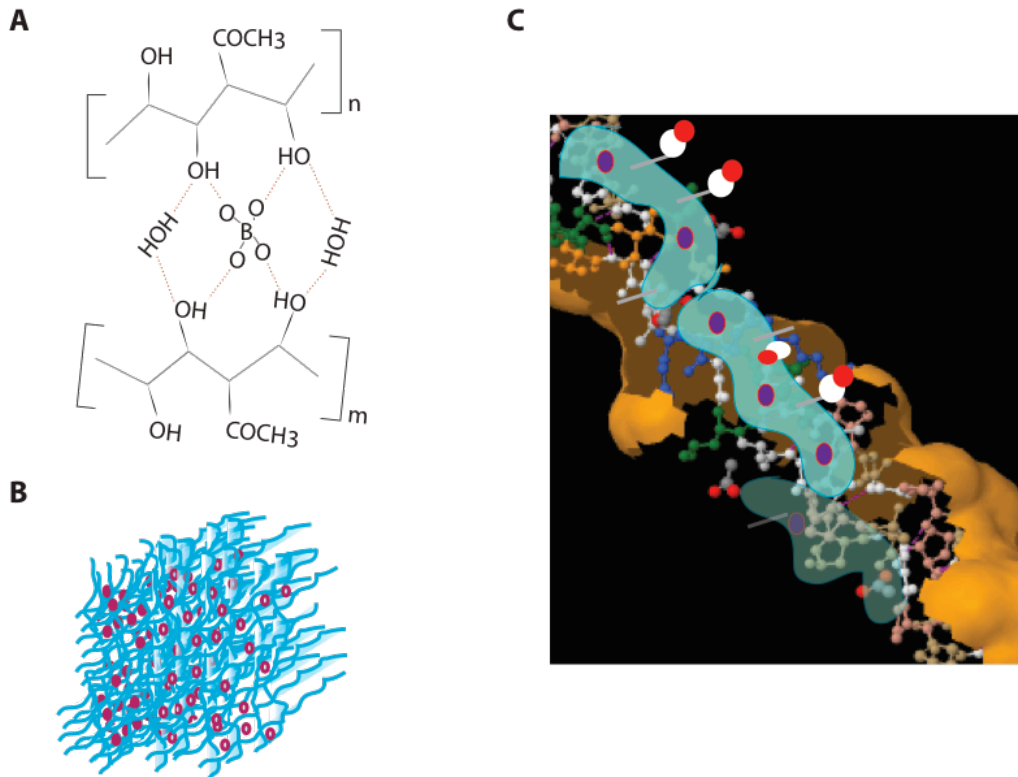


Figure 1.4. Structure and interactions of polyvinyl alcohol (PVA)².

(A) Structure and functional relationship of PVA with borate molecules (typically tetraborate decahydrate) at pH >7. (B) 3D hydrogel lattice representation of orthogonal crosslinking borate to PVA chains. Purple dots and blue chains represent borate and PVA respectively. (C) PDB image of a collagen triple helix, showing ball and stick structure and solvent surface (orange) (PDB1KBV). Proposed stabilization of the triple helix through PVA hydrogel interaction of non-solvated/solvated surfaces (blue) Hydroxyl functional group interaction with aqueous solvent is represented by red (hydrogen) and white (oxygen) balls.

² PDB1KBV RSCB Protein Data Bank ID reference for structure of triple helix found in panel "C" with modifications.

1.8 Hypothesis and objectives

Regardless of the source and site of trauma sequential biological mechanisms of repair, aim to prevent further damage and restore structure. Tissue structure, as a microenvironment, is integral for cell survival and *normal* physiology. As a result of numerous disease and trauma conditions such as burns, chronic wounds and transplantation there is inadequate structure within which cells can repair the tissue to its un-injured state. Hydrogels are a semi-solid structure that can easily integrate with the interface of a wounded tissue. Collagen, as a core physiological building block, is opportune for structural tissue repair, but in its native form lacks the physical properties required to rapidly form a tissue engineered scaffold *in-situ*. Although there are ways to circumvent this issue by extensively genetically or chemically modifying collagen, most of these solutions are not feasible for clinical translation. *My primary aim was to find a simple and commercially feasible alternative to conventional approaches.*

My general hypothesis is that a composite matrix comprising collagen and a semi-crosslinked PVA hydrogel would result in a material that could be easily stored and used to form an engineered skin within a wound bed, ultimately improving healing outcome and alleviating logistical challenges associated with currently available materials. The individual core objectives of this work are fourfold:

Objective 1 Develop and evaluate the chemistry, mechanics and functionality of a reconstitutable in situ forming scaffold in vitro;

Objective 2 Evaluate the efficacy of the scaffold to perform in vivo within a wound environment;

Objective 3 Evaluate methods to tailor the in situ forming scaffold to be used as a cell delivery vehicle to tissue engineering matrix that may satisfy other unmet research and medical needs;

Objective 4 Develop a prototype model product that could be ultimately translated to the clinic.

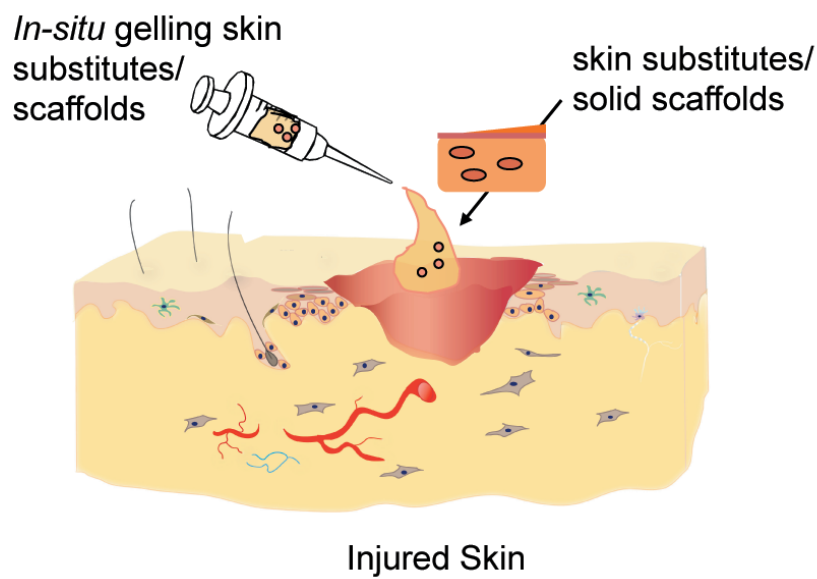


Figure 1.5. Cartoon representation of an in-situ forming skin substitute system either applied alone or in combination with pre-made skin substitutes in the solid form.

2 A novel hydrogel-collagen composite improves functionality of an injectable extracellular matrix

2.1 Introduction

The extracellular matrix (ECM) is a major determinant of cell survival, and ultimately organ function. Delivery and transplantation of cells is quickly becoming recognized as a feasible clinical strategy for the repair and regeneration of organs, in part because it offers a less invasive approach. Whereas the success of skin cell and pancreatic islet transplantation are quickly improving, clinical methods in muscle and nerve cell transplantation stand to benefit from the advent of tailored delivery systems that mimic ECM when formed *in situ* (54, 74, 75).

Improved vehicles for cell delivery and encapsulation have stemmed from principles in tissue engineering and drug delivery (54, 74, 76). Tissue engineering strategies often employ collagen and glycosaminoglycan (GAG) matrices as scaffolds to mimic tissue architecture. Simple crosslinking methods using either glutaraldehyde or 1-Ethyl-3-(3-dimethylaminopropyl) carbodiimide:N-hydroxy-succinimide (EDC:NHS) have been exhaustively investigated as ways to improve mechanical properties and stability (74, 77-80). These strategies are in most cases utilized to fabricate solid (dry) scaffolds, however, solid scaffolds have limited application in cell transplantation. Even as wound coverage, pre-formed solid scaffolds are unable to immediately integrate with the surrounding tissue. In this regard, a liquid matrix that would integrate with the surrounding tissue upon application would be advantageous. Furthermore, as a liquid, cells could be embedded prior to casting. This is particularly important for injectable cell transplants such as pancreatic islets (54, 81, 82). Unfortunately, the use of unmodified natural biomaterials has had limited success in producing useful injectable gels (74, 83). Encapsulation of cells within injectable synthetic mixtures of either pluronic acid, poly(ethylene glycol)-poly(caprolactone)-poly(ethylene glycol) (PEG-PCL-PEG), polylactic acid (PLA), and poly(lactic-co-glycolic acid) (PLGA) provide non-toxic, rapid gelling systems that can be modified to improve

stability, but often lack natural architecture when gelled *in situ* (74, 76). More recently *Fitzpatrick et al. (2010)* demonstrated the functionality of poly(N-isopropylacrylamide) (PNIPAAm)-collagen thermoreversible scaffolds for the delivery of retinal pigment epithelial (RPE) cells (84). However, as with other synthetic polymers, degradation of this material may expose the tissue to potentially cytotoxic products (74). In general, a major drawback with many new synthetic polymer systems is the length of time that is required to demonstrate safety and translate them to the clinic.

The development of an injectable ECM, using clinically approved polymers, which could mimic biological structures would be advantageous for a number of medical procedures including dermal reconstruction (as a filler), islet transplantation and as a skin graft for wound coverage. Polyvinyl alcohol is a well-known, clinically approved, synthetic analogue of hyaluronic acid (82, 85-87). It is an amphiphilic polymer that can be crosslinked to form a hydrogel in the presence of sodium borates at a $\text{pH} \geq 7$ and mechanically resembles soft tissues (86, 88-90). Generally, crosslinked PVA gels are isotropic and maintain a uniform shape that has shown to be useful for tissue engineering (91). In this regard, we hypothesized that the incorporation of PVA hydrogels within the collagen matrix would induce a faster fiber formation by aiding in both hydrogen bond formation, space-filling and nucleation of collagen fibrils within a restricted environment. Although it remains to be fully understood, PVA (at neutral pH) provides an unsuitable substrate for cell adhesion (90, 92). We also expected that the lack of cell adhesion would also restrict cell proliferation and contraction. In this study, we describe the preparation of an injectable collagen scaffold containing PVA-networks and evaluate its efficacy for use in tissue engineering and as an ECM for the application of skin cells.

2.2 Materials and methods

2.2.1 Collagen-glycosaminoglycan scaffolds

Three types of collagen-chondroitin sulfate scaffolds were prepared as reported by *Surronen et al.* with modifications (79). Briefly summarized in Table 2.1, rat tail collagen type I (BD, Canada) was neutralized with HEPES buffer and 1N NaOH to pH 7.0 and combined with chondroitin-6-sulfate (1:5 w/w). Crosslinked gels were prepared by crosslinking for 2 hours in the dark with 0.02%w/v glutaraldehyde. A 2 hour glycine wash was performed to deactivate remaining aldehyde groups. PVA composites were prepared by adding a mixture of 5%w/w PVA (Alfa Aesar, Ma, USA) in 10X DMEM (GIBCO, Ontario, Canada) pH 7.5 (2.5%w/w PVA 86, 2.5% PVA 99, 1% glycerol (Alfa Aesar, Ma, USA)) to 0.0625M sodium tetraborodecahydrate (Sigma, Ontario, Canada) pH 8.0 (final concentration 0.05%w/w sodium tetraborodecahydrate, 0.2%w/v PVA). PVA mixtures were combined with glycine-washed crosslinked scaffolds and allowed to settle overnight at 4°C prior to use. Sodium ascorbate (ascorbate) (in filtered water pH 7.0) was added to each scaffold to a final concentration of 100µM. Crosslinked scaffolds not containing PVA were prepared by adding sodium borate and ascorbate to the scaffold mixture following the glycine wash. Ascorbate was added to the non-crosslinked scaffolds during initial preparation. All scaffolds were prepared at the same time to a final collagen concentration of 3mg/ml. Prepared liquid composites were stored at 4°C and used within 1 week.

Table 2.1 Scaffold formulation

	Col	xCol	xCol HG
Collagen	3 mg/ml	3 mg/ml	3 mg/ml
Chondroitin-Sulfate (in 1x PBS)	15 mg/ml	15 mg/ml	15 mg/ml
Glutaraldehyde / Glycine	No	Yes	Yes
PVA (pH 7.0)	No	No	0.2%w/v
Sodium Borate decahydrate (pH 8)	0	0.05%w/v	0.05%w/v
Sodium Ascorbate (pH 7.0)	100 μ M	100 μ M	100 μ M

2.2.2 Cell populated scaffolds

Primary keratinocytes and fibroblasts were isolated from human neonatal foreskin that were obtained from consenting donors in accordance with the ethical guidelines set forth by the University of British Columbia. Briefly, keratinocytes were isolated from the epidermis following enzymatic digestion using 1x Trypsin:EDTA (Gibco, Ontario, Canada) and Dispase (Gibco, Ontario, Canada). Fibroblasts were isolated from sections of dermis cultured in 1x DMEM (10% FBS and 1% Penicillin, Streptomycin and Amphotericin B) (Gibco, Ontario, Canada). Fibroblast populated scaffolds were established at a density of 200,000 - 250,000 cells/ml with the exception of the proliferation assay which used 100,000 cells/ml. Cell numbers were counted using a hemocytometer and combined with the liquid matrix in a suspension equivalent to 10% of the final gel volume producing a collagen gel of 3mg/ml. Other cell numbers were as follows: Primary keratinocytes 10⁶/ml, Baby Hamster Kidney cells (BHK) 5 x 10⁵/ml,

HaCat's 10^6 /ml. Cells were cultured for 1 hour at 37°C prior to the addition of fresh media (200-300 μ l) specific to cell type: Keratinocytes (KSFM; Gibco, Ontario, Canada), BHK (DMEM:F12; Gibco, Ontario, Canada).

2.2.3 Cell viability and morphology

Viability was assessed using Live/Dead toxicity assay (Molecular Probes, Gibco, USA). Cells (primary or cell line) were cultured for 24 hours in or on top of scaffolds (fibroblasts and BHK cultured within and keratinocytes and HaCat's on top). After 24 hours, scaffolds containing cells were washed 3 times with 1x PBS (pH 7.0) and a mixture of ethidium-homodimer and calcein-AM according to manufacture's instructions. After 30min scaffolds were washed 3 times with 1x PBS and visualized using a Zeiss Axiovert 200M fluorescence microscope and Axiovision software. Cell counts were obtained using Image J software (NIH, USA). Cell morphology was visualized using a wheat germ agglutinin conjugated AlexaFluor 488 (Invitrogen, Canada) membrane staining of fibroblasts seeded in the collagen scaffolds 24 hours after casting. Images were captured using a Zeiss Axiovert 200M fluorescence microscope and Axiovision software.

2.2.4 Cellularity

Primary human fibroblasts were grown in 200 μ l volume scaffolds (uncrosslinked (Col), crosslinked (xCol), crosslinked with PVA (xColHG)) for a period of 10 days. Briefly, gels were prepared as described above and 100,000 cells/ml of gel were combined with the liquid matrix resulting in 20,000 cells total per scaffold. To confirm cell totals at time 0 gels were digested with collagenase (Sigma, USA) 1U/mL and cells were subsequently counted using Trypan blue to ensure similarity (data not shown). Fibroblasts were then grown for 10 days with gel harvest at days 2, 6 and 10. Culture media was changed every 48 hours. Gels were removed from wells and fixed in 4% w/v paraformaldehyde (Sigma, USA) for 24 hours at 4°C. Gels were then transferred to 70% ethanol and prepared for paraffin embedding. Six cross-sections (5 μ m) per gel obtained from 3-batches of

gel were de-waxed and stained with DAPI nuclear stain (Vector Labs, Ontario, Canada). Cell counts (per low power field) were obtained using Zeiss Axioplan 2 upright fluorescence microscope.

2.2.5 Time to fibril formation

The time it took for collagen gels to form fibers was used to indicate of casting time. Gels were prepared as described previously. Initial simple inverted test tube assays, as described previously (83), were used to estimate casting time during formulation (data not shown). Chilled gel resins (100 μ l) were aliquoted into 96 well plates (Corning, USA). DMEM containing 10% FBS and 1% Penicillin/streptomycin was used as a blank. Gel resins were chilled on ice until the absorbance measurements were taken as described previously (93, 94). Absorbance at 313nm was recorded every 60s over a 1 hour period at 35°C demonstrating the rate of collagen fiber formation.

2.2.6 Mechanical strength

Gels were cast in 5-well rectangular chamber slides (500 μ l each) and incubated for 24 hours at 37°C. Tensile testing was done using a KES-G1 Micro-Tensile Tester (Kato Tech, Japan), with a 1kg load cell. Prior to loading, gels were dried of excess liquid using KimWipes™ (Kimberly Clark, USA) and weighed. Two pieces of KimWipe™ were then used to firmly secure the gel onto the specimen holder. Gels were then stretched until breaking at a deformation rate of 0.02 cm/s. Tensile strength was calculated by dividing breaking load (g) with sample width (mm) and area density (g.sq.m) of the polymerized gels. For statistical purposes, six batches of gels were evaluated.

2.2.7 Differential scanning calorimetry (DSC) and scanning electron microscopy (SEM)

The same preparation procedure was used to prepare samples for both DSC and SEM, except that gels were not fixed for DSC analysis. Collagen scaffolds

(100µl) were cast in 96 well plates for 24 hours followed by fixation in 4% Formalin solution for 24 hours at 4°C. After fixation the gels were dehydrated twice for 12h in 70% ethanol and then frozen at -80°C prior to lyophilization. Lyophilized scaffolds were then weighed and evaluated on a Q1000 Differential Scanning Calorimeter (TA Instruments, USA) at 5°C/min within a range of 20°C to 100°C. SEM samples were first gold coated prior to loading inside the vacuum of a Hitachi S-3000N SEM (Hitachi, Japan).

2.2.8 Gel contraction

Primary fibroblasts were populated within each of three collagen gels: Col, xCol and xColHG which were prepared as described previously and cultured at 37°C. Cell media (DMEM containing 10% FBS and 1% antibiotics) was changed daily. Fibroblast populated collagen gels (250,000 cells/ml) were released from the plate walls 24 hours after gel casting (on day 0) and allowed to contract. Images were taken on days 1, 3, 5, 7 and 10 using a Sony CyberShot H9 digital camera at a standardized range. Gel size was measured using Image J (NIH, USA).

2.2.9 Collagenase digestion

Collagen gels (100µl) were cast in 96 well plates as described previously. Each gel was placed into 20µl of 1x PBS (pH 7.0) containing 0.3U of *Closteridium* Serine Peptidase A (CLSPA) purified from *Clostridium Histolyticum* (Worthington, USA). The mixture was then incubated at 37°C for either 1, 2, 6, 12 or 24 hours to determine the optimal ratio of gel digestion (data not shown). Hydroxyproline measurements were carried out on digested samples (supernatant and pellets). Following digestion gels were centrifuged 3 times at 15,000x g for 10 minutes at 4°C with 1x PBS wash. The supernatants were separated from the pellet and recombined with 200µl of concentrated hydrochloric acid (HCl) for a final concentration of 6N. The hydroxyproline analysis was as preformed as described previously (95) with minor modifications. Briefly, digested pellets were washed 3 times with PBS prior to adding concentrated HCl. Both pellets and supernatants

were hydrolyzed for 16 hours using 6N HCl. Hydroxyproline concentrations were obtained by reading OD at 550nm.

2.2.10 Bi-layered skin substitute

Collagen gel scaffolds were prepared as described previously. Primary human fibroblasts were combined with the liquid matrix at 200,000 cells/mL prior to casting in Transwell™ permeable supports (Corning, USA). Fibroblasts-populated gels were then incubated for 48 hours at 37°C in DMEM containing 10% FBS and 1% antibiotic (Gibco, USA). Primary human keratinocytes were cultured until 60% confluent in KSFM containing Bovine Pituitary Extract (BPE), Epidermal Growth Factor (EGF) and 1% antibiotic (Gibco, USA). After 48 hours, keratinocytes (1×10^6 cells) were seeded on top of cultured gel scaffolds and the media was changed to 49%DMEM, 49% KSFM and 1% FBS, and 1% antibiotic (50/50 media) as previously described (37). Media was changed after 24 hours and after 36 hours the gels were raised to the liquid air interface in order to differentiate keratinocytes. The gels were cultured in the Transwell™ (with a dry surface) for 10 days (5% CO₂) with 50/50 media containing 100µM ascorbic acid. Media was changed daily. After 10 days the bi-layered skin substitutes were removed from the Transwell™ and cast in a 1% agar gel. The gel was then fixed in 4% formalin for 24 hours. Paraffin embedded sections (5µm) were stained with hematoxylin and eosin (H&E) and images were captured using a Zeiss Axioplan 2 (Carl-Zeiss, Ontario, Canada) upright microscope.

2.2.11 Statistics

The number of repeats represents different batches of gels. Experimental results were evaluated using Analysis of Variance (ANOVA) with a post-hoc Tukey Test. Statistical significance was estimated with an alpha value ≤ 0.05 . Measurements were reported as means \pm standard deviation.

2.3 Results

2.3.1 Casting time

Two key characteristics of an injectable ECM are rapid gelation and immobilization of cells. Our goal is to create a system that could be applied through injection or topically within a working window of 15 minutes prior to solidification. Fibril formation *in vitro*, through entanglement of the collagen coiled-coiled structure, is the final step of collagen gelation. As such, acellular liquid collagen solutions either uncrosslinked (Col, figure 2.1. panel A), crosslinked (xCol, figure 2.1. panel B) or crosslinked containing PVA-borate hydrogels (xColHG, figure 2.1. panel C) were evaluated for their rate of fibril formation. Time to fibril formation is calculated by the time to half max absorbance at 313nm. The lag time (t_{lag}) is described as the time difference between the time at A_i and the time at the intersect between the slope (dA/dt) and the initial baseline absorbance (A_i) (93), represented by the following equation:

$$t_{lag} = ((A_i) - b)/(dA/dt), \text{ where } b \text{ is the intercept of the line } (dA/dt).$$

Results shown in Figure 2.1 (Panel D) suggest that PVA-borate gels (xColHG) require less than half the time to form ($p < 0.001$) and with a reduced lag time to initiate fibril formation compared to other gels ($p < 0.001$). The time to initiate fibril formation when heated from 4°C to 37°C is 13.65 minutes (819.1s \pm 153.7), where fibrils are formed at 16.3 minutes (978s \pm 268.4). Although both crosslinked gels with and without PVA-borate undergo shorter transitions to complete fibril formation, both the lag time and the time to half maximum absorbance for crosslinked gels without PVA-borate (1556.6s \pm 203.9 and 2096 \pm 196.4) were not significantly different from uncrosslinked collagen gels (1589.2 \pm 186.9 and 1920 \pm 128.6).

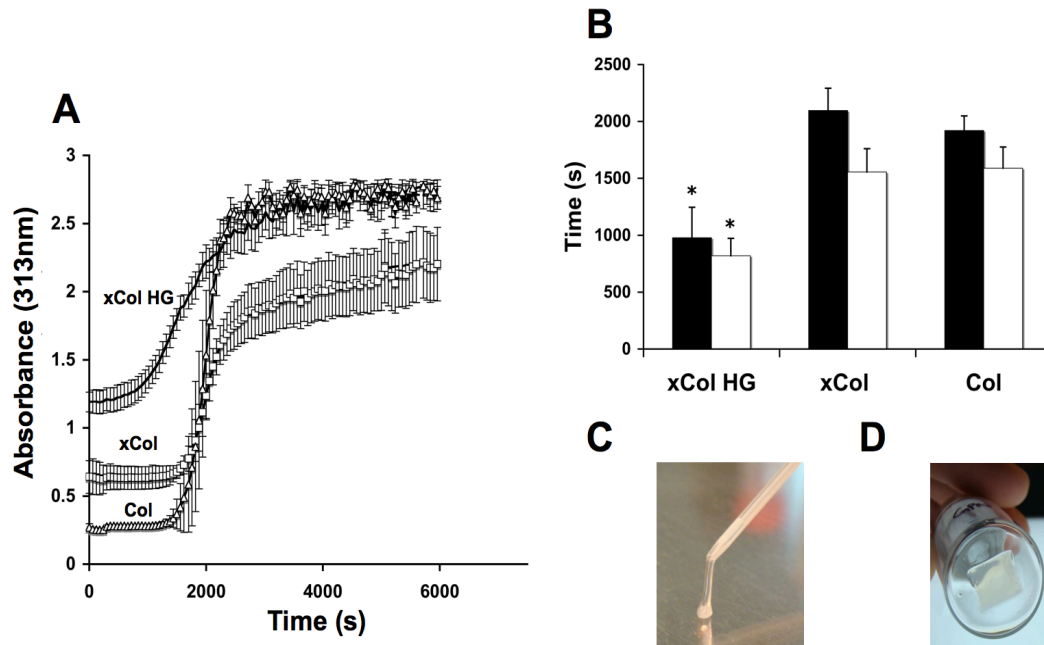


Figure 2.1. Time to fibril formation and gelation of collagen-GAG scaffolds.

(A-B) Three collagen gels: collagen-GAG (Col), crosslinked collagen-GAG (xCol) and crosslinked collagen-GAG containing PVA-borate networks (xCol HG) were prepared on ice and maintained at 4°C. To measure turbidity and rate of fibril formation gels were incubated from 4°C to 37°C and absorbance was measured every 30s at 313nm. DMEM (cell media), DMEM with borate and DMEM containing PVA-borate were used as respective blanks. (A) Turbidity shift of collagen scaffolds. (B) Time to fibril formation ($t_{1/2max}$ absorbance) (solid bars) and Lag time to initiate fibril formation (open bars). (C) Ejected xCol HG scaffold after casting in catheter tube at 37°C for 7 min. (D) xCol HG scaffold after casting in rectangular tray at 37°C. (n=9, $p < 0.05$) * $p < 0.05$

2.3.2 Mechanical strength

Matrix strength is integral in predicting functionality of an engineered tissue. Although it is well known that crosslinking of collagen increases matrix strength, we were interested to whether the addition of PVA-borate networks at a dilute concentration had any effect on the tensile properties of the matrix. Stress/Strain curves of collagen gels, shown in Figure 2.2 panels A-C, depict good agreement among different batches and are consistent with previous findings [9, 26]. Results demonstrate that maximum strain at break was statistically similar among uncrosslinked ($8.4\% \pm 1.2\%$), crosslinked ($12.5\% \pm 7.02\%$) and crosslinked with PVA-borate ($8.0\% \pm 1.3\%$) systems. However the Young's modulus (Y' ($\Delta\text{stress}/\Delta\text{strain}$)) of the crosslinked collagen containing PVA-borate ($1.414 \pm 0.5015\text{MPa}$) was significantly greater than that of the crosslinked collagen ($p=0.03$) and uncrosslinked collagen ($p<0.001$). Furthermore, the maximum stress at break was also significantly greater in the xCol HG ($0.074 \pm 0.0498\text{N/m}^2$) system compared to uncrosslinked collagen ($0.014 \pm 0.0056\text{N/m}^2$, $p=0.01$).

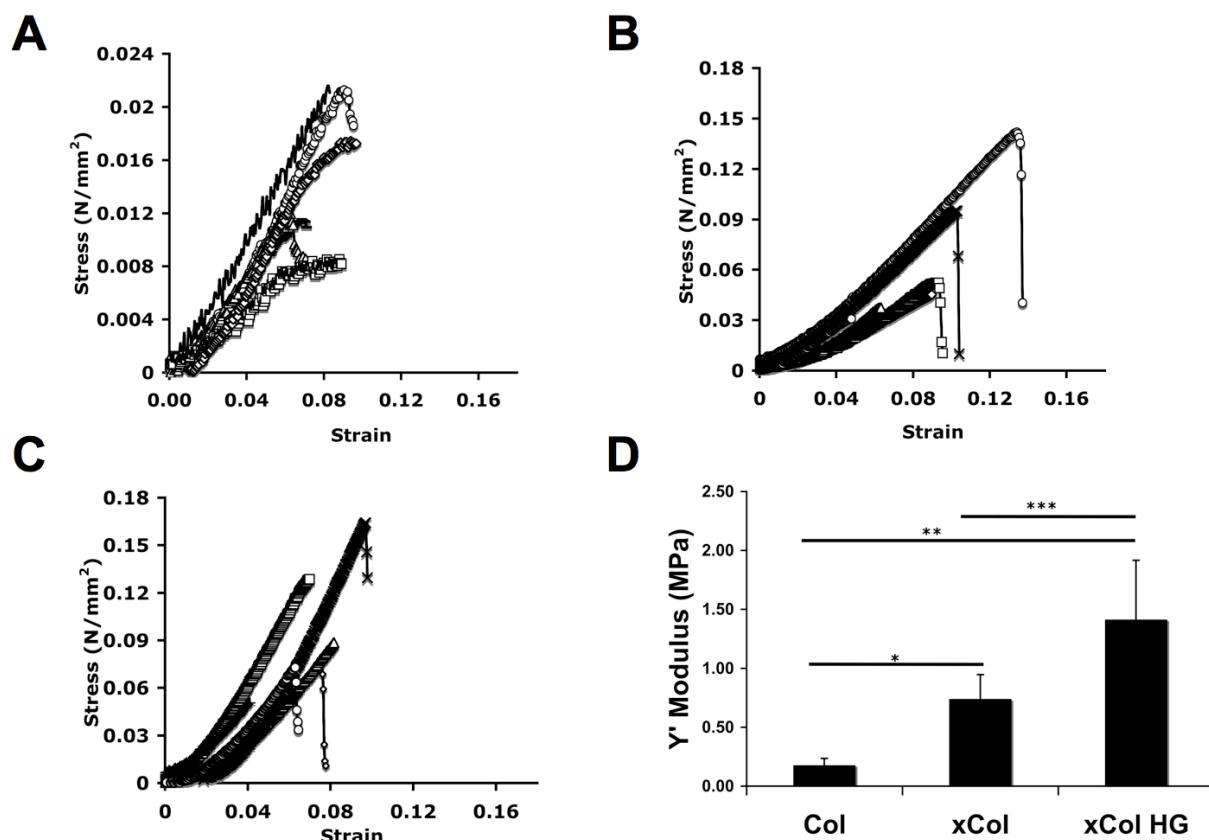


Figure 2.2. Mechanical properties of hydrated collagen-GAG gels.

Three collagen gels: collagen-GAG (Col), crosslinked collagen-GAG (xCol) and crosslinked collagen-GAG containing PVA-borate networks (xCol HG) were cast in 500 μ l rectangular wells at 37°C for 24 hours prior to testing. Following incubation gels were weighed and loaded on the tensile mounts. Gels were then stretched until breakpoint at a rate of 0.1cm/s. The results represent six different batches of gel. Young's modulus (Y), as one indicator of mechanical strength, was measured as the slope of the stress/strain curve (σ/ϵ) using engineering stress (force/ unit area density). (A-C) Stress vs. Strain curves for six different trials of each collagen scaffold: (A) Col, (B) xCol and (C) xCol HG. (D) Average Young's modulus for six batches of collagen scaffold. The error is represented as standard deviation. ($p < 0.05$) * $p = 0.03$, ** $p < 0.001$, *** $p = 0.01$.

2.3.3 Cell viability and morphology

Although glutaraldehyde crosslinked collagen matrices have been used and studied extensively, it was essential to determine if the PVA-borate systems exhibited toxicity. As there is potential for this scaffold to be used as a cell delivery matrix, as wound coverage or injection, we assessed and compared toxicity across a range of cell lines and primary cells. As shown in Figure 2.3, primary human fibroblasts and keratinocytes, two key cellular components of skin exhibited $86\pm 12\%$ and $78.8\pm 3.2\%$ viability respectively when cultured in or on the xCol HG composite. Similarly, BHK cells and HaCat cell lines remained $79.6\pm 9.7\%$ and $84.8\pm 4\%$ viable when cultured on the xCol HG composite scaffolds. With the exception of primary human keratinocytes, this viability for crosslinked scaffolds was similar to uncrosslinked scaffolds. Primary human keratinocytes cultured on either crosslinked scaffold were on average 12% less viable ($p < 0.001$) than those cultured on uncrosslinked collagen. Morphology of fibroblasts cultured inside the xCol HG gels for 24 hours (Figure 2.3, C) displayed a linear pattern compared to those cultured in either uncrosslinked or crosslinked collagen gels. Interestingly cell spreading in both uncrosslinked and crosslinked gels was random where as in xCol HG gels appeared to be uni-directional relative to a given location (i.e. plane) in the scaffold.

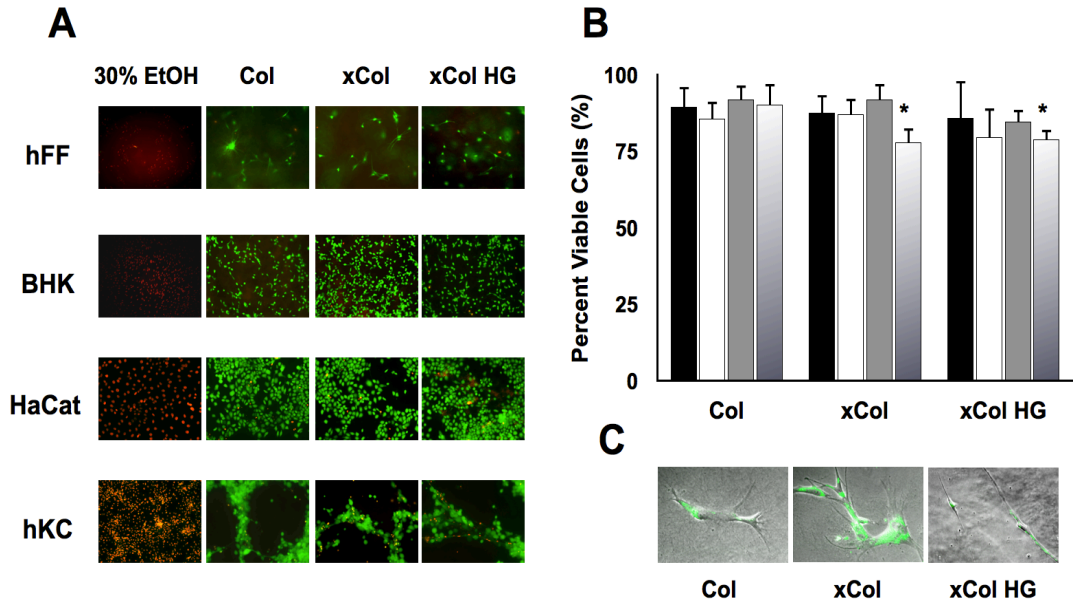


Figure 2.3. Viability and morphology of cells cultured in or on collagen-GAG scaffolds.

Three collagen gels: collagen-GAG (Col), crosslinked collagen-GAG (xCol) and crosslinked collagen-GAG containing PVA-borate networks (xCol HG) were prepared at 4°C. (A-B) Primary human fibroblasts (hFF, solid bars); baby hamster kidney cells, an epithelial cell line (BHK, open bars); immortalized human keratinocyte cell line (HaCat, grey bars); and primary human keratinocytes (hKC, gradient bar) were evaluated for viability after 24 hours on each of the different scaffolds. HaCat, hKC and BHK were all cultured on top of the collagen scaffolds, where hFF were cultured within. Cells were stained with a mixture of Calcein AM (green- viable) and Ethidium-homodimer (red- dead) to indicate cytotoxicity of the scaffolds. 30% Ethanol was used as a negative control. Cell numbers were obtained from low powered field images Axiovision lite software. Cell numbers and standard deviation reflect the entire of population of cells in triplicate (3 batches of gels). (C) Phase-contrast micrograph of fibroblasts within xCol HG gels. Fibroblasts were pre-treated with a fluorescent-n-glutenin membrane label (green) to depict cell morphology and surface area inside the casted scaffold after 24 hours. (n=3, p<0.05) *p=0.045

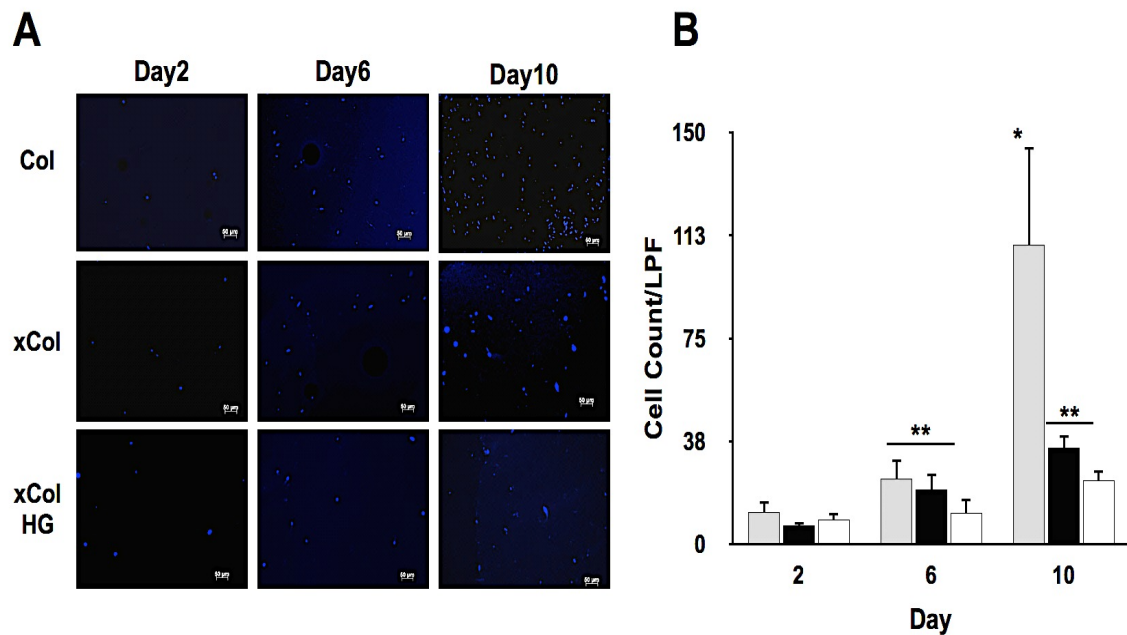


Figure 2.4. Fibroblast cellularity when cultured within collagen-GAG scaffolds over a 10-day period.

Again, three collagen gels: collagen-GAG (Col, grey bar), crosslinked collagen-GAG (xCol, closed bar) and crosslinked collagen-GAG containing PVA-borate networks (xCol HG, open bar) were prepared at 4°C. Primary fibroblasts were incorporated within the gel-resin prior to casting at 37°C. Gels were, washed and fixed in 4% paraformaldehyde for 12 hours prior to paraffin embedding on days 2, 6 and 10. Sections were de-waxed and stained with DAPI nuclear stain in order to count total cell numbers per low powered field (LPF). Six sections were counted from 3 different batches of gels. (A) Representative low power images of DAPI stained gel sections. (B) Average cellularity of scaffolds on days 2, 6 and 10. (n=3, p<0.05) *p=0.01, **p<0.001 (scale bar = 50mM)

2.3.4 Cellularity

High cellularity is a marker of tissue fibrosis. Control of fibroblast proliferation can be beneficial to reduce the degree of post-wound scarring and capsular contracture around implanted materials. It has been established that cells grown in a collagen gel (3D) exhibit reduced cellularity than those cultured on a plate surface (2D). In order to evaluate cellularity in these collagen systems, paraffin embedded gels were sectioned and analyzed under fluorescence microscopy using a low powered field (LPF). Results in Figure 2.4, panel B describe a marked increase in cellularity from day 6 to day 10 in uncrosslinked scaffolds. As of Day 10 xCol HG scaffolds have appreciably 5 fold less cells/LPF ($p < 0.001$) compared to uncrosslinked collagen-GAG gels. Furthermore, the addition of PVA-borate hydrogels to the scaffold significantly reduces cellularity (23 cells/LPF ± 4) compared to the xCol gels (35 cells/LPF ± 5 , $p < 0.001$).

2.3.5 Resistance to contraction

Hallmark determinants of contracture are high cellularity and reduction in gel strength (96). In order to evaluate if the xCol HG could mitigate cell-mediated contraction, casted gels were released from the plate surface and the surface area was measured daily over 10 days. As shown in Figure 2.5, panel A uncrosslinked collagen gels rapidly undergo contraction to nearly half the original size within 1 day of being released from the plate surface ($p < 0.001$). Both crosslinked gels are able to mitigate contraction over a 3 day period (above 75% original size), where following day 3 the xCol scaffolds significantly reduce in size (day 5 $p < 0.0001$; day 7 $p = 0.004$; day 10 $p < 0.0001$) relative to the xCol HG. On day 5 uncrosslinked scaffolds have reduced to near their minimum size at 25% $\pm 6\%$ of their original surface area, whereas xCol HG scaffolds retain 91% $\pm 5\%$ (Figure 2.5, panel B). Furthermore by day 10 the xCol HG are able to resist contracture by 57% $\pm 7.2\%$ compared to xCol scaffolds at 38% $\pm 9.6\%$ ($p < 0.001$).

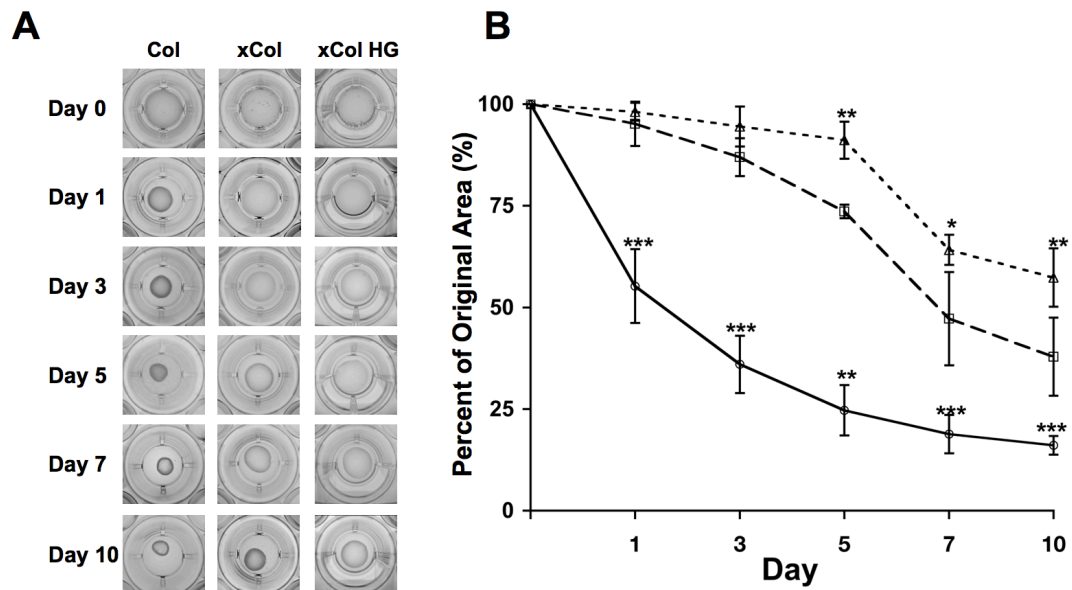


Figure 2.5. Contraction of free-floating fibroblast populated collagen-GAG scaffolds (FFPC).

Primary fibroblasts were cultured within each of three collagen gels: collagen-GAG (Col, open circle), crosslinked collagen-GAG (xCol, open square) and crosslinked collagen-GAG containing PVA-borate networks (xCol HG, open triangle) and cultured at 37°C. Cell media (DMEM containing 10x FBS and 1x antibiotics) was changed daily. FFPC's were released from the plate walls on day 0 and allowed to float. (A) Contraction images of FFPC's over the course of 10 days. (B) Resistance to gel contraction as marked by the percent of original gel on day 1, 3, 5, 7 or 10 where day 1 represents 24 hours following release of the scaffold from the plate walls. (n=3 batches of gel, $p < 0.05$) *** $p < 0.001$, ** $p < 0.01$, * $p < 0.05$

2.3.6 Thermal stability

Thermal stability and heat capacity is not only important for 'shelf-life' but also as an indicator of molecular bonding. Separately, it has been established that PVA and collagen exhibit distinct thermal properties, and that a combination of these polymers can produce enhanced effects (87). Lyophilized collagen gels were evaluated using DSC at a rate of 5°C/min. Representative DSC isotherms found in Figure 2.6 (panels A-C) show that crosslinking of collagen eliminates the glass transition observed with uncrosslinked collagen. The heat loss by crosslinked collagen (figure 2.6, panel B) is much greater than uncrosslinked collagen approaching its crystallization point at 90°C (consistent with both scaffolds). However, the addition of PVA-borate (figure 2.6, panel C) (even at 0.2%) distinctly changes the isotherm of the crosslinked scaffold (Figure 6, panel B). The heat capacity is notably increased at a T_g (glass transition temperature) of 30°C through to a second peak at 45°C in the xCol HG with no evident sign of crystallization at temperatures under 100°C (figure 2.6, panel C). It is known that PVA has a T_g of 85°C, which may explain the slight change in heat flow at around 90°C (97). The homogeneity of the heat flow curve does suggest that the addition of the PVA-borate hydrogel produces a stable polymer network.

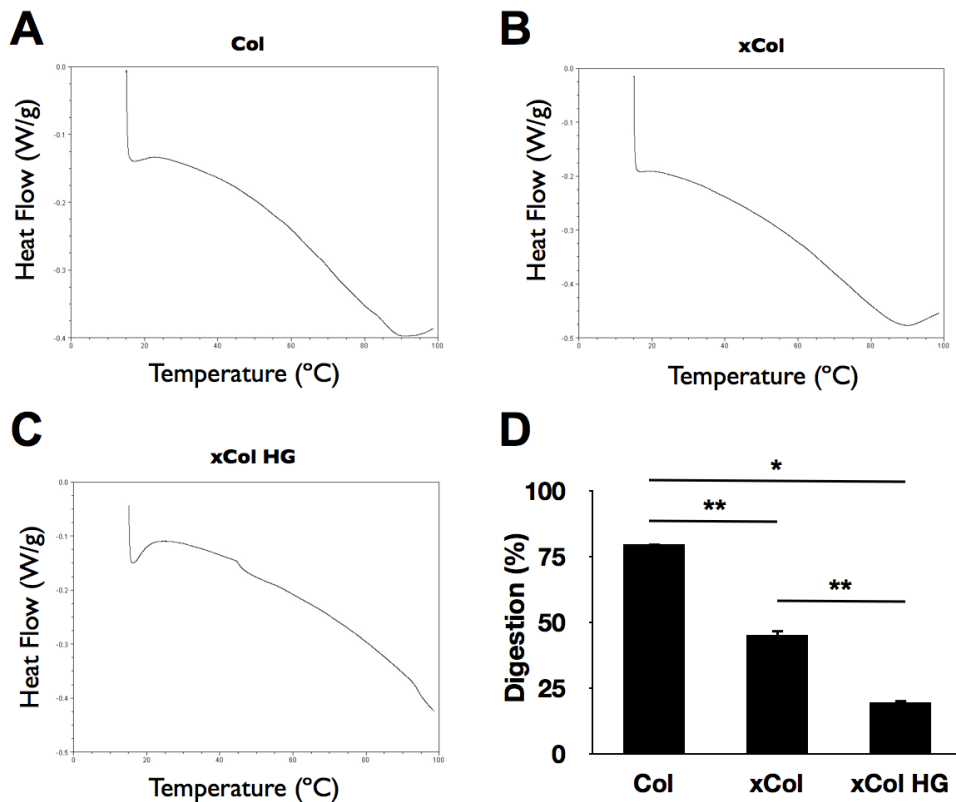


Figure 2.6. Thermal and enzymatic stability of collagen-GAG scaffolds.

Three collagen gels: collagen-GAG (Col), crosslinked collagen-GAG (xCol) and crosslinked collagen-GAG containing PVA-borate networks (xCol HG) were prepared at 4°C and cast at 37°C. (A-C) Differential scanning isotherms representative of different lyophilized scaffolds. Temperature was raised at 5°C/min, within a range of 20°C – 100°C. (D) Hydroxyproline content of digested supernatant calculated as percent of the total gel content. (n=3, p<0.05) **p=0.01, *p<0.001

2.3.7 Resistance to enzyme degradation

It has been previously established that the level of matrix metalloproteinases (MMP's), matrix degrading enzymes, increases when fibroblasts are cultured within a collagen gel. In order to investigate if the addition of PVA-borate hydrogels to the scaffold could mitigate enzymatic degradation, acellular gels

were incubated in the presence of pure collagenase (CLSPA) for 24 hours. Results were quantified by measuring the hydroxyproline content, where $80 \pm 0.4\%$ ($p < 0.001$) of the uncrosslinked collagen was digested (figure 2.6, panel D). Interestingly, evident by hydroxyproline content, PVA-borate hydrogels exhibited a reduced degradation ($19.5 \pm 1\%$) compared to those of both crosslinked ($45.2 \pm 2\%$) and uncrosslinked collagen (mentioned above) after 24 hours.

2.3.8 Scanning electron microscopy (SEM)

Pore size and fiber diameter are key modulators of cell physiology in a collagen scaffold. SEM imaging in Figure 2.7 revealed a distinct network of fibers in the crosslinked collagen scaffolds (panel B&E), with resembling a mesh unlike the larger fibers found in the uncrosslinked gels (panel A&D). Unexpectedly, the addition of the PVA-borate to the crosslinked networks created a heterogeneous network of channels, which appeared to be separated by a thin film rather than fibers (Figure 2.7, panel C&F). The topography of the xCol HG network suggests that it contains fibrous elements that are filled with PVA-borate (or glycosaminoglycan) similar to previous findings (87, 90, 92, 98).

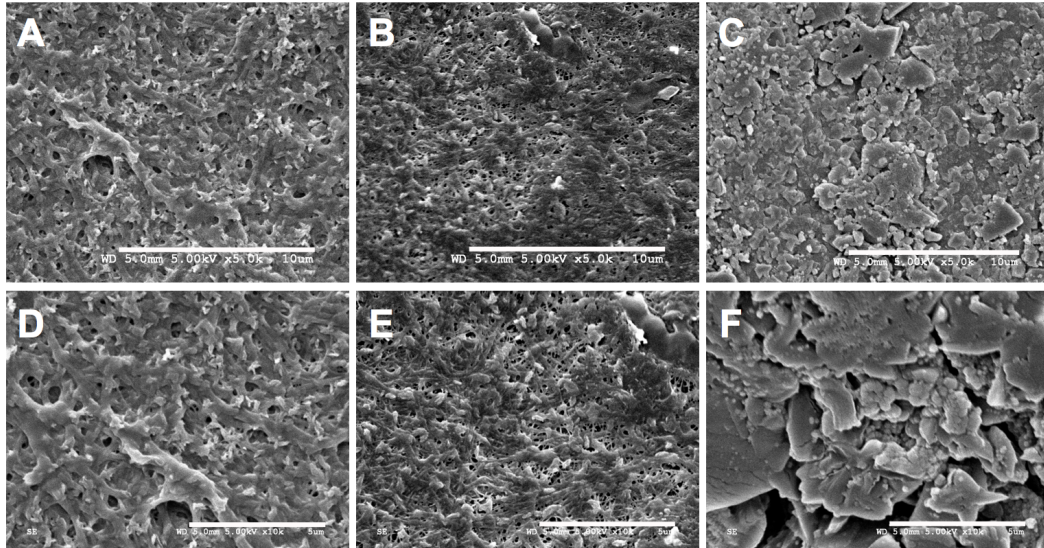


Figure 2.7. SEM micrographs of three different collagen gels.

(A&D) collagen-GAG, (B&E) crosslinked collagen-GAG and (C&F) crosslinked collagen-GAG containing PVA-borate networks. Gels were cast at 37°C, dehydrated in 70% ethanol and freeze dried at -80°C prior to gold plating. Scale bar: 10µm (A-C) and 5µm (D-F).

2.3.9 Engineered skin substitute (ESS)

The development of a liquid matrix system for cell delivery may be advantageous for application as a skin substitute. *In vitro* morphology of cells cultured in the xCol HG composite ESS showed an ordered arrangement, which differed from the random attachments observed in either uncrosslinked or crosslinked collagen scaffolds. In order to evaluate architecture of skin substitutes prepared over a 14-day period using both primary fibroblasts and keratinocytes. Paraffin embedded sections of ESS were mounted on slides and analyzed using H&E staining. Results demonstrated that fibroblasts, depicted in Figure 2.3, panel C, exhibited a similar linear morphology to was also achieved in the xCol HG ESS (figure 2.8, panel C). On the other hand, cellular organization was random in both of the other ESS. Furthermore the cellularity was also markedly less, in the xCol HG (Figure 2.8, panel C) and resembled a cross section of full thickness skin. Finally,

it was also evident that the thickness of both crosslinked scaffolds (Figure 2.8, panels A&B) was consistent across the entire section where in the uncrosslinked scaffolds the middle of the gel was thinner than at the edge.

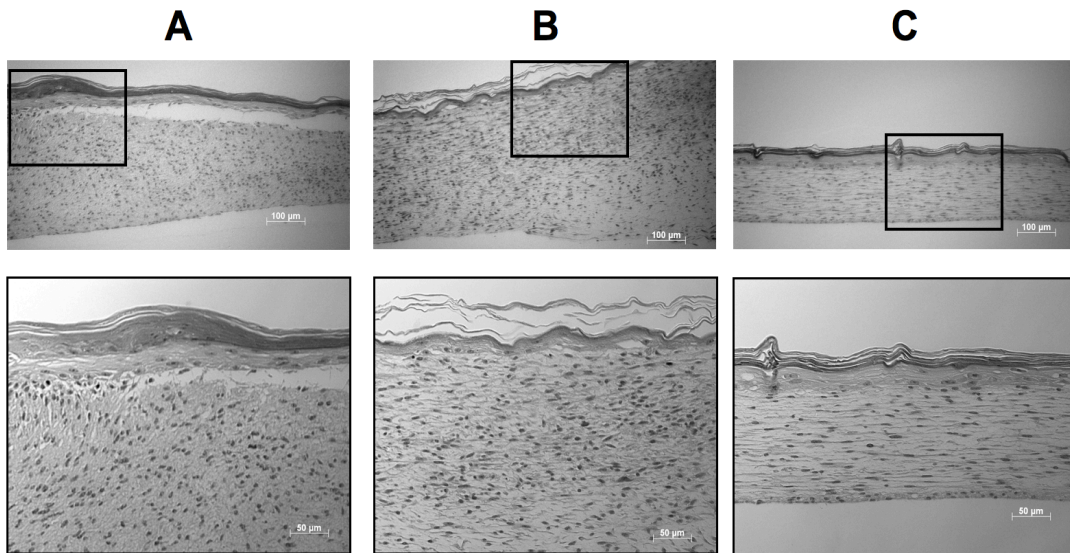


Figure 2.8. Phase-contrast micrographs of engineered skin substitutes ESS.

Three different collagen gels: collagen-GAG (Col), crosslinked collagen-GAG (xCol) and crosslinked collagen-GAG containing PVA-borate networks (xCol HG) were used to prepare ESS's. First, primary fibroblasts were combined with gel resin prior to casting in a permeable support for 48 hours at 37°C. After 48 hours primary keratinocytes were seeded on top of the scaffolds and the media was changed to 50/50 (DMEM/KSFM) as described in methods. After 36 hours media was lowered to expose the gel liquid interface and allow keratinocytes to develop over a 14 day period. Images represent H&E stained sections from paraffin embedded ESS. Scale bars: 100µm (A-C) and 50µm (D-E).

2.4 Discussion

Cell transplantation offers significant advantages over solid organ transplants for tissue repair and regeneration as a less invasive approach with potentially reduced immunosuppression (54, 99). One of the main hurdles for cell transplantation is the development of a viable injectable cell matrix system that will integrate with surrounding tissue while mitigating fibrotic responses. Several approaches to creating injectable scaffolds have employed crosslinking reagents, as well as modified synthetic and natural polymers that undergo crosslinking *in situ*. In this study we chose the use of glutaraldehyde as a rapid, well established collagen-crosslinker. Notably, we found our crosslinked gels to be non-toxic for both cell lines and primary cells. Although primary fibroblasts were used throughout the study, the viability of primary keratinocytes cultured on the gels was also evaluated in order to assess the usefulness of the scaffolds as skin substitutes. Furthermore, the viability of Baby Hamster Kidney cells (an epithelial cell type) and HaCat (immortalized keratinocyte) cell lines were included within our investigation to ensure that a variety of cells could grown in our scaffold. Importantly, all cultured cells remain viable in the presence of polyvinyl alcohol-borate, in or on any of the collagen-GAG scaffolds.

PVA is a neutral polymer that easily undergoes hydrogen bonding under physiological and basic conditions (88, 89, 92, 100). The formation of a gel as a result of hydrogen bonding is most pronounced in the presence of sodium borates. The bonding between borate and PVA is well known to cause rapid gelation under concentrated conditions (89). In this study we added a dilute PVA-borate mix to collagen-GAG resins in order to produce a rapidly forming injectable ECM. Using a simple inverted tube assay (86, 101) we were able to observe the crosslinking of collagen at 37°C in less than 10 minutes (data not shown). Although a solid gel may form within 10 minutes, the formation of fibrils (i.e. complete gelation) will take longer. Crosslinked collagen scaffolds that contained the PVA-borate hydrogels (xCol HG) showed a significantly increased rate of fibril formation (16.3 min), as well as a reduction in the lag time. This could

be explained as the result of hydrogen bonding between PVA-borate and collagen complexes that in turn increases viscosity and enhances nucleation of collagen fibers at 37°C (102, 103). Bonding between PVA and collagen was shown previously to create stronger biomaterials (87). *In vivo* collagen provides strength and toughness. Hyaluronic acid (HA) is a tissue abundant glycosaminoglycan providing lubrication and resiliency. It was thought that the addition of PVA-borate hydrogels, similar to HA, would not only increase strength but also elasticity. Where in fact xCol HG's demonstrated a significantly higher tensile strength ('Y') (1.414 ± 0.5015 MPa) than either of the control gels, the ultimate elasticity was not improved. One possibility is that there is more extensive bonding between the collagen and PVA networks, which exists at dilute PVA concentrations, that requires a greater force per unit area of strain (103). Thus, once the breaking force is obtained the bond energies are broken and the gel tears. The DSC results (Figure 2.6) suggest that there is a more extensively bonded (hydrogen) network in the PVA-borate and Collagen-GAG crosslinked composites, compared to the other two scaffolds as marked by an increased heat capacity. These data suggest that the intermolecular bonding between polymer species (PVA and collagen) may have an additive effect in improving the strength of the gel (104). In comparison, the elastic modulus of actual dermis (*in vivo* and *ex vivo*) has been found to be in the range of 0.6-5 MPa, with rat dermis slightly less at 0.4 MPa and simple dermal equivalents in the order of 8-10 kPa (50, 51, 105). Normal loads (using indentation) have recently been reported to be in the range of 1-10 kPa (106). In actual dermis it was shown that below a 10% strain rate the mechanical properties of the dermis differ significantly from higher strain rate, and this may be do to the presence of elastin-unwinding and adhesion of proteoglycans. Where patient age, matrix composition, hydration, relative humidity and the method can alter these values considerably, our results demonstrate that even in the absence of cells the hydrogel-containing injectable scaffold (once formed) can exhibit comparable mechanical stiffness to actual dermis. More importantly, these data demonstrate that the composite collagen matrix confers a greater tensile strength when

compared to crosslinked and uncrosslinked scaffolds, and may in part, explain the resistance to fibroblast contraction in free-floating gels.

Free-floating collagen gels have a tendency to contract when populated with fibroblasts (96). Contraction *in vitro* is a function of both the mechanical force required to cause contraction and the total number of fibroblasts to apply a given force (107). Thus, it is reasonable to suggest that a stiffer material will require more fibroblasts to produce contraction. Our results suggested a significant decrease in proliferation from days 5 -10 in both crosslinked gels compared to an uncrosslinked gel. The addition of PVA further reduced proliferation from days 6 - 10 as the total number of cells on day 10 was significantly less in the xCol HG than that of the xCol gel. Previously, PVA composites were found to be inadequate growth substrates for fibroblasts, as suggested by the possible lack of adhesion points. In our study we used a significantly lower amount of PVA within our composites, whereby cells could adhere. Cell morphology (Figure 2.3) in the presence of PVA-borate was visibly different, maintaining spindle-shape morphology. The amount of PVA (0.2%w/v) is less than the amount of HA used in other gel composites, and also was the upper limit of what could be applied without causing premature gelation (data not shown) (108). Together the improved tensile strength and reduced proliferation observed in our composite gels suggested that they would provide greater resistance to contraction when compared to either crosslinked or uncrosslinked gels. The significant difference in contraction between the crosslinked collagen gels and those containing PVA-borate occurred after day 3. In fact, with the exception of day 7, scaffolds containing PVA resisted contraction significantly from days 5 - 10 (compared to crosslinked without PVA) and maintained nearly 60% of their original size at the end of the study. Interestingly these data follow the same trend observed in cell counts over the same period (Figure 2.4).

Within a short period of time, fibroblasts are able to remodel collagen scaffolds, causing them to degrade. Fragmented collagen and GAG have been shown to

induce proliferative, fibrotic and immune responses (107). As a cell transplant delivery system, we were interested to learn if this composite system would be able to withstand specific degradation by collagenase. *Clostridium serine-peptidase A* is the most purified clostridium collagenase responsible for initiating digestion by unwinding and cleaving collagen, ultimately exposing it to other proteolytic enzymes (109). The hydroxyproline content in digested samples demonstrated that the PVA-borate gels were more resistant to degradation than either of the other gels. Similar to previous findings, crosslinked collagen was more resistant than uncrosslinked collagen. One explanation for these observations is that in addition to the glutaraldehyde crosslinks, the entanglement of PVA-borate networks among collagen fibrils further inhibited enzymatic attack (104). In support of this explanation, SEM images of the PVA-borate composites unlike Col and xCol gels, show lack of any fibers, and rather film formed crevasses. Compared to the SEM of other PVA-borate mixtures, thin films in the void space between and around the crosslinked collagen bundles may in part explain the absence of fibers in the xCol HG images (86). Most interesting is that the 'crack and crevasse' appearance of Figure 2.7F is similar to the SEM topography of decellularized pig and human dermis (110, 111).

Skin substitutes, as a cell transplant, are now becoming a more attractive option for the treatment of severe burns and chronic wounds. When we compared the histology of skin substitutes that were created using uncrosslinked, crosslinked or crosslinked PVA-borate containing collagen-GAG scaffolds it was found that those containing PVA were most similar to skin. Cellularity, cell morphology and even skin appendages (dermis and epidermis) were more consistent to normal anatomy. Furthermore the evident reduction in cell proliferation within the skin substitute containing PVA-borate (Figure 2.8) was also consistent with our findings in Figure 2.4. Interestingly, fibroblasts maintained a linear shape (similar to the morphology found in Figure 2.3) that may be caused by a restrictive environment created by the PVA-borate networks. Ultimately, this could produce a niche in which fibroblasts can survive, but not overgrow. The extensively

hydrogen bonded, and perhaps charge neutralization as a result of PVA-borate networks could reasonably create regions that are unfavorable for cell adherence. Further studies are required to better understand the morphological response of fibroblasts cultured within the PVA-borate containing skin substitutes. The use of injectable gels has the potential to improve the success of skin cell transplants as *in situ* forming skin substitutes. At present, there exist a variety of materials in which to deliver cells. Refinement of these injectable systems is needed to produce a matrix, that once gelled assume a desired architecture similar to solid, pre-formed scaffolds.

2.5 Conclusion

Our study evaluated the formulation of a simple, injectable collagen-GAG ECM containing networks of PVA-borate. Specifically, we demonstrated that the incorporation of PVA-borate networks was not only provisional for timely gelation of the ECM, but also improved architecture and mechanical properties. Where high cellularity and contracture is usually associated with fibrosis, these gels demonstrated the potential to dampen cell proliferation and contraction, without compromising cell viability. Altogether the improved functionality of our simple, PVA-borate containing collagen system warrants its further investigation in cell transplantation as a dermal substitute or injectable matrix.

3 Polyvinyl alcohol-*graft*-polyethylene glycol hydrogels improve fibrillation kinetics, mechanics and utility of collagen:glycosaminoglycan scaffolds

3.1 Introduction

The fabrication of collagen scaffolds for medical and research purposes has been studied extensively. Characterization of collagen and the fibrillation process, both *in vivo* and *in vitro*, is well known to occur at a neutral pH through a transition at 37°C that involves the denaturation of collagen into a linear form that can undergo hydrogen bonding between triple-helix chains of soluble collagen (59, 60, 93, 112, 113). The result of the process is an insoluble gel structure. The addition of glycosaminoglycan can further stabilize this process (33, 63). In the body collagen is in a dynamic state. Stability is achieved, in part, through the hydrophobic interactions collagen chains coupled with the solvation effects of water and hydrogen bonding and physical crosslinking. Collagen is the most abundant protein in the human body. There are over 28 types of collagen all of which assume a right-handed helix and an amino acid sequence that has been well conserved throughout evolution (56, 114). In fact, marine species such as hydra are known to comprise of a collagen that resembles type IV in humans. Marine collagen, unlike mammalian collagen, must undergo transition states at lower temperatures in order to form into a gel-like structure (114). The amino acid sequence of marine species provides for a lower gel transition temperature (T_g) and melting point (T_m) than that of mammalian collagen. The ability to form a scaffold at a lower temperature is provisional for improved utility of a scaffold for both medical and research purposes as a vehicle for cell transplantation. Aside from modification of the collagen amino acid sequence or the use of detergents, there are no known methods to both reduce the gelation temperature of collagen. In previous work it was determined by Li Y. (2009) that sodium dodecyl sulfate (SDS) could be used to reduce gelation points of collagen scaffolds, however it is known that SDS is also toxic to cells (64). Polyvinyl alcohols (PVA) and polyethylene glycol (PEG) have been known to be useful, and biocompatible

surfactants (68, 69). Variations of these polymer-surfactants have the added advantage of stabilizing the collagen structure, and altering its mechanical properties once gelled (62, 87, 97, 104). Toward the development of a simple cell delivery system the polymer additions would allow for rapid gelation of a collagen matrix *in situ*. In our earlier work we discovered that the addition of a single variant PVA-borate hydrogel to a crosslinked collagen-GAG scaffold could improve mechanical and physical properties (62). Through optimization of our earlier system, we can move toward the fabrication of cost effective injectable extracellular matrix that is opportune to satisfy several unmet needs in cell transplantation and tissue engineering (54, 115). In this work we further investigated the role that PVA variants play in enhancing the properties of collagen gel. As long chain polymer surfactants, the PVA and PEG variants could potentially be used to improve stability of neutralized collagen, where typically commercially available collagen is only available in an acidic medium. The second objective of this study was to investigate the potential of the polymers to stabilize a collagen scaffold for storage as a powder. Herein we described the use of PVA and PVA-*graft*-PEG copolymers to reduce the gelation temperature of collagen fibrillogenesis *in vitro* and the benefit of such polymers to stabilize a neutralized collagen system that can be lyophilized and reconstituted to form a scaffold *in situ*.

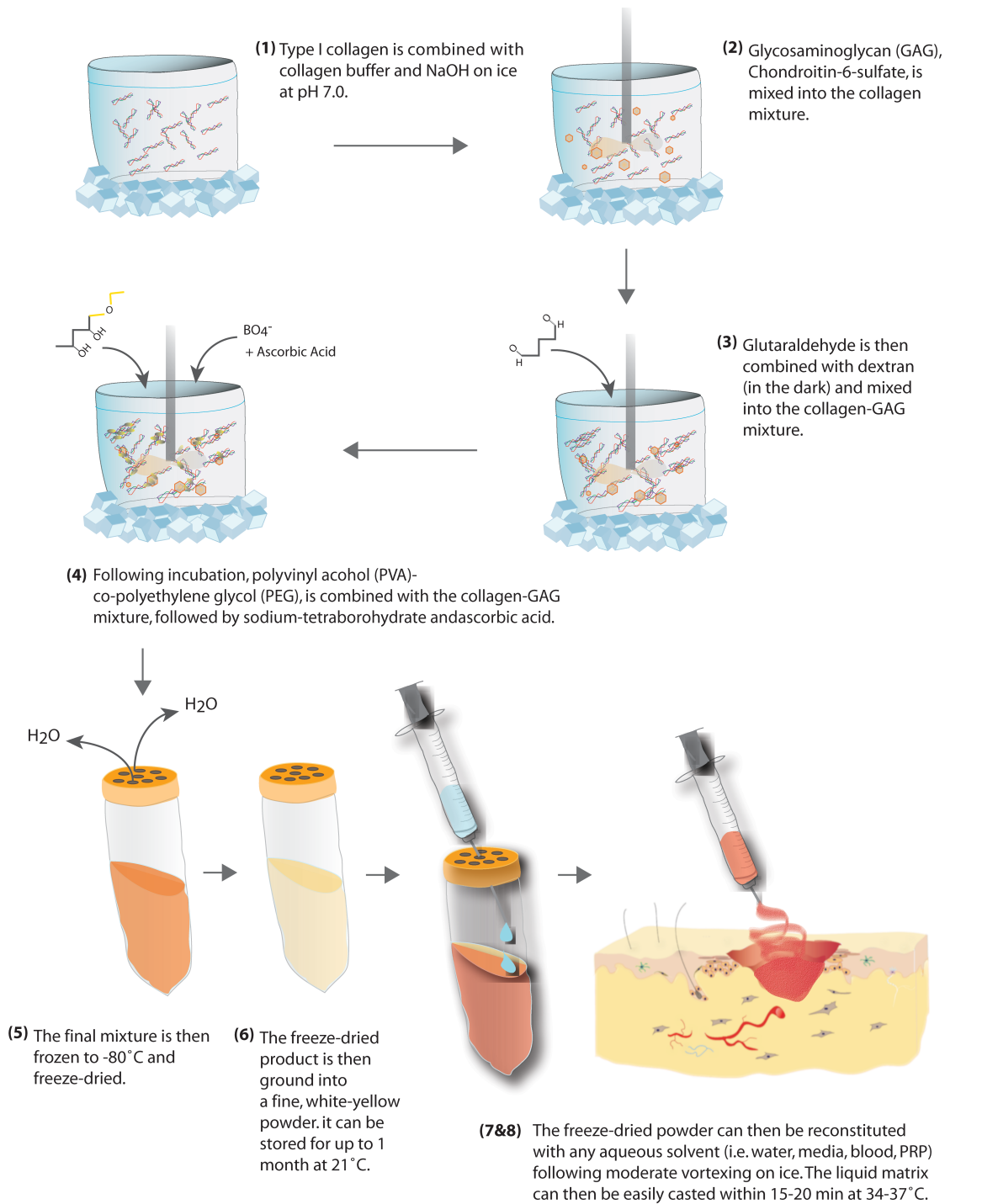


Figure 3.1. Process-schematic for the fabrication of the reconstitutable, collagen scaffold. Steps 1-8 describe the process by which one can manufacture the scaffold, freeze-dry, then reconstitute using water or other aqueous media and easily apply to a wound bed or cell culture container.

3.2 Materials and methods

3.2.1 Materials

Type I fibrous-bovine collagen (Advanced Biomatrix, USA), polyvinyl alcohol (PVA) 88% and 99% hydrolyzed (Alfa Aesar, USA), Kollicoat IR (polyvinyl alcohol-*graft*-polyethylene glycol) (Sigma Aldrich, Oakville, Can), sodium tetraborate decahydrate (borate) (Sigma Aldrich, Can), glutaraldehyde (25%v/v, Sigma Aldrich, Can), Dulbecco's Modified Essential Medium (10x, Life Technologies, Can), Chondroitin-6-sulfate (GAG) (Sigma Aldrich, Can), Dextran (40,000Da, Sigma Aldrich, Can), Ascorbic acid (Sigma, Aldrich, Can), Tween20 (Sigma Aldrich, Can), Tween80 (Sigma Aldrich, Can), Sodium dodecyl sulfate (Sigma Aldrich, Can), (Live/Dead viability assay kit (Molecular Probes, Invitrogen, Can), Phalloidin-488 Alexa Fluor (Invitrogen, Can).

3.2.2 Fabrication of collagen-polymer hybrid scaffolds

Type I fibrous-bovine collagen in 1N HCl was combined with a collagen buffer (10x DMEM, 10x PBS, 10x HEPES and 1x Antibiotic, pH 7.5) and pH adjusted using 1N NaOH as depicted in Figure 3.1. Once neutralized Chondroitin-6-sulfate was added to scaffolds (1:6, collagen:GAG). Non-crosslinked controls were combined with either remaining hydrogel reagents, or DMEM (1x). Crosslinked Gels were mixed thoroughly with a high molecular weight dextran (40,000Da)-glutaraldehyde mixture (0.02%v/v or as reported in Table 3.1) and allowed to incubate on ice in the dark. Incubation times varied as per the concentration and experimental object as outlined in Table 3.1. To optimize the crosslinker effects, gel-mixtures were exposed to glutaraldehyde concentrations that were either of proportion to a reaction volume (c1) or to the amount of collagen (c2) (Figure 3.1.A) or proportional to the incubation time (Figure 3.1.B). Different time periods were selected for each of the two treatment conditions such that exposure would

be similar. Table 3.2 describes the composition of variants used in all other investigations which followed the same crosslinking procedure as found in the variant in Table 3.1 (i.e. “Fig 3.2.B 21min”). Following incubation polymer hybrid gels were combined with respective amounts of PVA or PVA-PEG copolymer and gelling agent (sodium tetraborate decahydrate, 0.04-05%w/v) in a 1:4 ratio of borate molecule to hydroxyl functional group. All gel-mixes were brought to a final volume with 1x DMEM and ascorbic acid (100uM). Gel-mixes were stored at 4°C until casted or frozen at -80°C for lyophilization. Select scaffolds were lyophilized (freeze-dried) for 36 hours, then ground into a powder using a mortar and pestle and reconstituted to their original concentration using distilled and deionized water.

Table 3.1 Crosslinking conditions for scaffold variants depicted Figure 3.1

Scaffold	Stock Collagen	Glutaraldehyde	Incubation time
Col	9.9mg/ml	-	-
C1/45	9.9mg/ml	0.013 %w/v	
C1/60	9.9mg/ml	0.013 %w/v	
C1/70	9.9mg/ml	0.013 %w/v	
C1/90	9.9mg/ml	0.013 %w/v	
C2/15	9.9mg/ml	0.032 %w/v	
C2/30	9.9mg/ml	0.032 %w/v	
C2/60	9.9mg/ml	0.032 %w/v	
Fig 3.2.B. 60min	9.9mg/ml	0.02 %w/v (reaction volume corrected to represent stock collagen of 6mg/ml)	60min
Fig 3.2.B. 42min	9.9mg/ml	0.02%	42min
Fig 3.2.B. 21min	9.9mg/ml	0.02%	21min

Table 3.2 Composition of scaffold variants

Scaffold	Collagen (final)	Glutaraldehyde	Additive
Collagen (Col)	3mg/ml	-	-
Crosslinked collagen (xCol)	3mg/ml	0.02%w/v	-
(50/50)	3mg/ml	0.02%w/v	0.4%w/v of a 48% PVA (99% hydrolyzed) / 48% PVA (88% hydrolyzed) / 2%w/v glycerol and 0.05%wt borate
K99	3mg/ml	0.02%w/v	0.4%w/v of a 48% PVA (99% hydrolyzed) / 48% Kollicoat IR® / 2%w/v glycerol and 0.05%wt borate
K88	3mg/ml	0.02%w/v	0.4%w/v of a 50% PVA (88% hydrolyzed) / 48% Kollicoat IR® / 2%w/v glycerol and 0.05%wt borate
PVAnb	3mg/ml	0.02%w/v	0.4%w/v of a 48% PVA (99% hydrolyzed) / 48% PVA (88% hydrolyzed) / 2%w/v glycerol
TW80	3mg/ml	0.02%w/v	0.015mM Tween80(116)
TritonX100	3mg/ml	0.02%w/v	0.22mM TritonX100 ³

³ Sigma Aldrich, MSDS.

3.2.3 Crosslinker, polyvinyl alcohol and copolymer effects on gelation kinetics

Gel-mixes were aliquoted (150ul/well) into a 96 well plate on ice. Gelation kinetics were captured using a heated plate reader (Tecan, USA) with a 313nm uv/vis polarized filter set and Magellan Software™. The plate reader was first heated to the appropriate temperature (30, 32, 34, 37°C) and measurements were captured at either 1 or 2-minute intervals. Three batches (triplicate) of gel variants were used for each analysis (n=3) unless otherwise reported. Turbidity is the best indicator of collagen fibrillogenesis, and more indicative of gelation when combined with translucent hydrogels such as PVA and PEG (62-64, 93). The *time to gelation* is represented by the time at half the maximum absorbance at 313nm. The *lag time* is the time from the start of gelation to the time at half the maximum. The slope of the curve dA/dt indicates the rate fibrillogenesis. Using the Arrhenius equation [3.1] the activation energy can be calculated using first order kinetics of gel variants at different temperatures plotted as $\ln k$ vs. $1/T$, where k is the rate constant and T is the temperature in Kelvin. The rate constant for a first order reaction can be derived from the gelation time ($t_{1/2}$) using equation [3.2].

$$[3.1] \ln k = \ln A^{-E_a/T}$$

$$[3.2] k = \ln(2)/t_{1/2}$$

Using similar principles the change in rate fibrillogenesis (dA/dt) with respect to the polymers can also be determined through the comparison of the slope of the curve in the linear region.

3.2.4 Mechanical strength

Gels were cast in 5-well rectangular chamber slides (400ul each) and incubated for 24 hours at 37°C. Tensile testing was done using a KES-G1 Micro-Tensile

Tester (Kato Tech, Japan), with a 1kg load cell. Prior to loading, gels were dried of excess liquid using a KimWipe™ (Kimberly Clark, USA) and weighed. Two pieces of KimWipe™ were then used to firmly secure the gel onto the specimen holder. Gels were then stretched until breaking at a deformation rate of 0.02 cm/s. Tensile strength (engineering stress) was calculated by dividing breaking load (g) with sample width (mm) and area density (g.sq.m) of the polymerized gels, thereby to obtain the elastic modulus (E). For statistical purposes, three batches of gel were evaluated.

3.2.5 Scaffold architecture using Scanning Electron Microscopy (SEM)

Collagen scaffolds (100µl) were cast in 96 well plates for 24 hours followed by fixation in 4% Formalin solution for 24 hours at 4°C. After fixation the gels were dehydrated twice for 12h in 70% ethanol and then frozen at -80°C prior to lyophilization. SEM samples were first gold coated prior to loading inside the vacuum of a Hitachi S4700 SEM (Hitachi, Japan).

3.2.6 Contact angle

Gel-mixtures were formulated as described and then cast into thin films on glass slides at 37°C and then allowed to dry in a laminar flow hood for 24 hours. Using a contact angle tool (KSV Instruments), contact angle of a water droplet on the surface of the thin film was calculated using Attention Theta Software V4.1.

3.2.7 Cell viability

Viability was assessed using Live/Dead toxicity assay. Cells (primary or cell line) were cultured for in scaffolds for 24 hours. After 24 hours, scaffolds containing cells were washed 3 times with 1x PBS (pH 7.0) and a mixture of ethidium-homodimer and calcein-AM according to manufacture's instructions. After 30min scaffolds were washed 3 times with 1x PBS and visualized using a Zeiss Axiovert 200M fluorescence microscope and Axiovision software. Cell counts were obtained using Image J software (NIH, USA).

3.2.8 Cell adhesion and migration

Cell attachment and spreading was evaluated using phalloidin-Alexa-fluor 488 for staining of actin in fibroblasts cultured within collagen scaffolds 24 and 48 hours after casting. Briefly, gels were created and combined with cells as per the assessment of cell viability (above). Evaluation of cellular migration consisted of creating 4mm punch biopsies in the center of the gels and then filling the hole with acellular gel. Images were captured over a 10-day period, and migrating cells were designated as those that crossed into the new gel from the margin of the old. Images were captured using a Zeiss Axiovert 200M fluorescence microscope and Axiovision software.

3.2.9 Statistics

The number of repeats represents different batches of gels. Experimental results were evaluated using Analysis of Variance (ANOVA) with a post-hoc Tukey Test. Error calculations for linear regression represent the mean standard error of the fit for a given R^2 value of triplicate samples. Statistical significance was estimated with an alpha value of 0.05 ($p < 0.05$). Measurements were reported as means \pm standard deviation.

3.3 Results

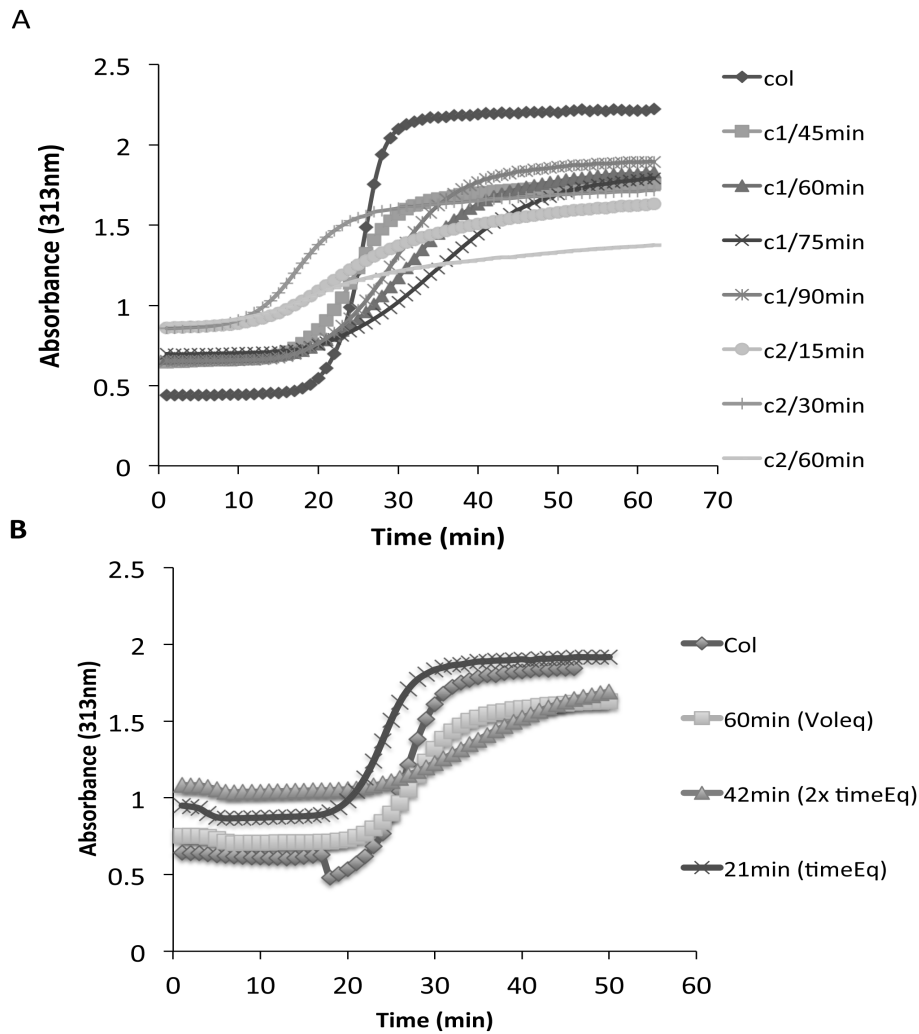


Figure 3.2. Effect of crosslinker concentration on fibril formation kinetics and turbidity.

Collagen solutions (3mg/ml) were fabricated either in the absence (Col) or presence of glutaraldehyde crosslinker. Collagen solutions were maintained on ice until being placed in a TECAN® spectrophotometer at 37°C to measure turbidity as an indicator of fibril formation (gelation) at 313nm. Panel (A) depicts collagen fibril formation kinetic profiles of three conditions described in Table 3.1. Panel (B) depicts a third condition with collagen alone as a control (col). Here the glutaraldehyde concentration is the same as C1 in panel A (0.002%wt) and the

incubation time is proportional to the reaction volume. The “60min Voleq” solution has a reaction concentration of collagen at 1.5mg/ ml, whereas the other two solutions contain 3mg/ml collagen.

3.3.1 Effect of crosslinker concentration, PVA and time on fibril formation

In order to optimize the formulation of the gel with respect to changes in stock collagen concentration we sought to first investigate the effect of both glutaraldehyde concentration and crosslinking incubation time on the change in fibril formation rate. First, when a change in glutaraldehyde concentration was proportional to a change in stock collagen concentration (where we previously utilized 6mg/ml (62)) the crosslinking reaction would result in gel solidification on ice. As such, it was found that increasing the concentration of would actually decrease the gelation rate, rather than increase it as might be predicted (Figure. 3.2.A (C1)). Furthermore higher concentrations of crosslinker resulted in a higher initial absorbance at 313nm. Interestingly, this pattern continued within the reaction-volume matched samples, which contained less glutaraldehyde crosslinker (C2). Collagen alone, without crosslinker exhibited the lowest initial absorbance and highest final absorbance, together with the fastest fibril formation as shown in Figure 3.2.A. Again $t_{1/2max}$ decreased, slightly, with the duration of incubation within the volume-matched reaction groups (Figure 3.2.A). It was apparent that a higher glutaraldehyde concentration in the reaction also corresponded to a reduction in $t_{1/2max}$ that was proportional to incubation time. This reduction in gelation time would ultimately correspond to both a reduction in the formulation time and time for gel solidification as a working mixture. Interestingly, when the incubation time was adjusted for the stock concentration of collagen used in the reaction vessel (Figure 3.2.B) the reaction kinetics could be controlled. This result demonstrated that the optimal final concentration of crosslinker is 0.02%w/v and that crosslinking incubation time should be adjusted in proportion to the stock concentration (reaction vessel concentration) of collagen.

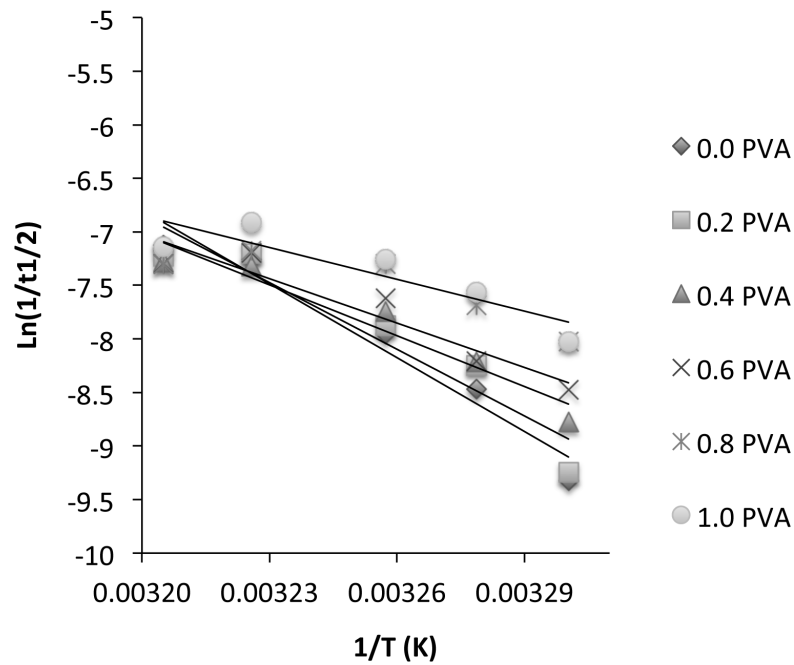


Figure 3.3. Arrhenius plot for collagen fibrillation as a function of PVA-borate hydrogel concentration

Uncrosslinked collagen scaffold variants were prepared as described in the materials and methods, containing 0 -1.0%w/v polyvinyl alcohol (PVA) (50%wt 99% hydrolyzed and 50%wt 88% hydrolyzed). Using Equation [1] a reduction in the activation energy for collagen fibrillogenesis is observed at 313nm as the concentration of PVA is increased.

Table 3.3. Effect of polyvinyl alcohol-borate gels on activation energy of collagen fibrillation

[PVA]	Ea (J/mol)		R ²	P value
0	2602.86	±424.88	0.93	*
0.2	2524.42	±487.56	0.90	
0.4	2025.82	±240.48	0.96	**
0.6	1504.28	±280.20	0.91	0.00035*/0.00612**
0.8	760.95	±237.50	0.78	<0.0001*/**
1	1276.45	±399.88	0.78	0.00024*/0.001**

The effect of polyvinyl alcohol-hydrogel addition to the gel-mixtures demonstrated an increase in rate of fibril formation when the concentration of PVA is increased from 0 to 1.0%w/v, which corresponded to a significant reduction in activation energy (Figure 3.3). As shown in Table 3.3 the addition of 1%w/v PVA resulted in more than 50% reduction in the required activation energy for fibril formation. The slight increase in gelation rate was also associated with a decrease in overall gelation time, however this change was not significant. Toward the formulation of a scaffold that could cast within a wound bed, or in the working range of 30°C-37°C for cell delivery and transplantation, gel-mixtures containing different PVA-hydrogel concentrations were explored. The results demonstrated that the PVA-borate hydrogels could in fact alter the fibril formation kinetics of Type I bovine collagen, in order to permit gelation at 30°C. Where typical inverted test-tube tests may demonstrate gelation at these lower temperatures, evaluation of turbidity at 313nm wavelengths remove the possibility of the PVA-hydrogel system to present artifact.

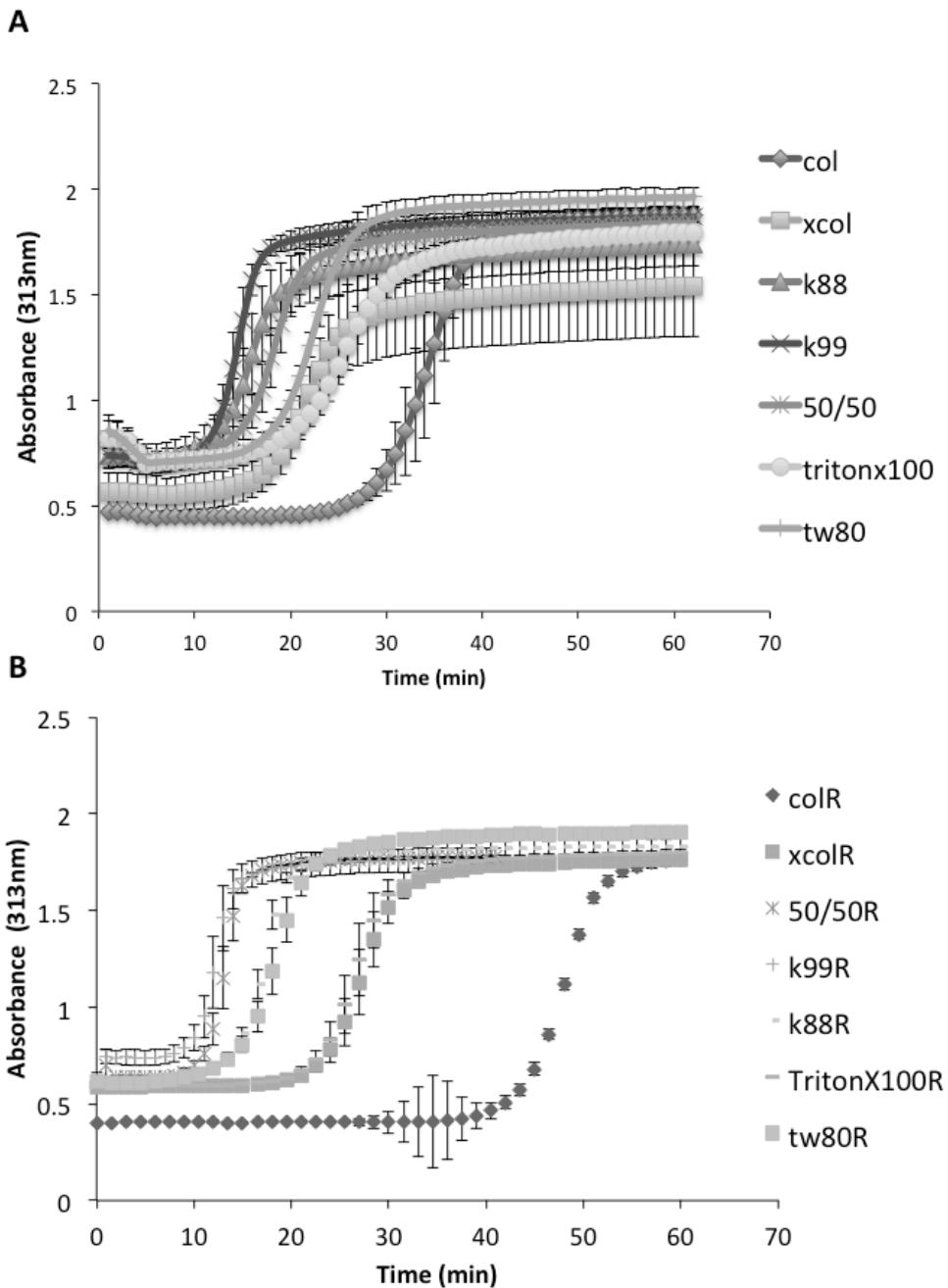


Figure 3.4. Effect of PVA variants on collagen fibrillogenesis pre- and post lyophilization/reconstitution.

Collagen solutions of (3mg/ml) alone (col) or crosslinked and combined with hydrogels or surfactants as follows: (xcol) crosslinked without any additives, (50/50) 50% PVA88/ 50% PVA99, (K99) 50% Kollicoat® / 50% PVA99, (K88)

50% Kollicoat®/ 50% PVA88, (TritonX100) TritonX-100, (tw80) Tween 80. Panel (A) depicts the shift in $t_{1/2max}$ for collagen fibrillogenesis with the addition of crosslinker, surfactant and PVA-hydrogel combination. Panel (B) depicts the fibrillogenesis of lyophilized and reconstituted collagen solutions matched to panel (A) and denoting the shifts in $t_{1/2max}$, with the exception of k99, k88 and 50/50.

3.3.2 PVA-hydrogel addition preserves gelation and mechanical properties of gel-mixtures following lyophilization

As an attempt to increase the stability of the gel-mixture (for transport and storage purposes), mixtures were lyophilized, ground into a powder and then reconstituted. Lyophilized mixtures were reconstituted with deionized and distilled water, without the need for pH neutralization. Interestingly, the PVA-hydrogel systems that were created using a PVA-PEG co-polymer (Kollicoat®) were most easily reconstituted. Collagen scaffold variants that were not crosslinked and did not contain PVA exhibited significantly longer gelation times when compared with the matched non-lyophilized scaffold mixture (52.6min \pm 1.52 v. 36min \pm 1.73) (Figure 3.4 & 3.5). The crosslinked-only (xcol) scaffolds were able to form fibrils, yet at a significantly longer gelation time than prior to lyophilization. Liquid mixtures of scaffold variants that contained PVA-hydrogels exhibited initial absorbances that were slightly higher than prior to lyophilization, yet formed fibrils within a statistically similar amount of time (Figure 3.4 & 3.5). The Kollicoat® samples, most notably K99, were among the fastest to gel (15.7min \pm 1.16) and exhibited the smallest change turbidity (from $t=0$ to t_{max} absorbance) suggesting that that the PVA-PEG must have had a protective effect on the collagen structure in powder form, and again when reconstituted. As shown in Figure 3.4 & 3.5 PVA-hydrogel scaffolds exhibited a significant reduction in gelation time when compared with col, xcol, Tw80 and Tritonx100 variants. The greatest reduction in gelation time was observed in scaffolds that contained the PVA-PEG hydrogels (2.02 fold). In comparison to previous studies that examined

the effect of surfactants on collagen gelation kinetics (64, 117) Tween 20, Tween 80 and Triton-x100 were combined within gel mixtures at their respective central micelle concentration's (CMC). (Note: The effect of Tween 20 was comparable to Tritonx100 and therefore was omitted for figure clarity). As shown in Figures 3.4 and 3.5 all surfactants increased the gelation rate (lowering $t_{1/2max}$) of both pre- and post-lyophilized samples, but to a significantly lesser extent than a majority of the PVA's.

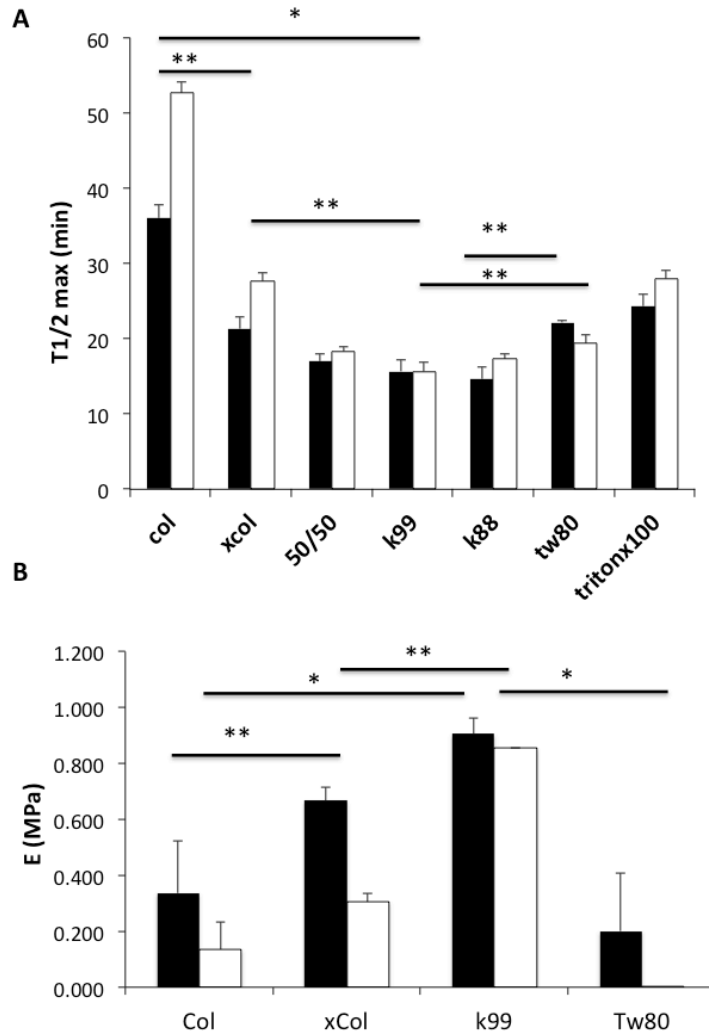


Figure 3.5 Quantification of collagen solution gelation kinetics and mechanical properties pre- and post lyophilization (freeze drying).

Panel (A) quantification of scaffold gelation time (fibrillation) as indicated by $t_{1/2max}$. Scaffolds were prepared as described in materials and methods. Panel (B) uniaxial mechanical strength (elastic modulus, E) of scaffold variants. Bar grouping with (*) denotes a statistical significance of $p < 0.001$ and (**) $p < 0.05$.

3.3.3 PVA-PEG and PVA-hydrogel systems exhibit a surfactant like effect on collagen gel-mixtures

A primary role of surfactants is to improve the hydrophilicity of a hydrophobic surface. The addition of Tween 20, 80 and Triton-x100 to the collagen gel mixtures significantly reduced the aqueous contact angle of a water droplet sitting on top of a casted, thin-film of a gel mixture from 108° (Collagen:GAG) to 51, 75° for Triton X100 and Tween 80 respectively (Figure 3.6). Additionally, there were differences in the contact angle depending upon the type of PVA that was used. Interestingly, when omitting borate (PVAnb) from the system the contact angle increased significantly from (52° to 72°). The crosslinked only gel-mixtures demonstrated the lowest contact angle suggesting the most hydrophilic surface formed by all gel mixtures (37°). PVA99, PVAnb and Tw80 were relatively similar at 75°, 76° and 75° respectively. Whereas Kollicoat® 99 and 88 blends were the next most hydrophilic with contact angles at 58° and 53° respectively. As would be expected the more hydrophobic PVA's had a greater surfactant-like effect and therefore a greater reduction in contact angle compared to similar molecular weight PVAs.

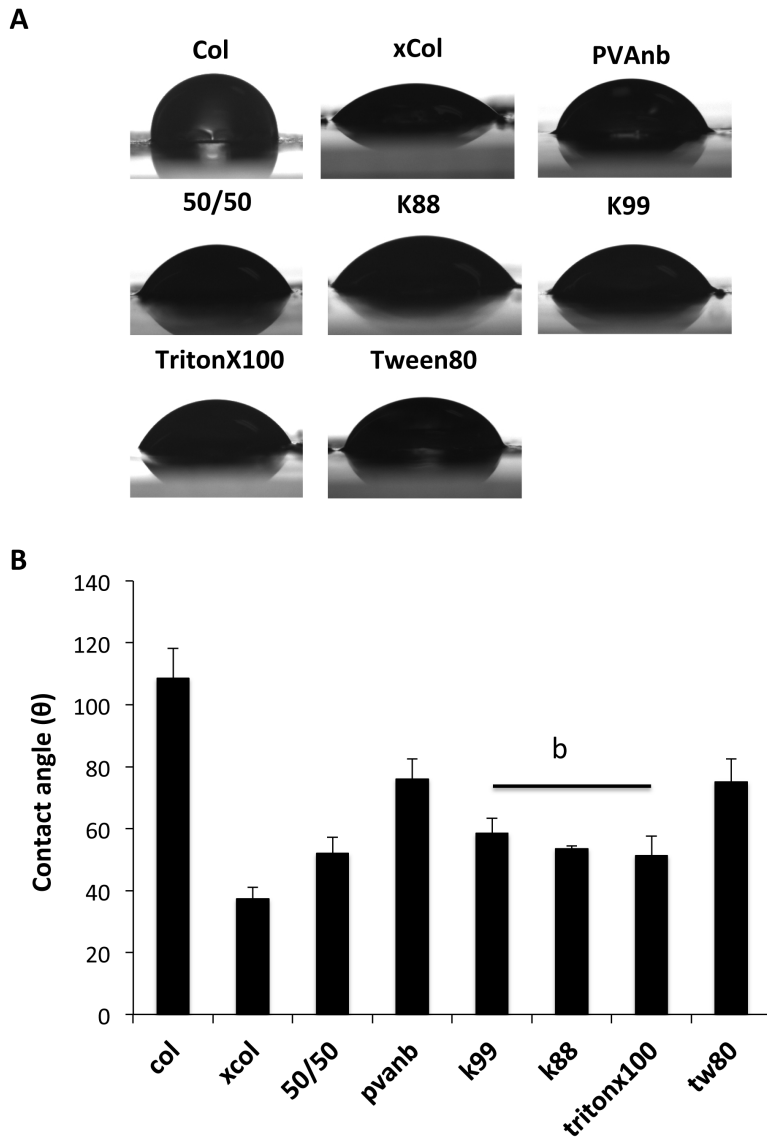


Figure 3.6. Contact angle measurements of dry gelled collagen films.

The effect of additive on surface hydrophilicity/hydrophobicity (surface wettability) was investigated through contact angle calculations. Variants were prepared as described in the materials and methods. Panel (A) photomicrograph images of a single water drop on the collagen scaffold surface. Panel (B) calculated contact angle of scaffold variants. Statistical significance of $p < 0.05$ was found between all treatments, with the exception of K88, k99, tritonx100 as denoted by the bar “b”. Statistical significance between the “b” group and all other treatments was observed.

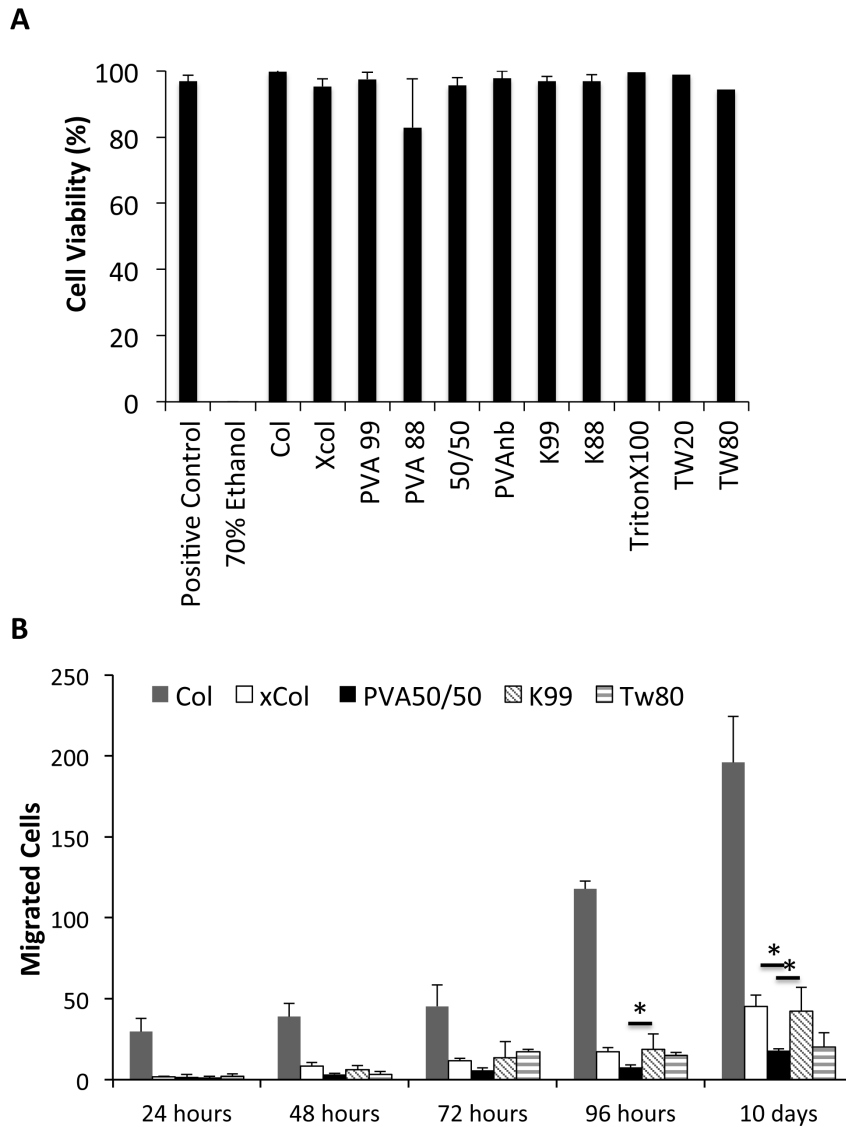


Figure 3.7. Cell viability and migration in collagen scaffold variants.

Panel (A) viability of primary fibroblasts cultured in collagen scaffold variants following 24 hours. Live/Dead ratios were utilized to calculate the percent of viable cells, using 70% ethanol as a dead control. Panel (B) 4mm punches were made in scaffolds and then refilled with an acellular scaffold variant. Cells were counted as they migrated from the old scaffold into the new scaffold over a period of 10 days. Cell numbers represent the total number of cells counted per scaffold variant at the denoted time point.

3.3.4 Cell viability and cell migration

Cells cultured in gel-mixture variants were cultured for 24 hours within scaffolds prior to staining. All scaffold variants were found to be non-toxic in vitro (Figure 3.7). Similar fibroblast populated collagen lattices were created to evaluate the migration. A punch biopsy was taken from the center of the scaffold and then filled with a matched acellular gel. There was no significant difference in cellular migration among all the scaffolds, with exception of the uncrosslinked, collagen:GAG scaffolds which exhibited the highest rate of cellular migration over a ten day period (Figure 3.7.B). On day 10, significantly more migrated cells were found in the k99 and xcol variants compared to PVA50/50 (Figure 3.7.B).

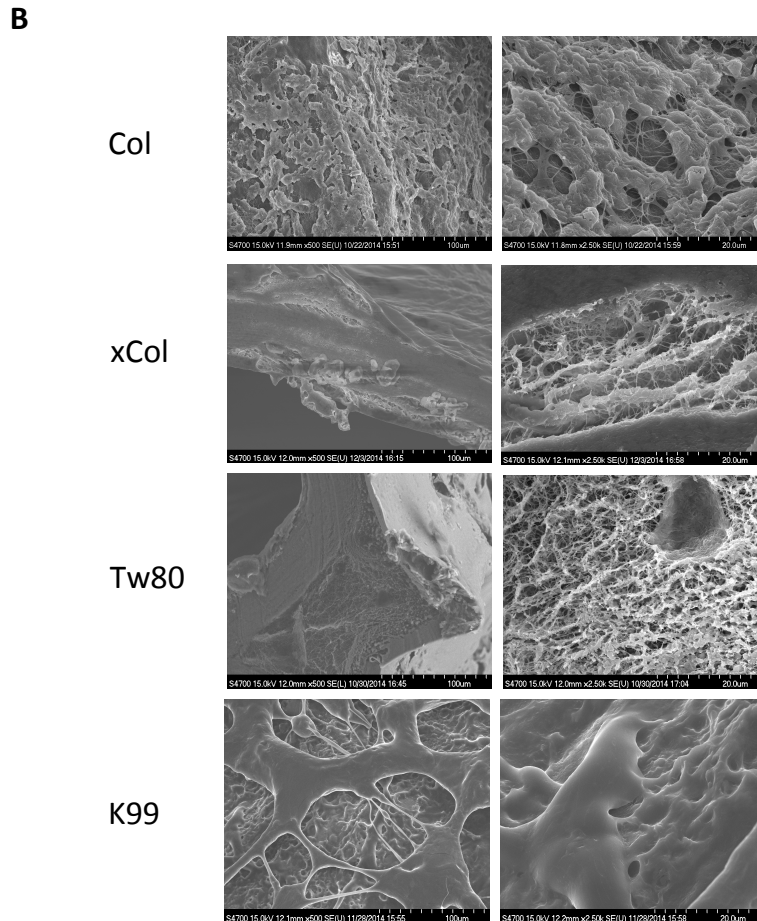
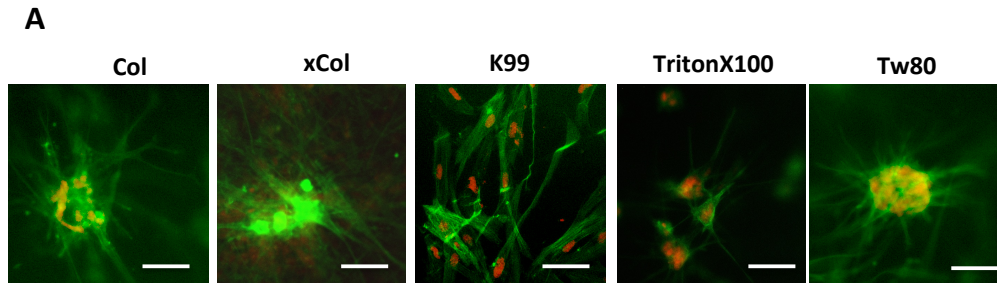


Figure 3.7. Fibroblast morphology and scaffold architecture in collagen variants.

Panel (A) depicts F-actin staining (green) of primary fibroblasts cultured in thin 100um scaffold variants. Nuclear stain (red) and scale bar (white) 100um. Panel (B) Scanning electron micrographs of freeze-dried collagen scaffold variants:

(col) collagen, (xcol) crosslinked collagen scaffold without additives, (Tw80) crosslinked collagen scaffold with tween 80 additive, and (K99) crosslinked collagen scaffold with kollicoat/PVA99 additive. Left panel scale bar: 100um and right panel scale bar: 20um).

3.3.5 Fibroblast morphology and scaffold architecture

Figure 3.7 depicts the morphology of fibroblasts cultured within five different scaffold variants. As found in our earlier work, cells cultured within an uncrosslinked collagen scaffold exhibit extensive spreading of lamellopodia and filopodia extensions, which is evident in panel (A) of stress fiber formation (filamentous actin) with phalloidin-488 stain (118, 119). Notable parallel fiber arrangement and reduced dendritic appearance, consistent with fewer filopodia, was observed fibroblasts cultured within a scaffold variant that contained a 50%wt Kollicoat®/ 50%wt PVA99 hydrogel (0.4%wt). Surfactant containing scaffolds exhibited a dendritic-like appearance with narrow filopodia-like extensions, and smaller cell bodies that are suggestive of cell stress and possible poor adhesion (Figure 3.7, Panel A) even though the cells remain viable (Figure 3.6). Scanning electron microscope cross-sectional images (Panel B) recapitulated our findings in the previous work, whereby larger, more irregular pores between collagen fibers are evident in the non-crosslinked scaffold (col) compared to other crosslinked scaffold variants. Interestingly surfactant treatment of collagen scaffolds with tween80 (tw80) resulted in a dense network of collagen fibers, with a smaller pore and a more tortuous void-path through the scaffold than any of the other scaffolds. The K99 scaffold demonstrated a similar film like appearance to what we have observed previously, where by the thin surface coatings of the fibers are evident by the lack of electron-beam penetration at high (2500x) magnification.

3.4 Discussion

Scaffold fabrication is core facet of tissue engineering. Modalities moving toward cell transplantation have prompted the demand for soft-materials that can conform to surrounding tissues, and exhibit tissue specific mechanical properties (strength, viscosity, elasticity, etc.) and physical characteristics (pore size, surface chemistry, gel transition temperature) (40, 54, 62, 120-122). Synthetic biocompatible polymers or modified biomaterials are often chosen for the creation of injectable scaffolds and hydrogels. Although type I collagen can also be used as an injectable material, its gelation temperature (and time) retard its utility as an *in situ* forming scaffold. To circumvent this issue, it can be chemically modified through crosslinking in order to create a more viscous material that would also avoid rapid degradation because of the chemical crosslinks. Excellagen® and Integra® flowable are two currently marketed injectable products for use as a dermal filler and wound healing modality respectively (15, 18, 123). Both Excellagen and Integra® flowable are new to the market, yet as soft materials are unable to form intact solid scaffolds (gels) *in situ*. Furthermore, most collagen scaffold preparation for tissue engineering research and clinical, first requires neutralization of a collagen solution prior to use. The utility of a reconstitutable collagen scaffold, as opposed to a gel-slurry, is that aside from forming *in situ* it would also have similar mechanical properties to preformed solid scaffolds, such as holding sutures or serving as an interface between an implant and tissue. Examples of the clinical utility of our reconstitutable system are shown in Figure 3.9.

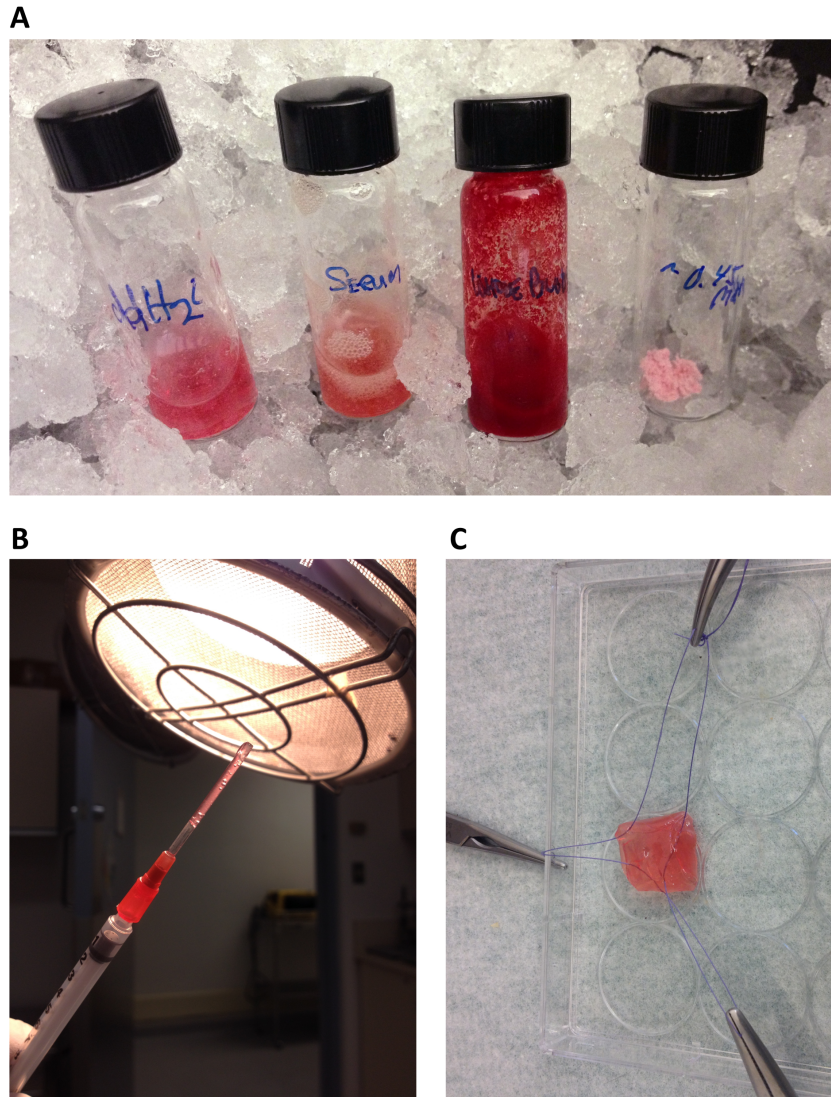


Figure 3.9. Utility of lyophilized (freeze-dried) collagen scaffold.

Panel (A) photomicrograph of K99 scaffolds reconstituted (left to right) with distilled and deionized water, serum, whole blood, and non-reconstituted powder. Panel (B) reconstituted k99 scaffold contained within a 16G BD® IV catheter. Panel (C) depicts the ability to suture a gelled, reconstituted k99 scaffold.

As shown in Figure 3.3 the addition of PVA to a crosslinked collagen:GAG gel-mixture significantly reduced the activation required to form fibrils and an intact

scaffold, without actually modifying the collagen itself. PVA-PEG (Kollicoat®) is a biocompatible synthetic biopolymer that is an accepted pharmaceutical component under most jurisdictions worldwide. In the paint and plastics industry, PVA is added as a surfactant and in the presence of borates (tackifying agent) the polymer chains can be ionically crosslinked, facilitating extensive hydrogen bonding (62, 67, 70, 71). Freeze-thaw cycling of the polymer, without crosslinker has been shown previously to produce robust cryogels (124). In vitro, biocompatibility data (Figure 3.7) demonstrated that none of the PVA variants examined were toxic to cells. Previous reports describe the lack of cell adhesion to PVA coated surfaces, and the differences in cell morphology among the variants may be due to the coatings that PVA make on the collagen fibers and fibrils. Although, higher concentrations may prove to be toxic they are outside the workable range, as at concentrations exceeding 1.0%w/v the gel-mixtures become too viscous to ensure homogeneity. Previous reports have demonstrated that surfactants could alter the kinetics of collagen gel formation (64, 117). It was postulated that the enhancement of fibrillogenesis was due to the surfactant destabilization of the collagen. The observed effects of the surfactants are similar to what was achieved using our PVA variants, and as such we further investigated the incorporation of biocompatible nonionic surfactants Tween 20, Tween 80 and Triton-x100 at their CMC. Interestingly, the surfactants did reduce the overall time to gelation without compromising cell viability, but had no overall improvement in gelation rate, mechanical strength and change in activation energy. Of the PVA variants, the best gel-mixture consisted of a combination of 48% PVA 99 and 48% Kollicoat® and 2% glycerol. The second best variant overall was the Kollicoat® mixture containing PVA 88 over PVA 99. As expected the surfactants and more hydrophobic PVA's provided the greatest improvement in surface wettability, with the exception of the crosslinked only gel-mixtures, which were unexpectedly the most hydrophilic Figure 3.5. The improved wettability of the scaffold surfaces compared to the uncrosslinked collagen scaffold could, in part, be related to the observed improvements in cellular morphology and migration (125-129). Furthermore the changes in surface

wettability are indicative of the coatings that the polymer variants are forming on the collagen scaffold architecture. As with pore sizes and mechanical stiffness, hydrophilic and hydrophobic effects have been shown to influence cell physiology *in vitro*. Optimization of the surface characteristics has been shown to reduce protein deposition and aggregation and alter cell attachment and expression of adhesion molecules. Given the amphipathic nature of PVA and to a greater extent, PVA-PEG, it is possible that the surface modification of the collagen scaffold provides adequate adhesion sites, as is achieved *in vivo* through proteoglycan interactions with collagens. For example heparin sulfates and other glycosaminoglycans have also been known to change the surface of collagen scaffolds, but unlike PVA they are also implicated in signaling cascades through receptor-ligand interactions (33, 44, 48).

3.5 Conclusion

Type I collagen is one of the most widely used biomaterials in tissue engineering but its use has primarily been limited to the fabrication of pre-formed solid materials and weak injectable gels rather than used as a material that could form solid structures *in vivo*. Herein we investigated the use of polymer variants of PVA that have surfactant-like effects and have shown that collagen could be destabilized in order to form a gel with reduced activation energy while maintaining its mechanical properties. Taking our approach one step further we were able to demonstrate that PVA could stabilize lyophilized collagen gel-mixtures (in powder form) in order to improve the handling and storage. With great advancements being made in bioprinting, tissue-bioreactors, and cell transplantation there is a large unmet need to *in-situ* forming scaffolds of biological origin. As collagen is the most abundant protein in the body, by weight, we are hopeful that the use of our hybrid (PVA-PEG)-collagen blends could offer a simple, cost effective solution for tissue repair and regeneration.

4 An in-situ forming skin substitute improves healing outcome in a hypertrophic scar model

4.1 Introduction

Wound healing is a complex and dynamic process, whereby skin cells orchestrate cell-cell communication in order to repair injured tissue. Use of engineered skin substitutes is intended to foster timely and normal healing. Unfortunately, not all wounds undergo organized healing and are often stuck in a non- or over healing phase (11, 12, 17, 34). Many diabetic and severe burn patients lack adequate donor sites to use for autografts. The need for a patient ready integratable skin substitute is underscored by the roughly 20 million diabetic ulcer patients each year in North America, many of which end up requiring amputation, and an excess of 400,000 hospitalized burn patients who desperately require a means of tissue repair (18, 130, 131). The medical device field has exploded with biological and tissue engineered products for advanced wound care (15, 18, 132, 133). Some of these commercially available products include biologics and biologic-hybrids such as bi-layered allografts and acellular scaffolds. As with any product, continuous development seeks to improve caveats that exist with current wound care modalities. For example, cost and supply chain logistics have retarded the economic advancement of many advanced wound care devices (15, 130). Secondly, allogeneic cellular scaffolds can elicit an immune rejection response that, albeit are often unpronounced, may further complicate healing (133, 134). In spite of these hurdles, the success of allo/xenogenic-tissue substitutes remains an ongoing discussion.

Many scaffolds that are currently used are pre-formed, solid materials. These scaffolds, including autografts, are unable to immediately integrate with the uneven surface of a wound bed. Without sufficient integration there is a risk of graft loss.

Hydrogels can be integratable, but are often created using components such as alginates, p-HEMA, chitosan and in some cases macro-sphere fillers (24-26, 121, 135, 136). The downside to many of injectable scaffolds is the poor mechanical

strength in comparison to solid structures. Ideally the interface between the scaffold and the wound bed should be seamless and therein promote vascular perfusion and innervation. We have previously proposed an *in situ* forming collagen-scaffold that, as an intact-scaffold sheet, can serve as a hydrated skin substitute. In combination with cells, this scaffold can also serve as an easily prepared, patient ready skin substitute for burns and chronic wounds (62). Earlier data, have demonstrated that Indoleamine 2,3-dioxygenase (IDO) expressing cells could protect xeno/allografts from T-cell mediated rejection (34, 37, 137, 138) but require lengthy preparation time (>2 weeks) to create a skin substitute. We have also demonstrated that a polyvinyl alcohol (PVA)-hydrogel system could be combined with a collagen-GAG network to produce a rapidly gelling matrix that exhibited superior mechanical and biological properties to traditional collagen based materials *in vitro* (62). In this study we present the results of a biohybrid hydrogel-collagen-GAG system that is able to rapidly transition from a viscous liquid into a solid scaffold within the wound. One primary objective of this study was to evaluate the effectiveness of this system to adequately form within the wound, in the presence of biological fluids, and integrate with surrounding tissue. Working toward the application of a patient-ready skin substitute this study demonstrates the functionality and feasibility of an *in situ* forming hydrogel collagen-GAG scaffold to be combined with IDO-expressing cells to thereby improve healing outcome in a hypertrophic animal model.

4.2 Materials and methods

4.2.1 Cell isolation and culture

In accordance with the human ethics policy at the University of British Columbia primary fibroblasts were isolated from the discarded foreskins of three-consenting donors. Likewise, primary hypertrophic scar fibroblasts were isolated from the skin of three-consenting donors (1 child (<18 years) and 2 adults (≥18 years)) that was discarded following surgical procedures. Skin specimens were

briefly washed several times with 1x Phosphate Buffered Saline (PBS) (pH 7), containing 1% antibiotic, minced into small pieces and then fixated with Fetal Bovine Serum (FBS) for 4 hours on a tissue culture plate. After 6 hours, one drop of 1x Dulbecco's Modified Essential Medium (DMEM) containing 10% FBS and 1% antibiotic was added to the FBS drops over night. The next day DMEM was used to cover fixated skin section in the dish. Skin pieces were maintained in culture until fibroblasts reached 60% confluency, after which cells were trypsinized and passaged as per previous studies (34, 37, 139). Fibroblast passages 6-7 were used for experimentation.

4.2.2 Preparation of IDO expressing cells

Dermal fibroblasts were stably transduced to over-express IDO using a recombinant lentiviral vector constructed by our group as performed previously (34, 37, 139) with modifications using a blasticidin selection gene. Infected IDO expressing cell population was then enriched through blasticidin addition (8ug/ml) to the media following exposure and washout of live virus. IDO expression in transduced fibroblasts was confirmed through PCR of hIDO mRNA (Fig 1.A) run on a 1% agarose gel. Primer sequences are shown in Table 1. Expression of functional IDO was confirmed by measuring kynurenine levels in the conditioned media (Figure 4.8).

Table 4.1. Primer sequences for IDO, MMP1, and Col-1alpha.

Gene	Sequence (F/R)
Col-α1	GGACCTCAAGATGTGCCACT / ACCACACGTGCTTCTTCTCC
MMP1	CAGCTTTATGGGAGCCAGTC / TGTTCTCACCCTCCAGAAC
hIDO	GGCAAAGGTCATGGAGATGT/ CTGCAGTCTCCATCACGAAA

4.2.3 Scaffold preparation

Crosslinked collagen-GAG scaffolds were prepared as described previously (62, 140). Briefly, Type 1 bovine collagen (Advanced Biomatrix, USA) and chondroitin-6-sulfate (Sigma Aldrich, CAN) were combined (1:6 w/w ratio) to a final concentration of 3mg/ml collagen and neutralized with DMEM and 1N NaOH. Glutaraldehyde (0.02%v/v; Sigma Aldrich, Mississauga, CAN) was used to crosslink the collagen for 1 hour on ice in the dark. Following crosslinking, glycine was used to de-activate residual aldehydes. Following washing, hydrogels comprising of polyvinyl-alcohol (PVA) (50:50/ 208,000 MW and 146,000 MW) (0.2%w/v; Sigma Aldrich, CAN), sodium borate decahydrate (0.05%w/v; Sigma Aldrich) and ascorbate (pH 7, 100uM; Sigma Aldrich) were added to the crosslinked collagen in order to fabricate in-situ forming scaffolds. All scaffolds were maintained at 4°C in liquid form until used for evaluation.

4.2.4 Cell viability and morphology

The viability of cells cultured within the scaffolds was examined using calcein AM and ethidium homodimer as described previously (62, 140). Briefly, cells within scaffolds were washed with 1xPBS and then exposed to calcein AM (1ul/ml) and ethidium homodimer (4ul/ml) and incubated for 30 min. Following incubation scaffolds were washed again with 1xPBS and then visualized and counted for live and dead cells using Image J (NIH software, USA). Grey-scale, phase contrast images of cell morphology were taken 24 hours following gelation. All cell images were captured using a Zeiss Axiovert microscope and Axiovision 4.8 software.

4.2.5 Scaffold contracture

Human fibroblasts from normal (NF) and hypertrophic scar tissues (HSC) were cultured within either collagen scaffolds without hydrogel (Col) or in-situ forming scaffolds (IPN) which were prepared as described previously (62). Cell media

(DMEM containing 10x FBS and 1x antibiotics) was changed daily. Fibroblast populated scaffolds (400µl volume with 250,000 cells/ml) were released from the plate walls 24 hours after gelation (on day 0) and allowed to float. Images were taken upon release and on days 1, 3, 5 and 7 using a Sony digital camera at a consistent range. Scaffold size was measured using Image J (NIH software, USA).

4.2.6 Animal model

All animal models were employed in accordance with protocols approved by the University of British Columbia and the Canadian Guidelines on Animal Care. Aseptic surgical techniques were used for all procedures. As a standard model of scar hypertrophy, four New Zealand white rabbits (~3kg) were used to investigate the utility of the in-situ forming scaffolds to be employed as skin substitutes as previously published (34, 141-143). Animals were anesthetized using ketamine (NMDA agonist)/xylazine (α 2 agonist) induction and isoflurane maintenance. Meloxicam (Non Steroidal Anti-Inflammatory Drug) (0.3 mg/Kg) prophylaxis was used as an analgesic. Four 6mm full thickness punch wounds were created on the dorsal surface of both ears and randomized by location. Groups and wound numbers were as follows: (8) untreated control (Con); (8) acellular in-situ forming scaffolds (Gel); (8) in situ forming scaffolds containing normal human fibroblasts (GelF); and, (8) in situ forming scaffolds containing normal human IDO-expressing fibroblasts (Gel IDOF). Cells were combined with scaffolds (pre-gelation) at a concentration of 500,000 cells per ml. Scaffolds were maintained in a liquid form on ice prior to creation of the wounds. Once wounds were formed, gels were aspirated within a 16G catheter and warmed for 5 minutes on a heating blanket prior to injecting onto the wound. Wounds were covered using Steri-Strips™ (3M Healthcare, Canada) and Tegaderm™ (3M Healthcare, Canada) occlusive dressing. Rabbits were inoculated with additional in situ forming scaffolds (once daily) for up to four days following wounding using a 16G catheter to overcome thinning of the scaffold that occurred following gelation. The catheter was placed within the Tegaderm™ dressing and subsequently

closed thereafter upon covering. Rabbits were evaluated over a 35-day period to assess scarring and healing outcome.

4.2.7 Healing outcome- scar elevation index, epidermal thickness & cellularity

Quality of wound healing can be measured in a number of ways, three of which are the scar elevation index (SEI), epidermal thickness (ET) and cellularity (34, 141-143). The SEI can easily be calculated using equation [4.1] as a measure of the ratio in epidermal and dermal thickness of the wounded area relative to that of the adjacent normal skin. Dermal and epidermal thicknesses are secondary markers of scarring and calculated as the average pixel thickness across the neo-tissue. Thickened dermis and/or epidermis are often observed in hypertrophic scars and keloids, with a marked abundance of collagen deposition.. Healing rate was assessed qualitatively on day 20, once wounds had begun to epithelialize. Increased cellularity is a hallmark indicator of fibroproliferative disorders such as hypertrophy especially in its early stages, and is easily quantified as cells/high powered field (hpf) using Image J (NIH software, USA).

[4.1] SEI = Cross Sectional Area of Healed Dermis/ Original Cross Sectional Dermal Area

4.2.8 Collagen staining, MMP-1 and collagen expression

In order to determine the abundance of collagen deposition, paraffin embedded sections were de-waxed and stained for collagen with Masson's Trichrome as described previously (142). Masson Trichrome contains four stains: (1) Weigert's Hematoxylin (ferric chloride in diluted hydrochloric acid, hematoxylin in 95% ethanol and potassium ferricyanide solution, alkalized by sodium borate; (2) Biebrich scarlet, glacial acetic acid, and distilled water; (3) phosphomolybdic acid in distilled water; and (4) Methyl blue. Staining colours are as follows: keratin and

muscle fibers stained red, collagen fibers are stained blue, cell cytoplasm and nuclei are stained light pink and dark brown. Total RNA was extracted from scar tissue using Trizol reagent according to the manufacturer's instructions (Invitrogen, Carlsbad CA, USA). Following DNase treatment and cDNA synthesis, gene expression of MMP1 and pro-alpha-1- collagen (col1a1) was determined using q-PCR (AB Biosystems, USA). Primers, described in Table 1, were designed and purchased from Invitrogen (Burlington, Canada). β -actin was used as the reference gene.

4.2.9 Immunofluorescence staining CD31, CD3 and PGP 9.5

Tissues were fixed in 10% formalin at room temperature and then embedded in paraffin followed by sectioning into 5 μ m sections. Embedded sections were then stained using both immunohistochemical and immunofluorescence techniques. Antigen retrieval was carried out in sodium citrate buffer (pH 6.0). Tissue was first incubated with blocking buffer (5% Goat Serum/5% Albumin in 1x PBS (pH 7)) for 1h and 2h for anti-CD3 (using 5% horse serum) at room temperature. Tissue sections were then incubated with primary anti-bodies CD31 (1:50) (Santa Cruz, USA), CD3 (1:50) and PGP 9.5 (1:25) (Abcam Inc., Cambridge, MA) overnight at 4°C. All sections were incubated with secondary antibody at room temperature (Alexa-fluor 488 anti-rabbit 1:2000, Alexa-fluor 568 anti-goat 1:1000 (Invitrogen, Carlsbad, CA, USA)). 4'-6-Diamidino-2-phenylindole (DAPI) (Vector Laboratories, Inc., Burlingame, CA, USA) was used as a counter stain. Sections were viewed using a Zeiss Axiovert microscope and Axiovision 4.8 software. Image analysis was conducted using Image J (NIH software, USA).

4.2.10 Statistics

All histological and *in vitro* experiments were performed in triplicate (n=3). Wound analysis consisted of 8 wounds per group (n=8), with the exception of the mRNA analysis (n=4). One-way ANOVA with Tukey post-hoc analysis was employed to

determine statistical significance. Standard deviation is represented in graphs and tables, and significance is indicated with an asterisk with an alpha of 0.05.

4.3 Results

4.3.1 IDO expression, skin cell viability and morphology within in-situ forming scaffolds

Validation of IDO expression and activity was confirmed through detection of hIDO mRNA in transfected fibroblasts (Figure 1.A) in conjunction with measurement of increasing concentrations of kynurenine in the culture media (S1.B). Primary human fibroblasts cultured on both plastic and in the in situ forming scaffolds were examined for viability 24 hours following gelation. Using calcein AM and ethidium homodimer as makers of viability it was found that cells remained similarly viable in all systems as found previously (62, 140) (Figure 1.B).

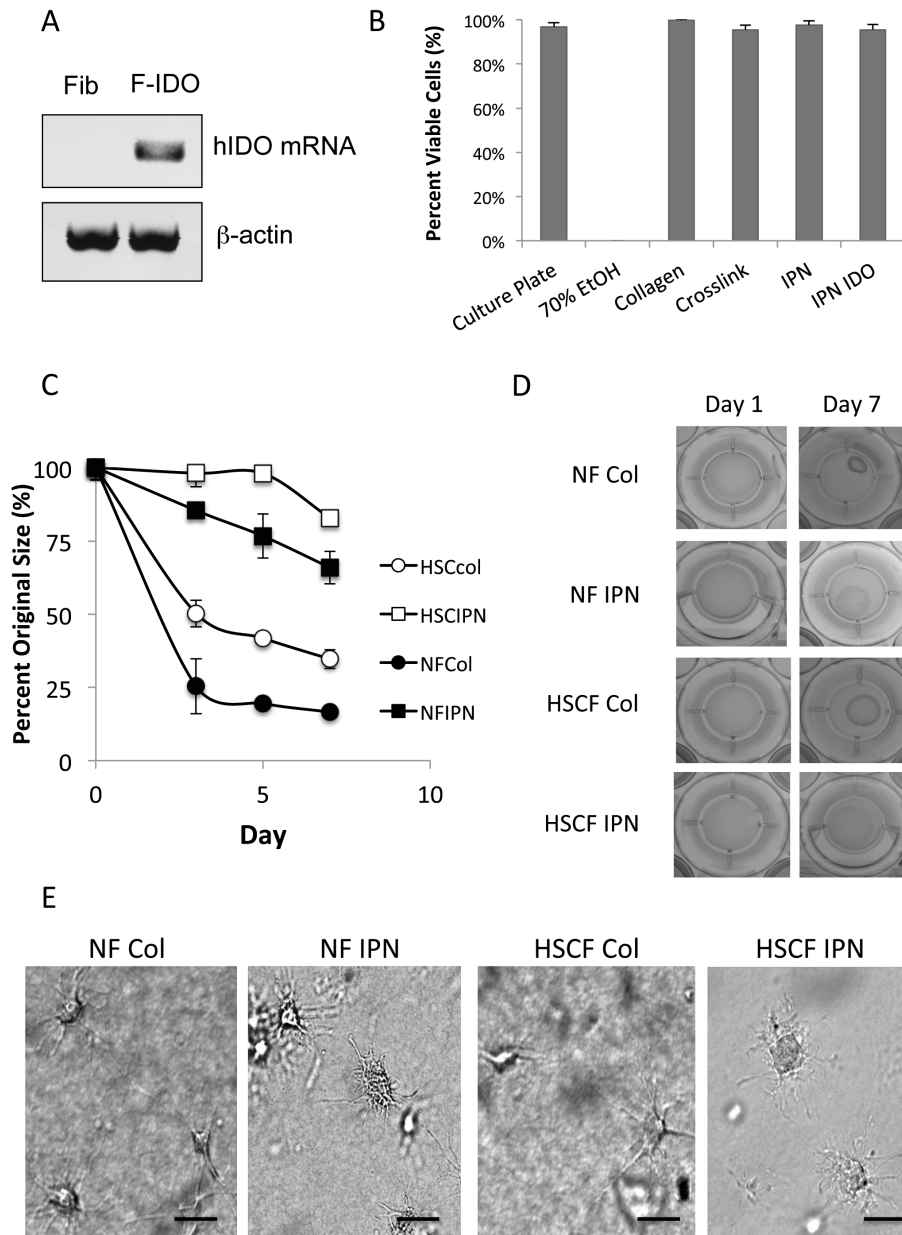


Figure 4.1. Biocompatibility and functional evaluation of scaffolds in-vitro.

(A) Validation of hIDO expression in human fibroblasts transfected with IDO using a lentiviral vector system driven by ef1 α as previously published (139). Detection of hIDO mRNA in transduced fibroblasts (IDOF) by PCR. No mRNA expression of hIDO was detected in non-transfected cells (Fib). **(B)** Viability of primary fibroblasts and IDO cultured in scaffolds: collagen (collagen+GAG), crosslinked (glutaraldehyde crosslinked collagen+GAG) and IPN (glutaraldehyde

crosslinked collagen+GAG+hydrogel) (n=3; p>0.05) **(C)** Graphical representation of free-floating scaffold resistance to contraction over a 7 day period. Fibroblasts derived from normal (NF) and hypertrophic (HSC) tissues were cultured in either standard collagen-GAG scaffolds (Col) or in-situ forming scaffolds (IPN) and observed for contracture over a 7-day period (n=3; p<0.05). **(D)** Photographic representation of free-floating scaffolds. **(E)** Inverted microscopic live cell imaging of fibroblasts cultured in scaffolds after 24 hours of incubation (scale bar=50µm).

4.3.2 Free-floating scaffold resistance to contraction and cellular morphology

Fibroblast populated free floating scaffolds (500,000 cells/ml) were created using the *in situ* forming scaffolds and a standard collagen-GAG scaffold similar formulation to our previous study (62). Four different scaffolds were fabricated to examine the efficacy of scaffolds to resist contraction of normal fibroblasts (NF) and hypertrophic scar fibroblasts (HSCF). Standard collagen-GAG scaffolds containing normal fibroblasts (NFCol) attained near maximum contraction (16% of original size) within the first 3 days (Figure 4.1.C-D), unlike the *in situ* forming scaffolds (NFIPN) that resisted contraction (within 85-98% of the original size) within the same period of time. As expected, all scaffolds contracted over the seven-day period, notwithstanding that the standard collagen-GAG scaffolds achieved an apparent plateau in contraction on, or nearest to the third day. *In situ* forming scaffolds significantly resisted contraction over the seven days compared to corresponding standard collagen-GAG scaffolds (82.8% ±0.01 v. 34.6% ±3.19 and 66% ±11.4 v. 16% ±0.01 of the original size, respectively). Interestingly, normal fibroblasts were more contractive than fibroblasts derived from hypertrophic scars (16% ±0.01 vs. 32% ±3.19 of the original size) whereby the initial contraction by these cells was found to be the greatest within the first 3 days. Cell morphology of cultured fibroblasts prior to scaffold release demonstrated cell spreading and attachment in both scaffolds with a marked reduction in refraction and an apparent difference in the morphology of cell extensions (Figure 4.1.E).

4.3.3 Application of the hydrogel scaffold and wound healing outcome

Treated wounds received treatment with the in situ forming hydrogel collagen-GAG scaffold and covered with Tegaderm™ (semi-occlusive, transparent film dressing) as shown in Figure 4.2.A. All wounds healed within the 35-day investigational period. Scaffolds containing xenofibroblasts (GelF) and untreated wounds were among the final wounds to heal (Figure 4.2.B). Wounds treated with either acellular in situ forming scaffolds (Gel) or with in-situ forming scaffolds containing IDO expressing fibroblasts (Gel IDOF) exhibited earlier epithelialization and minimal erythema on the margins. Untreated and GelF treated wounds presented a scab and raised scar or cyst-like structure that was evident on day 20, which further resulted in a thick-to-the-touch, raised scar on day 35 of the study. All Gel or Gel IDOF treated wounds had completed healing (free of scab) by day 20 without the formation of a raised scar or cyst-like structure (Figure 4.2.B).

Histological hallmarks of hypertrophic scars are a thickened epithelium, rete ridges in the epidermis, dense collagen bundle formations in the dermis, low levels of matrix metalloproteinase-1 (MMP-1), increased and disorganized collagen type I deposition and increased cellularity (34, 141). Figure 4.3, (A-D) depicts a thickened epidermis and dermis in the untreated and GelF treated wounds compared to normal skin and that of either Gel or Gel IDOF groups. In the GelF group this may be as a result of allo-tissue incompatibility. Using the scar elevation index (SEI), epidermal (ET) and dermal thickness (DT) analysis, it was found that the application of Gel significantly reduces scarring in general compared to that of untreated and GelF treated wounds respectively, even in the presence of an occlusive dressing (Figure 4.3.A-D and Figure 4.4.A-B). The thickness of both epidermis and dermis was significantly lower in Gel (9.48 ± 1.83 and 0.93 ± 0.15 pixels) and Gel IDOF (9.93 ± 2.60 and 0.67 ± 0.25 pixels) groups relative to untreated wounds (17.23 ± 2.6 and 1.61 ± 0.15 pixels) (Figure 4.2.A-B). Furthermore, Gel and Gel IDOF treated wounds resulted in relatively similar SEI (1.24 ± 0.05 and 1.25 ± 0.03). Interestingly, epidermal and dermal thicknesses

were relatively similar among Gel and Gel IDOF treated wounds (Figure 4.4.A). Cellularity, was also significantly lower in the Gel and Gel IDOF groups (124 ± 21 and 114 ± 17 cells/hpf), and greatest in the control group (242 ± 25 cells/hpf). Collagen bundle formations were absent in all Gel and Gel IDOF groups, and markedly higher in untreated wounds (Figure 4.3). GelF group displayed collagen bundle formation but to a lesser extent than untreated wounds. Rete ridges were notable in both untreated and GelF groups (Figure 4.3.E-L).

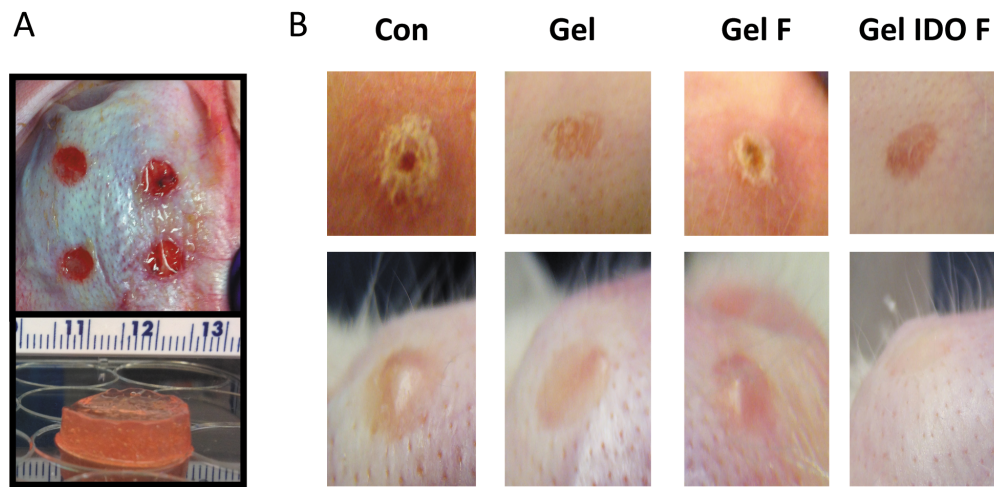


Figure 4.2. Macroscopic clinical evaluation of punch wounds in the rabbit ear.

Abbreviations: Con- untreated wounds, Gel- acellular in situ forming hydrogel collagen-GAG scaffold, GelF- in situ forming scaffolds containing xenofibroblasts, and Gel IDOF- in situ forming scaffolds containing IDO expressing fibroblasts. (A) Top Panel: Photomicrograph depicting post-surgical punch wounds filled with a layer of in situ scaffolds (right side) and covered with Tegaderm™ following solidification. Lower Panel: Free-standing in-situ forming scaffolds following gelation in a culture dish at 37°C for 15 minutes. (B) Follow-up micrographs on post-surgical day 20 (upper panel) and day 35 (lower panel) demonstrating wound healing progression.

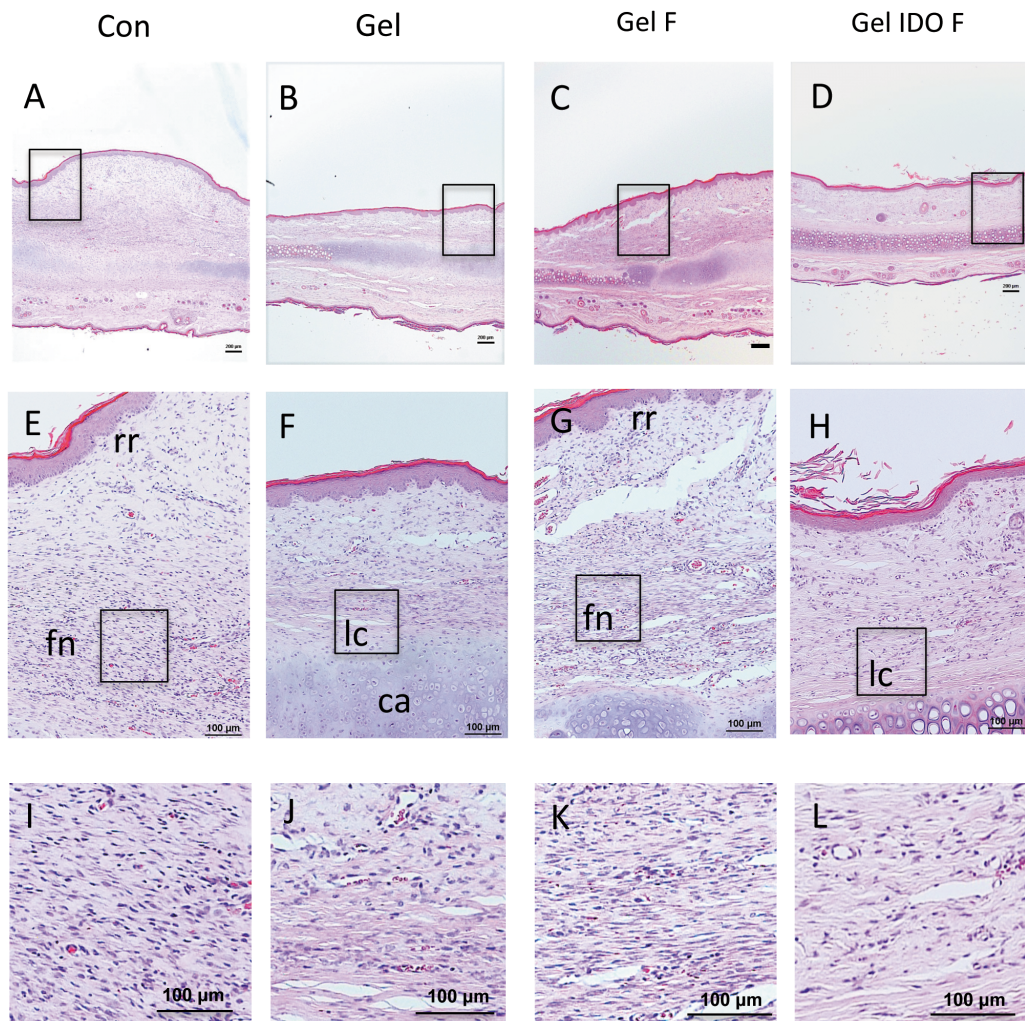


Figure 4.3. Histologic evaluation of hematoxylin and eosin stained sections of treated rabbit wounds on post surgical day 35.

Abbreviations: Con- untreated wounds, Gel- acellular in situ forming scaffolds
 GelF- in situ forming scaffolds containing xenofibroblasts, and Gel IDOF- in situ forming scaffolds containing IDO expressing fibroblasts. Abbreviations in (E-H) denote histological features: lc- linear collagen banding, ca- cartilage (mature and immature), fn- fibrotic nodules, and rr- rete ridges. Scale bars represent 200um (A-H) and 100um (I-L). Black boxes indicate the region represented in the corresponding lower panel higher magnification image.

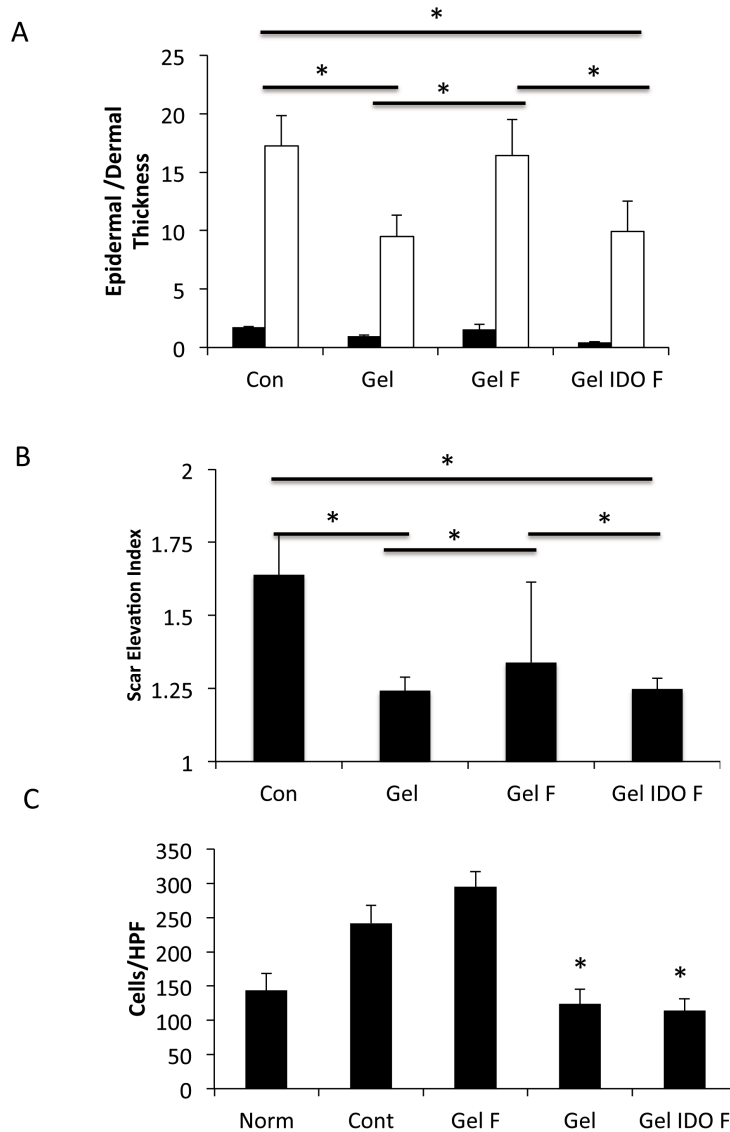


Figure 4.4. Evaluation of healing outcome in rabbit ear treated wounds using Scar Elevation Index, epidermal and dermal thickness, and tissue cellularity.

(A) Epidermal (open bars) and dermal (closed bars) thickness averages. Dermal thickness area scaled at 1:100000 pixels and epidermal thickness as linear pixels averages of the treated wound area. (B) Scar elevation index, represented as the ratio of the total hypertrophic tissue relative to the normal tissue area. (C) Cellularity of H&E stained tissue sections. (n=8; p<0.05).

4.3.4 Matrix deposition and expression of matrix metalloproteinase-1 (MMP-1) and collagen type 1

Collagen deposition was evaluated using Masson's trichrome staining (Figure 4.5.A). As expected the raised scar structures of the untreated and GelF groups corresponded with a greater amount of disorganized collagen deposition. Gel and Gel IDOF treated wounds demonstrated predominantly a parallel matrix organization that was contiguous with neighbouring unwounded tissue. At the mRNA level, untreated wounds expressed increased tissue levels of pro-alpha-1 collagen and low levels of MMP-1 (25.30 \pm 3.22 and 3.53 \pm 0.73 fold respectively), the primary collagen-remodeling enzyme (Figure 5.B-C). Wounds treated with Gel and Gel IDOF exhibited a significantly lower amount of tissue pro-alpha-1 collagen expression (9.57 \pm 3.1 and 10.23 \pm 1.95 fold respectively; p <0.05) compared to all other treatments on day 35 post-wounding. When compared to the untreated group, Gel treated wounds alone did not significantly alter the MMP-1 expression (1.28 \pm 0.6 v. 0.58 \pm 0.21 fold), however Gel IDOF treated wounds exhibited a significant 16-fold increase in tissue MMP-1 expression when compared to normal skin and all other treatments. Reduced expression of pro-alpha-1-collagen in the Gel treatment group corresponded with a decreased collagen type I deposition within the wound site and the absence of scarring.

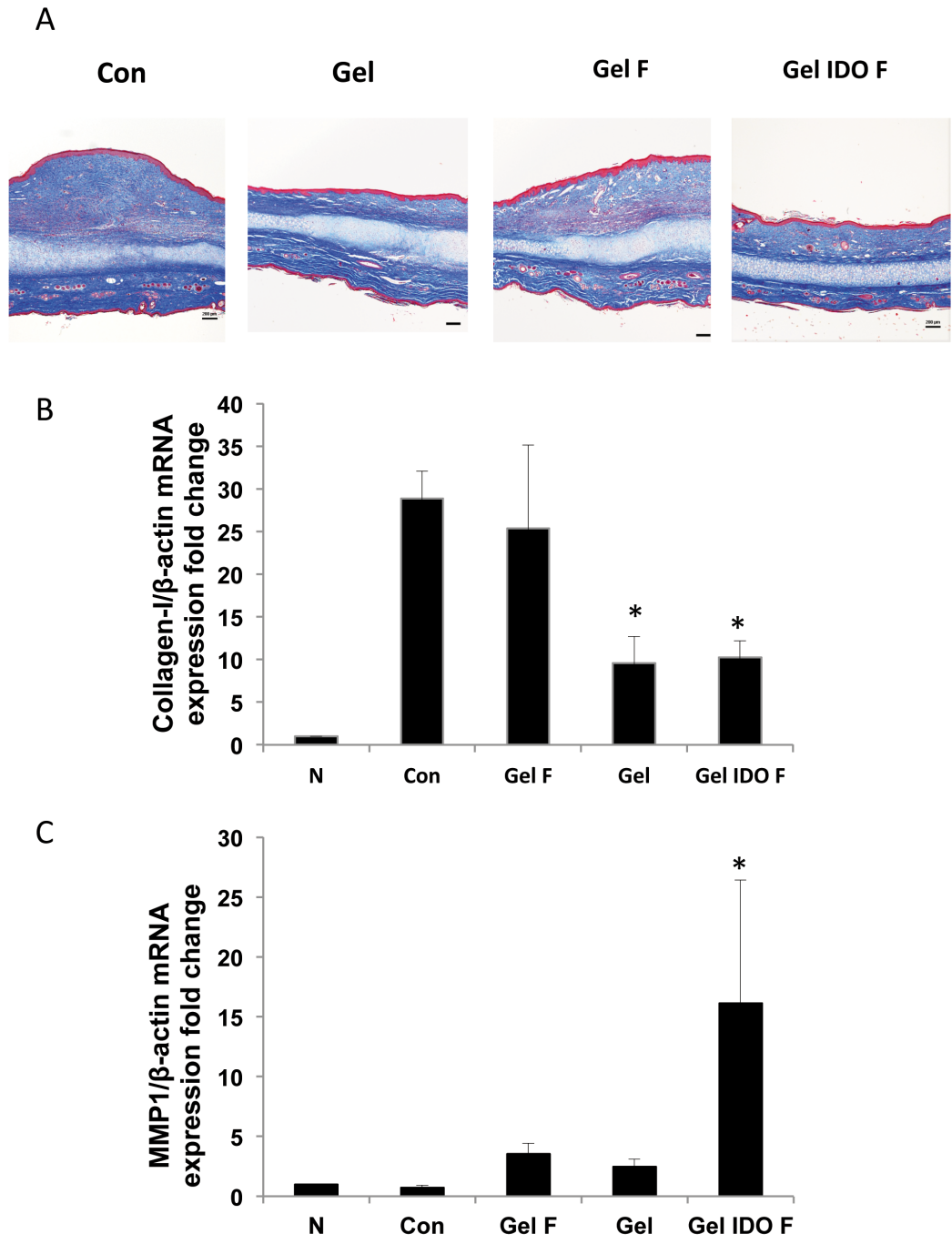


Figure 4.5. Collagen staining and gene expression of collagen and MMP-1 in treated rabbit wounds.

(A) Masson-trichrome staining of collagen in wounded tissue sections on day 35. Scale bar represents 400 μ m and 20 μ m for top and bottom panels respectively. (B) mRNA expression of pro-alpha 1 Collagen in treated rabbit ear tissue. (C)

mRNA expression of MMP-1 in treated rabbit ear tissue. All mRNA expression is expressed as a fold change in beta-actin and normalized to uninjured tissue. β -actin was used as a reference gene. (n=8; p<0.05)

4.3.5 CD3⁺ T-cells post wound healing

It is well known that localized IDO activity can prevent T-lymphocyte infiltration and proliferation (34, 37, 137). T-cell infiltration and persistence in healed wounds was evaluated by immunofluorescence staining using a rabbit monoclonal anti-CD3⁺ pan T-cell marker. Gel IDOF treated wounds demonstrated significantly reduced, if not entirely absent, infiltrated immune cells evaluated on day 35 compared to both untreated and GelF treated wounds (4 ± 2 v. 8 ± 3 and 14 ± 4 cells per high powered field respectively; Figure 4.6.A and C). Likewise, wounds treated with Gel alone exhibited relatively fewer CD3⁺ cells on day 35 compared to the untreated wounds, however this difference was not significant (8 ± 3 v. 5 ± 2 p>0.05). GelF treated wounds were heavily infiltrated with CD3⁺ cells, this may explain the increased cellularity found in these samples (Figure 4.3.D-L) and the number of these cells was significantly greater than the untreated wounds. Functional IDO expression was confirmed through kynurenine production within the Gel IDOF scaffold cultured *in vitro*. Gel IDOF scaffolds sustained IDO production throughout the experiment and were able to produce sufficient kynurenine concentrations (15-20 μ g/ml) (Figure 4.8.B), as per previous studies in this range (34, 37).

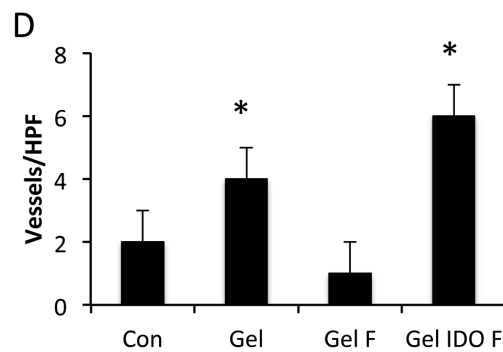
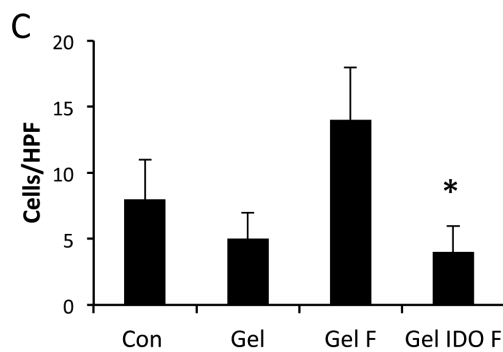
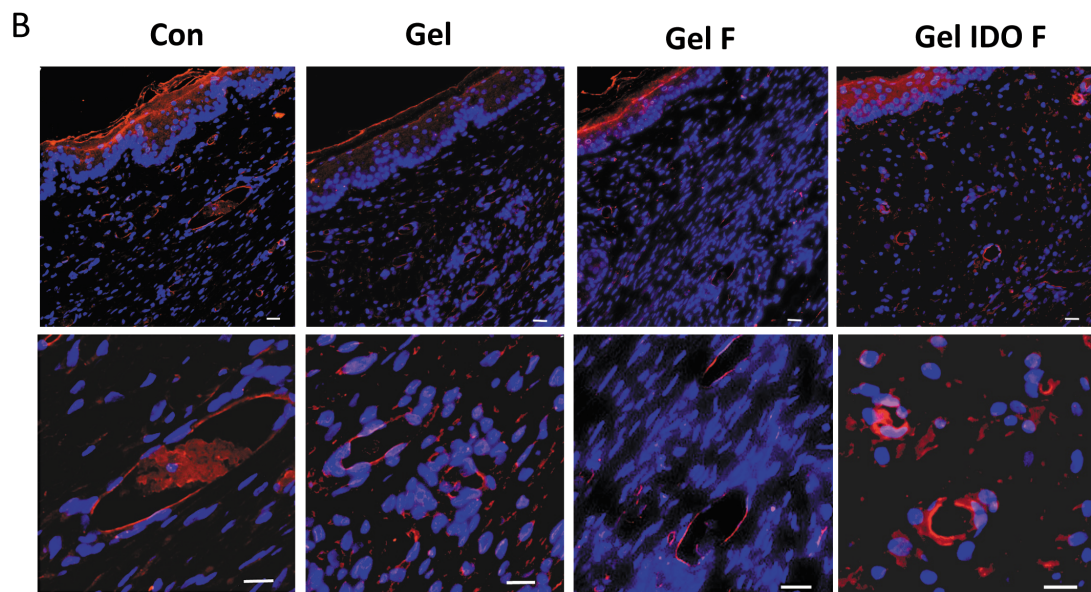
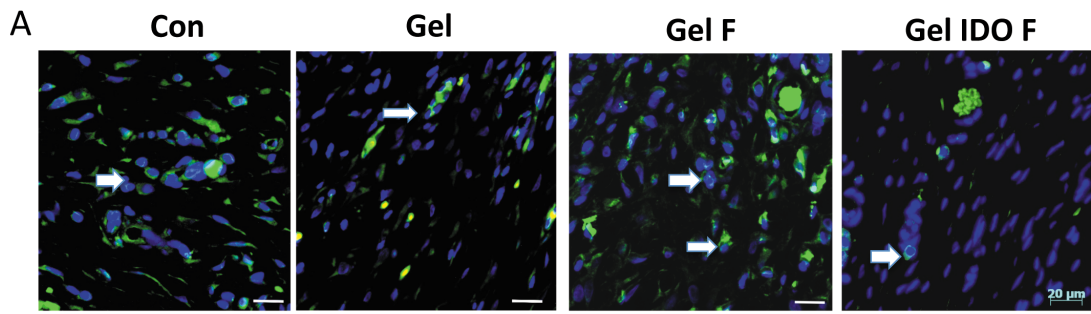


Figure 4.6. CD3⁺ lymphocyte and CD31⁺ (platelet cell adhesion molecule) marked vessel formation in treated rabbit tissue.

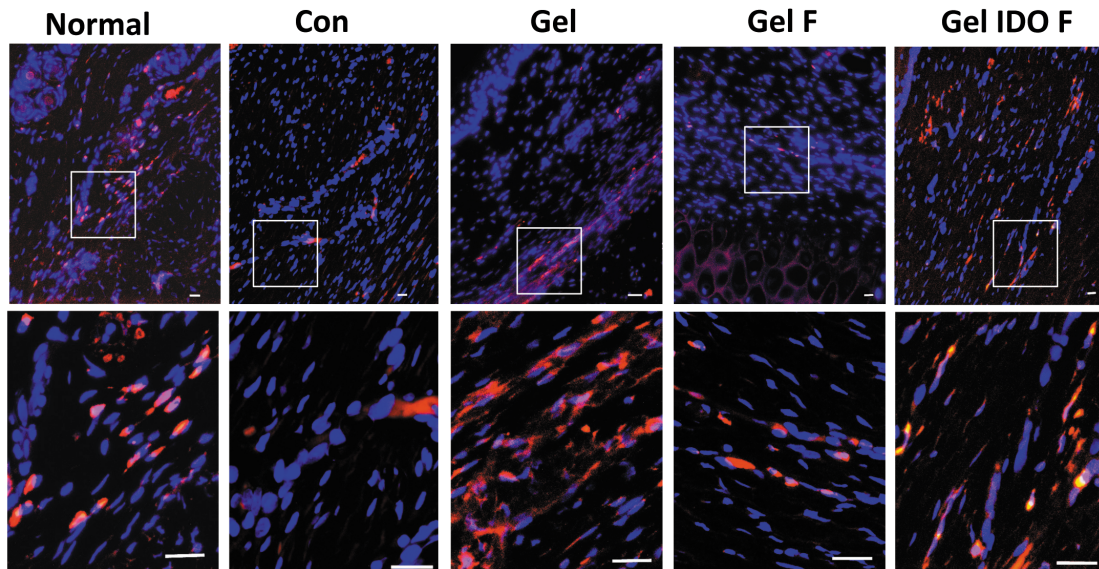
(A/C) Photomicrographs and corresponding quantification of CD3⁺ lymphocyte (pan-lymphocyte marker) infiltration into the wounded area represented as the

number of cells per high-powered field as denoted by white arrows (n=8). (B/D) Photomicrographs and corresponding quantification of vessel formation within the treated wounds. (n=8; p<0.05) (scale bars represent 50µm)

4.3.6 CD31⁺ immunostaining and vessel-like structures within healed wounds

Perfusion of a tissue or graft through angiogenesis is essential for oxygenation and nutrient flow (144, 145). Vessel formation was identified with immunofluorescence staining of CD31 (a specific endothelial cell marker) and confirming both cellular organization and structure (Figure 4.6.B). The CD31 and vessel architecture was significantly higher in the Gel and Gel IDOF treatment groups compared to the other treatments (4±1 and 6±1 vessels respectively per hpf, p<0.05; Figure 4.6.D).

A



B

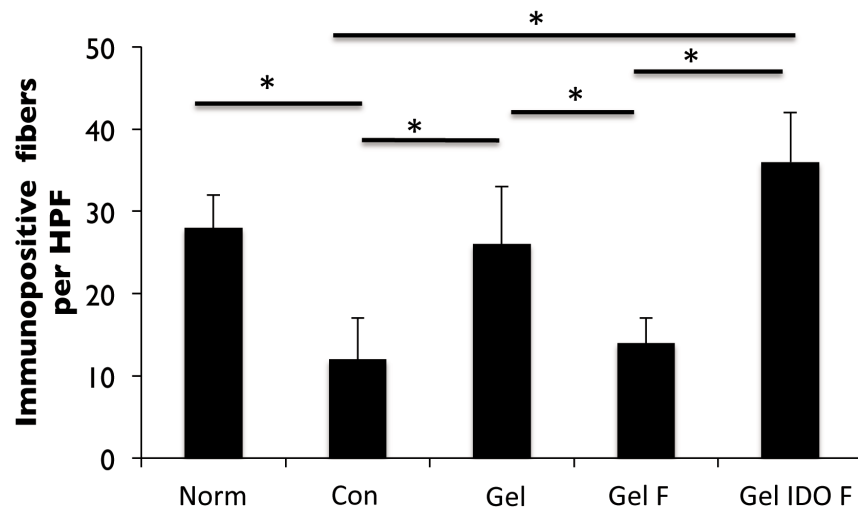


Figure 4.7. Distribution and quantification of cutaneous neoinnervation within the treated wound tissues 35 days post-surgery.

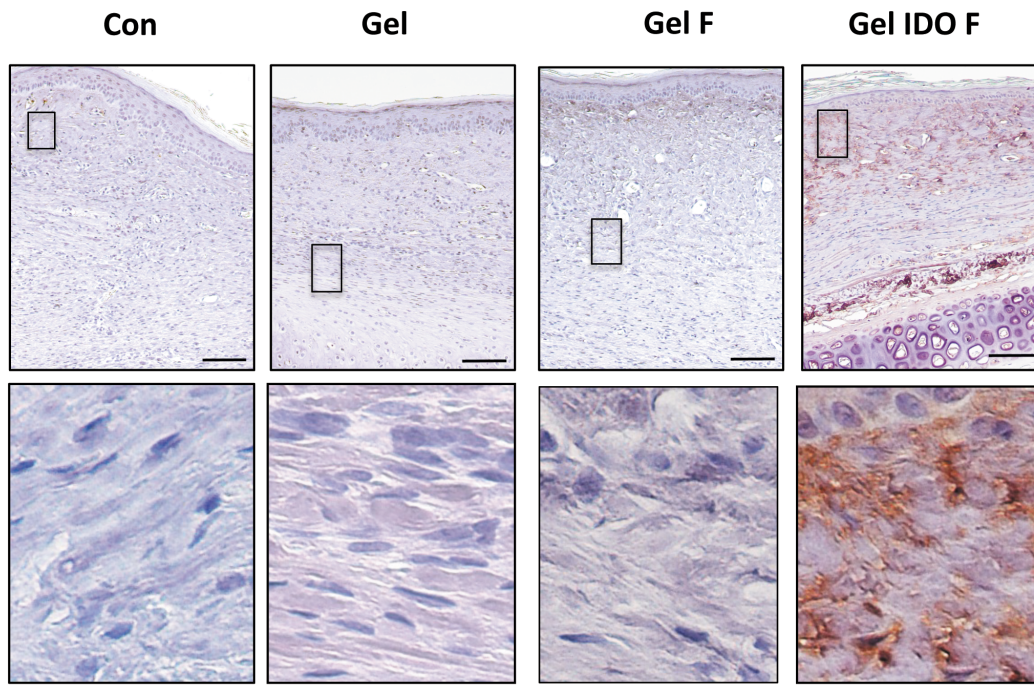
(A) Photomicrograph representation of panaxonal marker PGP 9.5, ubiquitin carboxy terminal hydrolase1) (red) in tissue sections display peripheral nerve

fiber formation. White boxes correspond to the lower panel images representing staining specificity. (B) Quantification of fiber density is represented by number of immunopositive fibers per high-powered field (n=8, p<0.05) Scale bar= 100 μ m.

4.3.7 Cutaneous innervation

Rabbit tissue from Day 35 was stained for PGP 9.5 (ubiquitin hydrolase), a panaxonal marker for ganglia and nerve sheath development and standard marker for intra-epidermal nerve fibers, including Langherans cells (146). All wounds treated with the Gel exhibited structural formation of innervated fiber-like structures within the neo-dermis (Figure 4.7.A-B). This was matched with both appendages and vascular structures that typically are associated with innervated structures. Gel and Gel IDOF treated wounds demonstrated significantly more innervation (26 \pm 6 and 36 \pm 6 immunoreactive fibers (IRF)/high power field (hpf)) than other treatments (Con 12 \pm 5 and GelF 14 \pm 3 IRF/hpf) and resembled that of normal skin (28 \pm 4 IRF/hpf). Gel alone was found to have a greater number of innervated structures than the GelF treated wounds and more closely reflects unwounded skin.

A



B

Day (post transfection)	Kynurenine (ug/mL)
1	2.76
3	13.69
6	14.36
9	17.26
12	18.08

Figure 4.8. Validation of IDO expression in transplanted fibroblasts.

(A) Detection of kynurenine in cell media of transfected fibroblasts. (B) Immunostaining of IDO in treated rabbit wounds of Gel IDOF administered scaffolds. Anti-human IDO (1:500/ incubation overnight at 4°C) (Abcam, USA) and Vector ‘ABC’ biotinylated polyclonal antibody (45 min at RT) (Vector Labs,

Canada) was used to detect IDO in tissue sections in conjunction with a 1,2-Diacetylbenzene chromophore (DAB).

4.4 Discussion

Wound healing requires a lengthy orchestrated sequence of biological events and any deviation in this process results in either over-healing or lack thereof. In this study we sought improve wound healing outcome by the application of a novel hydrogel-collagen scaffold that can be used to fabricate a skin substitute *in-situ* and integrate with all aspects of the wound bed. In principle, this solution seeks to also circumvent several issues with current solid scaffolds and engineered skin substitutes (15, 122, 130, 132, 133). It is well known that timely biological wound coverage has a direct impact on healing outcome. Wounds that remain open for greater than 21 days are likely to result in hypertrophy and excessive scarring, in addition to becoming susceptible to infection, water and heat loss (12, 130, 147). In our previous works we have demonstrated the benefit of using an Indoleamine 2,3 dioxygenase (IDO) expressing fibroblast as an allo/xeno-transplant that will be tolerated by the recipient (34, 37, 81). In the present study we constructed a skin substitute *in-situ*, with and without IDO expressing fibroblasts, which conferred greater feasibility for clinical application over previous works. Through the combination of a partially crosslinked hydrogel-collagen biohybrid system we are able to rapidly decrease the gelation time of the scaffold. Consistent with our previous work, the addition of a PVA hydrogel to the collagen network lends it self to produce a tacky rapidly forming scaffold that is easily applied to the wound bed without compromising cell viability (Figure 4.1.B & 4.8.a) (62, 140). It was previously demonstrated that PVA-hydrogel addition to the collagen composite produces a tacky scaffold, improves the gelation rate and mechanical stiffness (62) similarly to chondroitin-6-sulfate (33), which we found to be optimal for surgical application. The utility of this hydrogel blend is currently being explored to understand the molecular interactions that are provisional for the rapid gelation of the bio-hybrid system. Unlike other

animals, rabbit ear skin heals through secondary intention (similar to humans), as opposed to contracture due to the lack of the panniculus carnosus. If the dermis is not replaced in a timely manner, by engraftment or skin substitute, hypertrophy occurs likely due to the slow epithelialization process and prolonged fibroproliferative period (17). Application of the Gel, alone, significantly reduced scar formation resulting in a neodermis within which adjacent cells could infiltrate. In order to fabricate a patient-ready skin substitute we investigated the application of the *in situ* forming scaffold comprising IDO-expressing fibroblasts. In practice, our method could employ the use of harvested autologous cells (i.e. skin or adipose derived) as opposed to allogeneic and/or transduced cells. The utility of the scaffold as a cell delivery vehicle markedly reduced the days required for the fabrication of a fibroblast-populated scaffold (typically 7-14 days) using pre-formed solid scaffolds (34). Gel IDOF further improved the healing outcome through a reduction in SEI, ET, DT and cellularity when compared to GelF and untreated wounds. Notably the acellular *in-situ* forming hydrogel collagen-GAG scaffolds also provided significant improvements to wound healing outcome. Although acellular *in situ* forming scaffold is advantageous for the smaller acute wounds, the additional growth factor and immunomodulatory support from IDO expressing fibroblasts is opportune to improve healing outcome of the non-healing wounds or large burn wounds (12, 130, 148).

IDO expressing fibroblasts were easily combined with the *in situ* forming scaffold in the surgical suite prior to applying it to the wound. As expected GelF elicited an inflammatory response, which likely further exacerbated the fibroproliferative response despite the presence of the *in situ* forming hydrogel collagen-GAG scaffold. Importantly, our results herein correspond with previous studies demonstrating the efficacy of IDO to protect allo/xenogenic grafts and reduce scarring (34, 37, 81), assuming that necessary steps are taken to mitigate risks of disease transmission. Earlier studies on the *in-situ* forming scaffold identified that cells cultured within the scaffolds would align in a parallel arrangement, possibly in-line with fibers (62). The defined cellular organization did not occur

throughout the entirety of treated wounds, yet was prominent in the hypodermis and mid dermal sections closest to the cartilage (Figure 4.3.E-H). Two reasons for the lack of cellular alignment throughout the dermis could be that: 1) during remodeling cells will alter the architecture of the dermis, or 2) that the scaffold is reduced to a thinner layer that is subsequently covered with an endogenous neo-dermis. Although GelF became hypertrophic as expected, the extent of the hypertrophy appeared less than in our previous work using solid, pre-made skin substitutes (34). It is possible that because the number of transplanted cells, including the lack of highly antigenic keratinocytes is less than what was employed previously, the immune response is also reduced. This improved reduction in the infiltrated immune cell response would be similar to what we have observed through the use of the graft in islet transplantation models (81).

Surgical engraftment of engineered skin and even acellular scaffolds is often burdened by the lack of vasculature in the graft and in the later stages, a restorative lack of functional innervation. For many patients impaired re-innervation within a healed wound site can lead to idiopathic hypersensitivity and itchiness (149). It has been reported that neovascularization, which is only suggestive of a perfused tissue, can occur as early as 14 days following engraftment in human (144, 145). The application of a thin layer-by-layer scaffold may minimize hypoxia which has previously been shown to be detrimental for tissue reconstruction (145). As was demonstrated previously, IDO expression exhibited increased mature vessel formation compared to untreated and non-IDO expressing fibroblast engraftment (37, 150). Similarly it was found that both Gel alone and Gel IDOF treated wounds exhibited a greater abundance of immunoreactive nerve fibers within the hypodermis. It is unclear what type of peripheral nerve fiber (i.e. efferent or afferent, and subtypes) has resulted and whether or not a functional nerve network will result; however the distribution of the fibers suggests that the outcome is similar to normal tissue. Although PGP 9.5 is generally accepted as a neuronal-cell marker, it should be cautioned that recent evidence has discovered PGP 9.5 on other cell types (151). Further work

is warranted to investigate both neovascularization within early time points, modeling vascular perfusion, and long-term nerve functionality.

Typically grafted wounds will exhibit contracture at the margins (11). In order to correlate our *in vivo* findings to human tissue, scaffolds containing both human scar derived fibroblasts and normal fibroblasts were evaluated for contractility. Results demonstrated that our *in-situ* forming scaffold could withstand the contractile tendency of normal and hypertrophic fibroblast. Although it is known that fibroblasts from hypertrophic scars exhibit different phenotypic characteristics than normal cells, it was not expected that within the free-floating scaffolds they would exhibit reduced contraction when compared to normal, neonatal foreskin fibroblasts. It is well known that fibroblasts from young patients exhibit a more proliferative and active cell type (fetal being the most active), which may in part explain why we observed greater contractility when using neonatal fibroblasts (152).

4.5 Conclusion

This study demonstrates for the first time the application of a non-rejectable, *in situ* forming scaffold for skin engineering. Our approach offers a promising practice to reduce the logistical and physiological hurdles that are associated with current modalities. The findings herein underscore the advantages and utility of our *in-situ* gelling scaffold to be used in conjunction with non-rejectable, IDO expressing cells in order to create a patient-ready skin substitute at the bedside.

5 Applications of a reconstitutable matrix for in-situ tissue engineering strategies and suggestions for future work⁴

5.1 General discussion

Tissue engineering has gained significant traction over the last decade with examples of skin allograft engineering, the first engineered trachea transplant, heart cell transplants and islet transplantation for type 1 diabetics, among many others (14, 18, 54, 81, 153). Previous chapters described the use of collagen gel-mixtures comprising a PVA-based hydrogel that would in turn result in a solid, gel-like scaffold within minutes when heated to 37°C. This scaffold has the added benefit that it can be reconstituted from a powder form with water, without neutralization or additional reagents. Comparatively, dermal fillers and injectable gels, often composed of crosslinked hyaluronic acid or collagen, can achieve similar results; however, unlike our collagen-PVA hybrid, they are unable to completely solidify into a form that resembles a pre-formed solid scaffold.

The engineering of a tissue *inside* the human body (*in situ*) is not a novel concept. *In situ*-tissue engineering has largely been driven by cell transplantation methods. Islet transplantation is a prime example of the potential success of cell transplantation. Aside from the immunosuppressant medications, one of the major pitfalls is the lack of matrix (scaffold) for the transplanted islets. Previously, we demonstrated that islets (a mass of cells) are more viable when cultured within the PVA-collagen biohybrid than when cultured on a plate surface, and even more viable when combined with fibroblasts (81, 140). The resulting composite scaffold in fact better resembles a pancreas than the injection of free-islets into the portal vein. This strategy requires the islets to be transplanted within the collagen biohybrid scaffold and placed under the kidney capsule. Islets transplanted using the PVA-collagen biohybrid resembled that of normal

⁴ As described in the Preface, a version of this work has been published in:140. Azadeh Hosseini-Tabatabaei RBJ, Ryan Hartwell, Sanam Salimi, Ruhangiz T. Kilani, Aziz Ghahary. Embedding Islet in a liquid scaffold increases islet viability and function. Canadian Journal of Diabetes. 2013;37 (1):27-35.

pancreatic islets 100 days post-transfection, whereas islets transplanted in a simple collagen gel did not.

The same philosophy of using the reconstitutable biohybrid scaffold to create an ECM niche for islets within the body applies to other cell transplant modalities as well. The woundcare product Recell™ uses a simple trypsinization procedure to isolate cells from a punch biopsy of skin and create expansive wound coverage for burn patients. It has been well established that without the application of cells, a large surface area of skin cannot be repaired through the normal repair process; however, like free-islet transplantation, the cells are sprayed onto the wound without matrix. In this final chapter I conclude by describing the possible application of the reconstitutable system as a cell transplantation vehicle and the opportunity to advance other tissue engineering applications, modalities and research.

5.2 Suggestions for future work

This thesis has described a collagen-based matrix that, using simple processing techniques, can be combined with regulatory approved reagents to fabricate a reconstitutable scaffold system. The combination of collagen with PVA hydrogels, ideally PVA-PEG (Kollicoat®) produces a rapidly forming extracellular matrix that can be easily combined with cells to form a cell-populated skin substitute. As the lyophilized powder has already been neutralized it can easily be combined with water or other aqueous solvent, such as plasma, to produce a nutrient-tailored medium. Although this thesis demonstrates a *proof-of-principle*, further work is required to fully appreciate the extent of which the technology can improve upon current wound care and tissue engineered modalities. The following underscore the areas with which further research is suggested:

- i. In Chapter 2, I evaluated the utility of combining PVA within collagen to improve mechanical characteristics and biocompatibility (with a wide range of cell types) of engineered skin. The study suggested that cell

- morphology and organization more appropriately resembled that of normal tissue. As this was the initial *proof of principle* work, there is no suggested future work required.
- ii. In Chapter 3, I further evaluated the utility of PVA in the optimization of a fully reconstitutable scaffold system. In this Chapter I looked at PVA variants, such as PVA-PEG, and the ability of these agents to reduce the activation energy of type 1 bovine collagen in order to produce a rapidly gelling collagen scaffold. The idea of using PVA to improve the kinetics initially stemmed from 1) the surfactant nature of the polymer and 2) it's thickening capabilities when combined with borates. It would be advantageous to investigate the mechanism in which PVA and other surfactant-like polymers interact with collagen in order to improve gelation rate, stability and cell morphology. This exploration could be useful toward understanding the cell-scaffold interface as it pertains to implants in general (i.e. breast and bone). Furthermore, it would be worthwhile to explore the use of other collagen sources, such as marine based biomaterials.
 - iii. In Chapter 4, I further demonstrated the benefit of the biohybrid scaffold system as a means to generate in situ forming allogeneic scaffolds on full thickness fibrotic wounds. The full thickness wounds in the rabbit ear become fibrotic due to the lack of muscle-driven contracture. As a result the wounds remain open for longer, similar to a chronic wound, yet develop a robust scar. Scar formation could be mitigated simply by application of the biohybrid. Currently chronic wounds, pressure ulcers and diabetic ulcers present the largest expenditure by wound type within wound care (14, 18). Further research is warranted to explore the use of this reconstitutable system in these wounds. The splinted wound model would be a good model to determine the utility of the scaffold under chronic, non-contractile healing conditions.

- iv. Future work should focus on the fabrication of a *low cost, patient ready skin substitute kit*. The generation of a non-rejectable patient ready skin substitute kit could prevent scarring, preserve neighbouring tissue and promote recovery in patients burdened by complicated wounds. Here we propose the development of a skin substitute system that can be fabricated with or without cells at the bedside, fill a wound and completely integrate with the tissue surfaces. Future investigations should consider examining the combination of scaffold with platelet rich plasma (PRP) and adipocytes to determine if these classical modalities can be further enhanced. Commercially available skin substitutes have offered a biological fix to complicated wounds, but have an array of pitfalls. These include cost, logistics and integration with the wound bed, otherwise known as graft-take. *The technology described herein lends itself to a low cost manufacturing process (2-steps) and comprises low cost materials (collagen and simple polymers). The stability of the lyophilized powder is superior to hydrated materials, such as hydrogels and cellular skin substitutes, and the ability to reconstitute the powder into a scaffold that can mold to the wound site (with or without cells) confers greater utility over commercially available skin substitutes at present.* Moving down the development pipeline we foresee that the addition of either autologous cells (using a punch biopsy or fat-cell harvest) or genetically modified non-rejectable cells could render a cellular, patient ready skin substitute. *The benefit is simple: accessible tissue replacement in minutes.*

Bibliography

1. Locono JA, Ehrlich HP, Gottrup F, Leaper PJ. In: Wounds. Eds. 1998:10-22.
2. Hinz B, Dugina V, Ballestrem C, Wehrle-Haller B, Chaponnier C. Alpha-smooth muscle actin is crucial for focal adhesion maturation in myofibroblasts. *Molecular biology of the cell*. 2003;14(6):2508-19.
3. Hinz B, Mastrangelo D, Iselin CE, Chaponnier C, Gabbiani G. Mechanical tension controls granulation tissue contractile activity and myofibroblast differentiation. *The American journal of pathology*. 2001;159(3):1009-20.
4. Terkeltaub RA GM. The molecular and Cellular biology of wound repair. 1 ed. Clark RA, editor. New York, NY: Springer US; 1988.
5. Nemeth GG BM, Martin GR. Growth factors and other aspects of wound healing clinical implications. 1988:1-17.
6. Johnston RB, Weedon D. Weedon's skin pathology essentials: Elsevier Churchill Livingstone; 2012. viii, 784 p. p.
7. Coulombe P. Towards a molecular definition of keratinocyte activation after acute injury to stratified epithelia. *Biochem Biophys Res Commun*. 1997;236:231-8.
8. Gniadecki R. Regulation of keratinocyte proliferation. *Gen Pharmac*. 1998;30(5):6119-622.
9. McCarty SM, Cochrane CA, Clegg PD, Percival SL. The role of endogenous and exogenous enzymes in chronic wounds: a focus on the implications of aberrant levels of both host and bacterial proteases in wound healing. *Wound Repair Regen*. 2012;20(2):125-36.
10. Ghahary A, Ghaffari A. Role of keratinocyte-fibroblast cross-talk in development of hypertrophic scar. *Wound Repair Regen*. 2007;15 Suppl 1:S46-53.
11. Curran TA, Ghahary A. Evidence of a role for fibrocyte and keratinocyte-like cells in the formation of hypertrophic scars. *J Burn Care Res*. 2013;34(2):227-31.
12. Medina A, Scott PG, Ghahary A, Tredget EE. Pathophysiology of chronic nonhealing wounds. *J Burn Care Rehabil*. 2005;26(4):306-19.
13. Park SA, Raghunathan VK, Shah NM, Teixeira L, Motta MJ, Covert J, et al. PDGF-BB does not accelerate healing in diabetic mice with splinted skin wounds. *PLoS one*. 2014;9(8):e104447.
14. FDA. Skin Substitutes for Treating Chronic Wounds. In: FDA, editor. Technology Assessment: FDA; 2011.
15. UILO. Skin Tissue Engineering. Vancouver: University of British Columbia, 2012 2012. Report No.: HLC101A_S003.
16. Margolis DJ, Malay DS, Hoffstad OJ, Leonard CE, MaCurdy T, de Nava KL, et al. Incidence of Diabetic Foot Ulcer and Lower Extremity Amputation Among Medicare Beneficiaries, 2006 to 2008: Data Points #2. *Data Points Publication Series* 2011.
17. Ghahary A, Karami-Busheri F, Marcoux Y, Li Y, Tredget EE, Kilani RT, et al. Keratinocyte-releasable stratifin functions as a potent collagenase-stimulating factor in fibroblasts. *J Invest Dermatol*. 2004;122:1188-97.

18. Crandall MA. World Wound Care Markets 2. publication. New York: 2010
2010. Report No.
19. FDA. Technology Assessment: Skin substitutes for treating chronic wounds.: FDA Publication Agency for Healthcare; 2011.
20. Gainer K. Regenerative medicines: Bone and joint applications. Wellesly, Mass.: 2013 PHM032C.
21. Shevchenko RV, James SL, James SE. A review of tissue-engineered skin bioconstructs available for skin reconstruction. *J R Soc Interface*. 2009;7(43):229-58.
22. OMJ Pharmaceuticals I. Product Monograph: Regranex. FDA2008.
23. Wang X, You C, Hu X, Zheng Y, Li Q, Feng Z, et al. The roles of knitted mesh-reinforced collagen-chitosan hybrid scaffold in the one-step repair of full-thickness skin defects in rats. *Acta Biomater*. 2013;9(8):7822-32.
24. Wang L, Stegemann JP. Thermogelling chitosan and collagen composite hydrogels initiated with beta-glycerophosphate for bone tissue engineering. *Biomaterials*. 2010;31(14):3976-85.
25. Gao L, Gan H, Meng Z, Gu R, Wu Z, Zhang L, et al. Effects of genipin cross-linking of chitosan hydrogels on cellular adhesion and viability. *Colloids and surfaces B, Biointerfaces*. 2014;117:398-405.
26. Yildirimer L, Thanh NT, Seifalian AM. Skin regeneration scaffolds: a multimodal bottom-up approach. *Trends in biotechnology*. 2012;30(12):638-48.
27. Zhong SP, Zhang YZ, Lim CT. Tissue scaffolds for skin wound healing and dermal reconstruction. *Wiley interdisciplinary reviews Nanomedicine and nanobiotechnology*. 2010;2(5):510-25.
28. Chae T, Yang H, Leung V, Ko F, Troczynski T. Novel biomimetic hydroxyapatite/alginate nanocomposite fibrous scaffolds for bone tissue regeneration. *Journal of materials science Materials in medicine*. 2013;24(8):1885-94.
29. Leung V, Hartwell R, Elizei SS, Yang H, Ghahary A, Ko F. Postelectrospinning modifications for alginate nanofiber-based wound dressings. *Journal of biomedical materials research Part B, Applied biomaterials*. 2014;102(3):508-15.
30. Chung EJ, Ju HW, Park HJ, Park CH. Three-layered scaffolds for artificial esophagus using poly(varepsilon-caprolactone) nanofibers and silk fibroin: An experimental study in a rat model. *Journal of biomedical materials research Part A*. 2014.
31. Dalton PD, Joergensen NT, Groll J, Moeller M. Patterned melt electrospun substrates for tissue engineering. *Biomedical materials*. 2008;3(3):034109.
32. Sham A, Martinez EC, Beyer S, Trau DW, Raghunath M. Incorporation of a prolyl hydroxylase inhibitor into scaffolds: a strategy for stimulating vascularization. *Tissue engineering Part A*. 2014.
33. Kinneberg KR, Nirmalanandhan VS, Juncosa-Melvin N, Powell HM, Boyce ST, Shearn JT, et al. Chondroitin-6-sulfate incorporation and mechanical stimulation increase MSC-collagen sponge construct stiffness. *Journal of orthopaedic research : official publication of the Orthopaedic Research Society*. 2010;28(8):1092-9.

34. Chavez-Munoz C, Hartwell R, Jalili RB, Carr M, Kilani RT, Jafarnejad SM, et al. Application of an indoleamine 2,3-dioxygenase-expressing skin substitute improves scar formation in a fibrotic animal model. *J Invest Dermatol.*132(5):1501-5.
35. Powell HM, Boyce ST. Engineered Human Skin Fabricated Using Electrospun Collagen-PCL Blends: Morphogenesis and Mechanical Properties. *Tissue Eng Part A.* 2009.
36. Boyce ST. Design principles for composition and performance of cultured skin substitutes. *Burns.* 2001;27(5):523-33.
37. Forouzandeh F, Jalili RB, Hartwell RV, Allan SE, Boyce S, Supp D, et al. Local expression of indoleamine 2,3-dioxygenase suppresses T-cell-mediated rejection of an engineered bilayer skin substitute. *Wound Repair Regen.*18(6):614-23.
38. Chavez-Munoz C, Nguyen KT, Xu W, Hong SJ, Mustoe TA, Galiano RD. Transdifferentiation of adipose-derived stem cells into keratinocyte-like cells: engineering a stratified epidermis. *PloS one.* 2013;8(12):e80587.
39. Jansen LA, De Caigny P, Guay NA, Lineaweaver WC, Shokrollahi K. The evidence base for the acellular dermal matrix AlloDerm: a systematic review. *Annals of plastic surgery.* 2013;70(5):587-94.
40. Al-Abboodi A, Fu J, Doran PM, Tan TT, Chan PP. Injectable 3D hydrogel scaffold with tailorable porosity post-implantation. *Advanced healthcare materials.* 2014;3(5):725-36.
41. Cheung HK, Han TT, Marecak DM, Watkins JF, Amsden BG, Flynn LE. Composite hydrogel scaffolds incorporating decellularized adipose tissue for soft tissue engineering with adipose-derived stem cells. *Biomaterials.* 2014;35(6):1914-23.
42. Wang LS, Du C, Chung JE, Kurisawa M. Enzymatically cross-linked gelatin-phenol hydrogels with a broader stiffness range for osteogenic differentiation of human mesenchymal stem cells. *Acta Biomater.* 2012;8(5):1826-37.
43. Akhtar N, Marlow R, Lambert E, Schatzmann F, Lowe ET, Cheung J, et al. Molecular dissection of integrin signalling proteins in the control of mammary epithelial development and differentiation. *Development.* 2009;136(6):1019-27.
44. Fthenou E, Zafiroopoulos A, Katonis P, Tsatsakis A, Karamanos NK, Tzanakakis GN. Chondroitin sulfate prevents platelet derived growth factor-mediated phosphorylation of PDGF-Rbeta in normal human fibroblasts severely impairing mitogenic responses. *J Cell Biochem.* 2008;103(6):1866-76.
45. Junker JP, Kratz C, Tollback A, Kratz G. Mechanical tension stimulates the transdifferentiation of fibroblasts into myofibroblasts in human burn scars. *Burns.* 2008;34(7):942-6.
46. Lee PH, Trowbridge JM, Taylor KR, Morhenn VB, Gallo RL. Dermatan sulfate proteoglycan and glycosaminoglycan synthesis is induced in fibroblasts by transfer to a three-dimensional extracellular environment. *J Biol Chem.* 2004;279(47):48640-6.
47. Pawlina MHRaW. *Histology: a text and atlas.* 5th ed. Baltimore, MD: Lippincott Williams & Wilkins; 2006. 906 p.

48. Webber J, Meran S, Steadman R, Phillips A. Hyaluronan orchestrates transforming growth factor-beta1-dependent maintenance of myofibroblast phenotype. *J Biol Chem*. 2009;284(14):9083-92.
49. Georges PC, Miller WJ, Meaney DF, Sawyer ES, Janmey PA. Matrices with compliance comparable to that of brain tissue select neuronal over glial growth in mixed cortical cultures. *Biophysical journal*. 2006;90(8):3012-8.
50. Silver Frederick H. SGP, Freeman Joseph W., Devore Dale. Viscoelastic properties of young and old human dermis: A proposed molecular mechanism for elastic energy storage in collagen and elastin. *Journal of applied polymer science* 2002;86(8):1978-85.
51. Zahouani H, Pailler-Mattei C, Sohm B, Vargiolu R, Cenizo V, Debret R. Characterization of the mechanical properties of a dermal equivalent compared with human skin in vivo by indentation and static friction tests. *Skin Res Technol*. 2009;15(1):68-76.
52. Boccafoschi F, Ramella M, Sibillano T, De Caro L, Giannini C, Comparelli R, et al. Human elastin polypeptides improve the biomechanical properties of three-dimensional matrices through the regulation of elastogenesis. *Journal of biomedical materials research Part A*. 2014.
53. Li J, Chen J, Kirsner R. Pathophysiology of acute wound healing. *Clin Dermatol*. 2007;25(1):9-18.
54. Turner R, Gerber D, Reid L. The Future of Cell Transplant Therapies: A Need for Tissue Grafting. *Transplantation*.
55. Tan H, Marra, Kacey G. . Injectable, Biodegradable Hydrogels for Tissue Engineering Applications. *Materials*. 2010;3(3):1746-67.
56. Kadler KE, Baldock C, Bella J, Boot-Handford RP. Collagens at a glance. *Journal of cell science*. 2007;120(Pt 12):1955-8.
57. Grisham RHGaCM. *Biochemistry*. 3rd ed. CA, USA: Thomson Learning Inc.; 2005. 169-71 p.
58. Gautieri A, Uzel S, Vesentini S, Redaelli A, Buehler MJ. Molecular and mesoscale mechanisms of osteogenesis imperfecta disease in collagen fibrils. *Biophysical journal*. 2009;97(3):857-65.
59. Jenkins CL, Raines RT. Insights on the conformational stability of collagen. *Natural product reports*. 2002;19(1):49-59.
60. Kar K, Wang YH, Brodsky B. Sequence dependence of kinetics and morphology of collagen model peptide self-assembly into higher order structures. *Protein science : a publication of the Protein Society*. 2008;17(6):1086-95.
61. Ushiki T. Collagen fibers, reticular fibers and elastic fibers. A comprehensive understanding from a morphological viewpoint. *Archives of histology and cytology*. 2002;65(2):109-26.
62. Hartwell R, Leung V, Chavez-Munoz C, Nabai L, Yang H, Ko F, et al. A novel hydrogel-collagen composite improves functionality of an injectable extracellular matrix. *Acta Biomater*.7(8):3060-9.
63. Alyssa Panitch JEP, Kinam Park, Katherine Stuart, Steve Higbee, inventor; Purdue Research Foundation, assignee. Collagen-binding synthetic peptidoglycans, preparation, and methods of use. USA patent US20110020298 A1. 2011.

64. Li Y. The Mechanism of Collagen self-assembly: hydrophobic and electrostatic interactions [Dissertation]. Florida: Univeristy of Florida; 2009.
65. Kita M, Ogura Y, Honda Y, Hyon SH, Cha W, 2nd, Ikada Y. Evaluation of polyvinyl alcohol hydrogel as a soft contact lens material. *Graefes Arch Clin Exp Ophthalmol*. 1990;228(6):533-7.
66. Mishra S, Bajpai R, Katare R, Bajpai AK. Preparation, characterization and microhardness study of semi interpenetrating polymer networks of polyvinyl alcohol and crosslinked polyacrylamide. *Journal of materials science Materials in medicine*. 2006;17(12):1305-13.
67. Cui Q, Ward Muscatello MM, Asher SA. Photonic crystal borax competitive binding carbohydrate sensing motif. *The Analyst*. 2009;134(5):875-80.
68. Menon JU, Kona S, Wadajkar AS, Desai F, Vadla A, Nguyen KT. Effects of surfactants on the properties of PLGA nanoparticles. *Journal of biomedical materials research Part A*. 2012;100(8):1998-2005.
69. Turk CT, Oz UC, Serim TM, Hascicek C. Formulation and optimization of nonionic surfactants emulsified nimesulide-loaded PLGA-based nanoparticles by design of experiments. *AAPS PharmSciTech*. 2014;15(1):161-76.
70. Carretti E, Grassi S, Cossalter M, Natali I, Caminati G, Weiss RG, et al. Poly(vinyl alcohol)-borate hydro/cosolvent gels: viscoelastic properties, solubilizing power, and application to art conservation. *Langmuir : the ACS journal of surfaces and colloids*. 2009;25(15):8656-62.
71. Murphy DJ, Sankalia MG, Loughlin RG, Donnelly RF, Jenkins MG, PA MCC. Physical characterisation and component release of poly(vinyl alcohol)-tetrahydroxyborate hydrogels and their applicability as potential topical drug delivery systems. *International journal of pharmaceutics*. 2012;423(2):326-34.
72. Murphy KP, Travers P, Walport M, Janeway C. *Janeway's immunobiology*. 8th ed. New York: Garland Science; 2012. xix, 868 p.
73. Black JP, Sefton MV. Complement activation by PVA as measured by ELIFA (enzyme-linked immunoflow assay) for SC5b-9. *Biomaterials*. 2000;21(22):2287-94.
74. Coutu DL, Yousefi AM, Galipeau J. Three-dimensional porous scaffolds at the crossroads of tissue engineering and cell-based gene therapy. *J Cell Biochem*. 2009;108(3):537-46.
75. Walsh S, Midha R. Practical considerations concerning the use of stem cells for peripheral nerve repair. *Neurosurg Focus*. 2009;26(2):E2.
76. Van Tomme SR, Storm G, Hennink WE. In situ gelling hydrogels for pharmaceutical and biomedical applications. *Int J Pharm*. 2008;355(1-2):1-18.
77. Duan X, McLaughlin C, Griffith M, Sheardown H. Biofunctionalization of collagen for improved biological response: scaffolds for corneal tissue engineering. *Biomaterials*. 2007;28(1):78-88.
78. McLaughlin CR, Acosta MC, Luna C, Liu W, Belmonte C, Griffith M, et al. Regeneration of functional nerves within full thickness collagen-phosphorylcholine corneal substitute implants in guinea pigs. *Biomaterials*. 31(10):2770-8.

79. Suuronen EJ, McLaughlin CR, Stys PK, Nakamura M, Munger R, Griffith M. Functional innervation in tissue engineered models for in vitro study and testing purposes. *Toxicol Sci.* 2004;82(2):525-33.
80. Powell HM, Boyce ST. EDC cross-linking improves skin substitute strength and stability. *Biomaterials.* 2006;27(34):5821-7.
81. Jalili RB, Forouzandeh F, Rezakhanlou AM, Hartwell R, Medina A, Warnock GL, et al. Local expression of indoleamine 2,3 dioxygenase in syngeneic fibroblasts significantly prolongs survival of an engineered three-dimensional islet allograft. *Diabetes.* 2010;59(9):2219-27.
82. Qi Z, Shen Y, Yanai G, Yang K, Shirouzu Y, Hiura A, et al. The in vivo performance of polyvinyl alcohol macro-encapsulated islets. *Biomaterials.*31(14):4026-31.
83. Zheng L, Ao Q, Han H, Zhang X, Gong Y. Evaluation of the chitosan/glycerol-beta-phosphate disodium salt hydrogel application in peripheral nerve regeneration. *Biomed Mater.*5(3):35003.
84. Fitzpatrick SD, Jafar Mazumder MA, Lasowski F, Fitzpatrick LE, Sheardown H. PNIPAAm-grafted-collagen as an injectable, in situ gelling, bioactive cell delivery scaffold. *Biomacromolecules.*11(9):2261-7.
85. Chiellini E, Cinelli P, Grillo Fernandes E, Kenawy el RS, Lazzeri A. Gelatin-based blends and composites. Morphological and thermal mechanical characterization. *Biomacromolecules.* 2001;2(3):806-11.
86. Cho SH, Lim SM, Han DK, Yuk SH, Im GI, Lee JH. Time-dependent alginate/polyvinyl alcohol hydrogels as injectable cell carriers. *J Biomater Sci Polym Ed.* 2009;20(7-8):863-76.
87. Fikai M, Andronescu E, Fikai D, Voicu G, Fikai A. Synthesis and characterization of COLL-PVA/HA hybrid materials with stratified morphology. *Colloids Surf B Biointerfaces.*81(2):614-9.
88. Valentin JL, Lopez D, Hernandez R, Mijangos C, Saalwachter K. Structure of Poly(vinyl alcohol) Cryo-Hydrogels as Studied by Proton Low-Field NMR Spectroscopy. *Macromolecules.* 2009;42(1):263-72.
89. Ani Idris NAMZ, Mohd Suardi Suhaimi. Immobilization of Baker's yeast invertases in PVA-alginate matrix using innovative immobilization techniques. *Process biochemistry.* 2008(43):331-8.
90. Ramires PA, Milella E. Biocompatibility of poly(vinyl alcohol)-hyaluronic acid and poly(vinyl alcohol)-gellan membranes crosslinked by glutaraldehyde vapors. *J Mater Sci Mater Med.* 2002;13(1):119-23.
91. Li L, Beniash E, Zubarev ER, Xiang W, Rabatic BM, Zhang G, et al. Assembling a lasing hybrid material with supramolecular polymers and nanocrystals. *Nat Mater.* 2003;2(10):689-94.
92. Wang CC, Lu JN, Young TH. The alteration of cell membrane charge after cultured on polymer membranes. *Biomaterials.* 2007;28(4):625-31.
93. Valli M, Leonardi L, Strocchi R, Tenni R, Guizzardi S, Ruggeri A, et al. "In vitro" fibril formation of type I collagen from different sources: biochemical and morphological aspects. *Connect Tissue Res.* 1986;15(4):235-44.

94. Stuart K, Panitch A. Influence of chondroitin sulfate on collagen gel structure and mechanical properties at physiologically relevant levels. *Biopolymers*. 2008;89(10):841-51.
95. Cope AP. *Arthritis Research Methods and Protocols Volume 1*. Totowa, NJ: Humana Press Inc.; 2007. Available from: http://link.library.utoronto.ca/eir/EIRdetail.cfm?Resources_ID=967305&T=F.
96. Li M, Moeen Rezakhanlou A, Chavez-Munoz C, Lai A, Ghahary A. Keratinocyte-releasable factors increased the expression of MMP1 and MMP3 in co-cultured fibroblasts under both 2D and 3D culture conditions. *Mol Cell Biochem*. 2009;332(1-2):1-8.
97. Sarti B, Scandola M. Viscoelastic and thermal properties of collagen/poly(vinyl alcohol) blends. *Biomaterials*. 1995;16(10):785-92.
98. Nilasaroya A, Poole-Warren LA, Whitelock JM, Jo Martens P. Structural and functional characterisation of poly(vinyl alcohol) and heparin hydrogels. *Biomaterials*. 2008;29(35):4658-64.
99. Heng TS, Dudakov JA, Khong DM, Chidgey AP, Boyd RL. Stem cells--meet immunity. *J Mol Med*. 2009;87(11):1061-9.
100. Nuttelman CR, Mortisen DJ, Henry SM, Anseth KS. Attachment of fibronectin to poly(vinyl alcohol) hydrogels promotes NIH3T3 cell adhesion, proliferation, and migration. *J Biomed Mater Res*. 2001;57(2):217-23.
101. Ballios BG, Cooke MJ, van der Kooy D, Shoichet MS. A hydrogel-based stem cell delivery system to treat retinal degenerative diseases. *Biomaterials*. 31(9):2555-64.
102. Pederson AW, Ruberti JW, Messersmith PB. Thermal assembly of a biomimetic mineral/collagen composite. *Biomaterials*. 2003;24(26):4881-90.
103. Alina Sionkowska JS, Marcin Wisniewski. Photochemical stability of collagen/poly(vinylalcohol) blends. *Polymer Degradation and Stability*. 2004;83:117-25.
104. Barbani N, Cascone MG, Giusti P, Lazzeri L, Polacco G, Pizzirani G. Bioartificial materials based on collagen: 2. Mixtures of soluble collagen and poly(vinylalcohol) cross-linked with gaseous glutaraldehyde. *J Biomater Sci Polym Ed*. 1995;7(6):471-84.
105. Eming SA, Whitsitt JS, He L, Krieg T, Morgan JR, Davidson JM. Particle-mediated gene transfer of PDGF isoforms promotes wound repair. *J Invest Dermatol*. 1999;112(3):297-302.
106. Bader DL, Bowker P. Mechanical characteristics of skin and underlying tissues in vivo. *Biomaterials*. 1983;4(4):305-8.
107. Linge C, Richardson J, Vigor C, Clayton E, Hardas B, Rolfe K. Hypertrophic scar cells fail to undergo a form of apoptosis specific to contractile collagen--the role of tissue transglutaminase. *J Invest Dermatol*. 2005;125(1):72-82.
108. Ko CS, Huang JP, Huang CW, Chu IM. Type II collagen-chondroitin sulfate-hyaluronan scaffold cross-linked by genipin for cartilage tissue engineering. *J Biosci Bioeng*. 2009;107(2):177-82.

109. Barrett AJ, Knight CG, Brown MA, Tisljar U. A continuous fluorimetric assay for clostridial collagenase and Pz-peptidase activity. *Biochem J.* 1989;260(1):259-63.
110. Eberli D, Rodriguez S, Atala A, Yoo JJ. In vivo evaluation of acellular human dermis for abdominal wall repair. *J Biomed Mater Res A.*93(4):1527-38.
111. Prasertsung I, Kanokpanont S, Bunaprasert T, Thanakit V, Damrongsakkul S. Development of acellular dermis from porcine skin using periodic pressurized technique. *J Biomed Mater Res B Appl Biomater.* 2008;85(1):210-9.
112. Miyahara M, Hayashi K, Berger J, Tanzawa K, Njieha FK, Trelstad RL, et al. Formation of collagen fibrils by enzymic cleavage of precursors of type I collagen in vitro. *J Biol Chem.* 1984;259(15):9891-8.
113. Persikov AV, Ramshaw JA, Brodsky B. Prediction of collagen stability from amino acid sequence. *J Biol Chem.* 2005;280(19):19343-9.
114. Zhang X, Boot-Handford RP, Huxley-Jones J, Forse LN, Mould AP, Robertson DL, et al. The collagens of hydra provide insight into the evolution of metazoan extracellular matrices. *J Biol Chem.* 2007;282(9):6792-802.
115. Kretlow JD, Young S, Klouda L, Wong M, Mikos AG. Injectable biomaterials for regenerating complex craniofacial tissues. *Adv Mater.* 2009;21(32-33):3368-93.
116. Mahmood MEaA-K, Dhafer A.F. Effect of Temperature Changes on Critical Micelle Concentration for Tween Series Surfactant. *Global Journal of Science Frontier Research Chemistry.* 2013;13(4):1-7.
117. Fathima NN, Dhathathreyan A. Effect of surfactants on the thermal, conformational and rheological properties of collagen. *Int J Biol Macromol.* 2009;45(3):274-8.
118. Kim MH, Sawada Y, Taya M, Kino-Oka M. Influence of surface topography on the human epithelial cell response to micropatterned substrates with convex and concave architectures. *Journal of biological engineering.* 2014;8:13.
119. Mattila PK, Lappalainen P. Filopodia: molecular architecture and cellular functions. *Nature reviews Molecular cell biology.* 2008;9(6):446-54.
120. Balakrishnan B, Mohanty M, Umashankar PR, Jayakrishnan A. Evaluation of an in situ forming hydrogel wound dressing based on oxidized alginate and gelatin. *Biomaterials.* 2005;26(32):6335-42.
121. Meng X, Stout DA, Sun L, Beingessner RL, Fenniri H, Webster TJ. Novel injectable biomimetic hydrogels with carbon nanofibers and self assembled rosette nanotubes for myocardial applications. *Journal of biomedical materials research Part A.* 2013;101(4):1095-102.
122. Prestwich GD. Engineering a clinically-useful matrix for cell therapy. *Organogenesis.* 2008;4(1):42-7.
123. New drugs/drug news. *P & T : a peer-reviewed journal for formulary management.* 2011;36(12):784-842.
124. Duboeuf F, Basarab A, Liebgott H, Brusseau E, Delachartre P, Vray D. Investigation of PVA cryogel Young's modulus stability with time, controlled by a simple reliable technique. *Medical physics.* 2009;36(2):656-61.

125. Dowling DP, Miller IS, Ardhaoui M, Gallagher WM. Effect of surface wettability and topography on the adhesion of osteosarcoma cells on plasma-modified polystyrene. *Journal of biomaterials applications*. 2011;26(3):327-47.
126. Arima Y, Iwata H. Effect of wettability and surface functional groups on protein adsorption and cell adhesion using well-defined mixed self-assembled monolayers. *Biomaterials*. 2007;28(20):3074-82.
127. Forest PO, Karoum R, Gagnieu CH. Influence of gradual introduction of hydrophobic groups (stearic acid) in denatured atelocollagen on fibroblasts behavior in vitro. *Journal of biomedical materials research Part A*. 2007;80(3):758-67.
128. Cote MF, Doillon CJ. Wettability of cross-linked collagenous biomaterials: in vitro study. *Biomaterials*. 1992;13(9):612-6.
129. Campillo-Fernandez AJ, Unger RE, Peters K, Halstenberg S, Santos M, Salmeron Sanchez M, et al. Analysis of the biological response of endothelial and fibroblast cells cultured on synthetic scaffolds with various hydrophilic/hydrophobic ratios: influence of fibronectin adsorption and conformation. *Tissue engineering Part A*. 2009;15(6):1331-41.
130. Clark RA, Ghosh K, Tonnesen MG. Tissue engineering for cutaneous wounds. *J Invest Dermatol*. 2007;127(5):1018-29.
131. Burn Incidence Fact Sheet [Electronic]. American Burn Association; 2014 [updated 2013; cited 2014 August 2014]. Available from: http://www.ameriburn.org/resources_factsheet.php.
132. US Tissue Engineering Markets: Overview, Analysis and Opportunities. 2012 Contract No.: N910-54.
133. FDA. Technology Assessment: Skin substitutes for treating chronic wounds. FDA Publication Agency for Healthcare, 2011.
134. Zaulyanov L, Kirsner RS. A review of a bi-layered living cell treatment (Apligraf) in the treatment of venous leg ulcers and diabetic foot ulcers. *Clin Interv Aging*. 2007;2(1):93-8.
135. Krebs MD, Sutter KA, Lin AS, Guldberg RE, Alsberg E. Injectable poly(lactic-co-glycolic) acid scaffolds with in situ pore formation for tissue engineering. *Acta Biomater*. 2009;5(8):2847-59.
136. Lu G, Ling K, Zhao P, Xu Z, Deng C, Zheng H, et al. A novel in situ-formed hydrogel wound dressing by the photocross-linking of a chitosan derivative. *Wound Repair Regen*. 2010;18(1):70-9.
137. Forouzandeh F, Jalili RB, Germain M, Duronio V, Ghahary A. Skin cells, but not T cells, are resistant to indoleamine 2, 3-dioxygenase (IDO) expressed by allogeneic fibroblasts. *Wound Repair Regen*. 2008;16(3):379-87.
138. Elmaagacli AH, Ditschkowski M, Steckel NK, Gromke T, Ottinger H, Hillen U, et al. Human chorionic gonadotropin and indoleamine 2,3-dioxygenase in patients with GVHD. *Bone marrow transplantation*. 2014;49(6):800-5.
139. Rezakhanlou AM, Habibi D, Lai A, Jalili RB, Ong CJ, Ghahary A. Highly efficient stable expression of indoleamine 2,3 dioxygenase gene in primary fibroblasts. *Biol Proced Online*. 2010;12(1):9028.

140. Azadeh Hosseini-Tabatabaei RBJ, Ryan Hartwell, Sanam Salimi, Ruhangiz T. Kilani, Aziz Ghahary. Embedding Islet in a liquid scaffold increases islet viability and function. *Canadian Journal of Diabetes*. 2013;37 (1):27-35.
141. Kloeters O, Tandara A, Mustoe TA. Hypertrophic scar model in the rabbit ear: a reproducible model for studying scar tissue behavior with new observations on silicone gel sheeting for scar reduction. *Wound Repair Regen*. 2007;15 Suppl 1:S40-5.
142. Rahmani-Neishaboer E, Jallili R, Hartwell R, Leung V, Carr N, Ghahary A. Topical application of a film-forming emulgel dressing that controls the release of stratifin and acetylsalicylic acid and improves/prevents hypertrophic scarring. *Wound Repair Regen*. 2013;21(1):55-65.
143. Li Y, Kilani RT, Rahmani-Neishaboer E, Jalili RB, Ghahary A. Kynurenine increases matrix metalloproteinase-1 and -3 expression in cultured dermal fibroblasts and improves scarring in vivo. *J Invest Dermatol*. 2014;134(3):643-50.
144. Kung EF, Wang F, Schechner JS. In vivo perfusion of human skin substitutes with microvessels formed by adult circulating endothelial progenitor cells. *Dermatol Surg*. 2008;34(2):137-46.
145. Auger FA, Gibot L, Lacroix D. The pivotal role of vascularization in tissue engineering. *Annual review of biomedical engineering*. 2013;15:177-200.
146. Wallengren J, Chen D, Sundler F. Neuropeptide-containing C-fibres and wound healing in rat skin. Neither capsaicin nor peripheral neurotomy affect the rate of healing. *Br J Dermatol*. 1999;140(3):400-8.
147. Deitch EA, Wheelahan TM, Rose MP, Clothier J, Cotter J. Hypertrophic burn scars: analysis of variables. *J Trauma*. 1983;23(10):895-8.
148. Werner S, Krieg T, Smola H. Keratinocyte-fibroblast interactions in wound healing. *J Invest Dermatol*. 2007;127(5):998-1008.
149. Cheng B, Liu HW, Fu XB. Update on pruritic mechanisms of hypertrophic scars in postburn patients: the potential role of opioids and their receptors. *J Burn Care Res*. 2011;32(4):e118-25.
150. Li Y, Tredget EE, Ghaffari A, Lin X, Kilani RT, Ghahary A. Local expression of indoleamine 2,3-dioxygenase protects engraftment of xenogeneic skin substitute. *J Invest Dermatol*. 2006;126(1):128-36.
151. Campbell LK, Thomas JR, Lamps LW, Smoller BR, Folpe AL. Protein Gene Product 9.5 (PGP 9.5) Is Not a Specific Marker of Neural and Nerve Sheath Tumors: An Immunohistochemical Study of 95 Mesenchymal Neoplasms. *Mod Pathol*. 2003;16(10):963-9.
152. Phillips CL, Combs SB, Pinnell SR. Effects of ascorbic acid on proliferation and collagen synthesis in relation to the donor age of human dermal fibroblasts. *J Invest Dermatol*. 1994;103(2):228-32.
153. Gonfiotti A, Jaus MO, Barale D, Baiguera S, Comin C, Lavorini F, et al. The first tissue-engineered airway transplantation: 5-year follow-up results. *Lancet*. 2014;383(9913):238-44.